Overview of Restructuring technologies of cereal polymers through processing and nanotechnology (for food and non-food applications)

Jozef L. Kokini

Department of Food Science
Purdue University

West Lafayette IN, USA

PURDUE
UNIVERSITY

Outline of Talk

- Extrusion cooking of cereals
- Development of state diagrams to understand phase changes
- Microwave expansion of unexpanded glassy pellets
- Understanding crispness
- Understanding tortilla stickiness
- Restructuring and functionalization using nanotechnology

PURDUE UNIVERSITY

Extrusion is primarily useful to cook, form and expand cereals-Mechanism of food extrudate expansion

1. **Order-disorder transformation and chemical complexing** (in the extruder)
2. **Nucleation**
3. **Extrudate swell**
4. **Bubble growth**
5. **Bubble collapse**

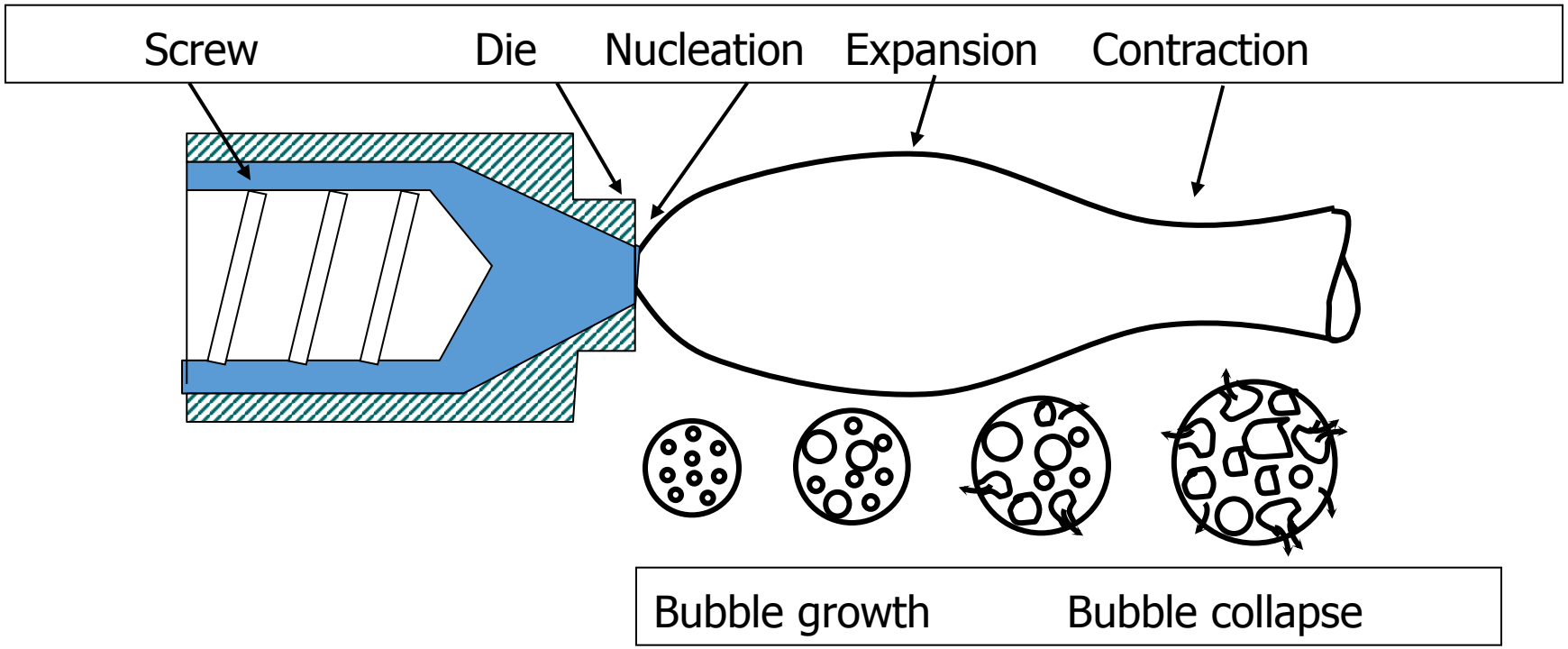

Mechanism of bubble nucleation in starch extrudates

A. Air pockets from interparticle, inter- and intragranular voids serve as water vapor nuclei

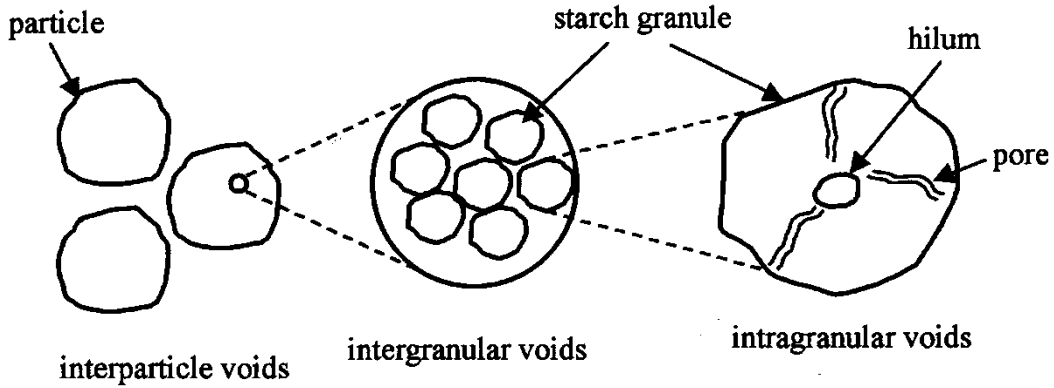

B. Hydrophobic surfaces decrease wetting

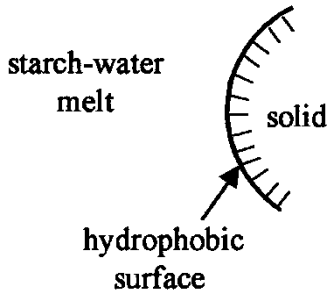

C. Mobility of water molecules increases with distance from polymer chains

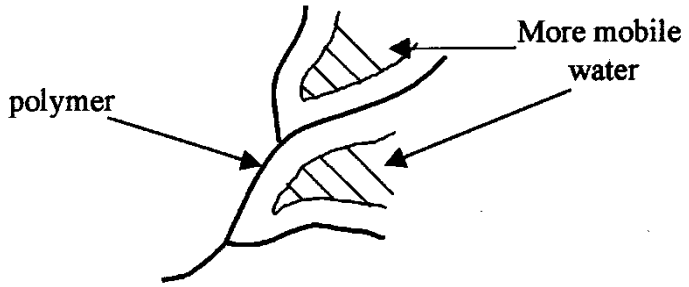

PURDUE UNIVERSITY

Air entrapment is determined by the barrel fill length

1. When EBFL is in the **"cold"** barrel section, the unexpanded extrudate has numerous air bubbles
2. When EBFL is in the **"hot"** zone, the unexpanded extrudate has few or no bubbles.

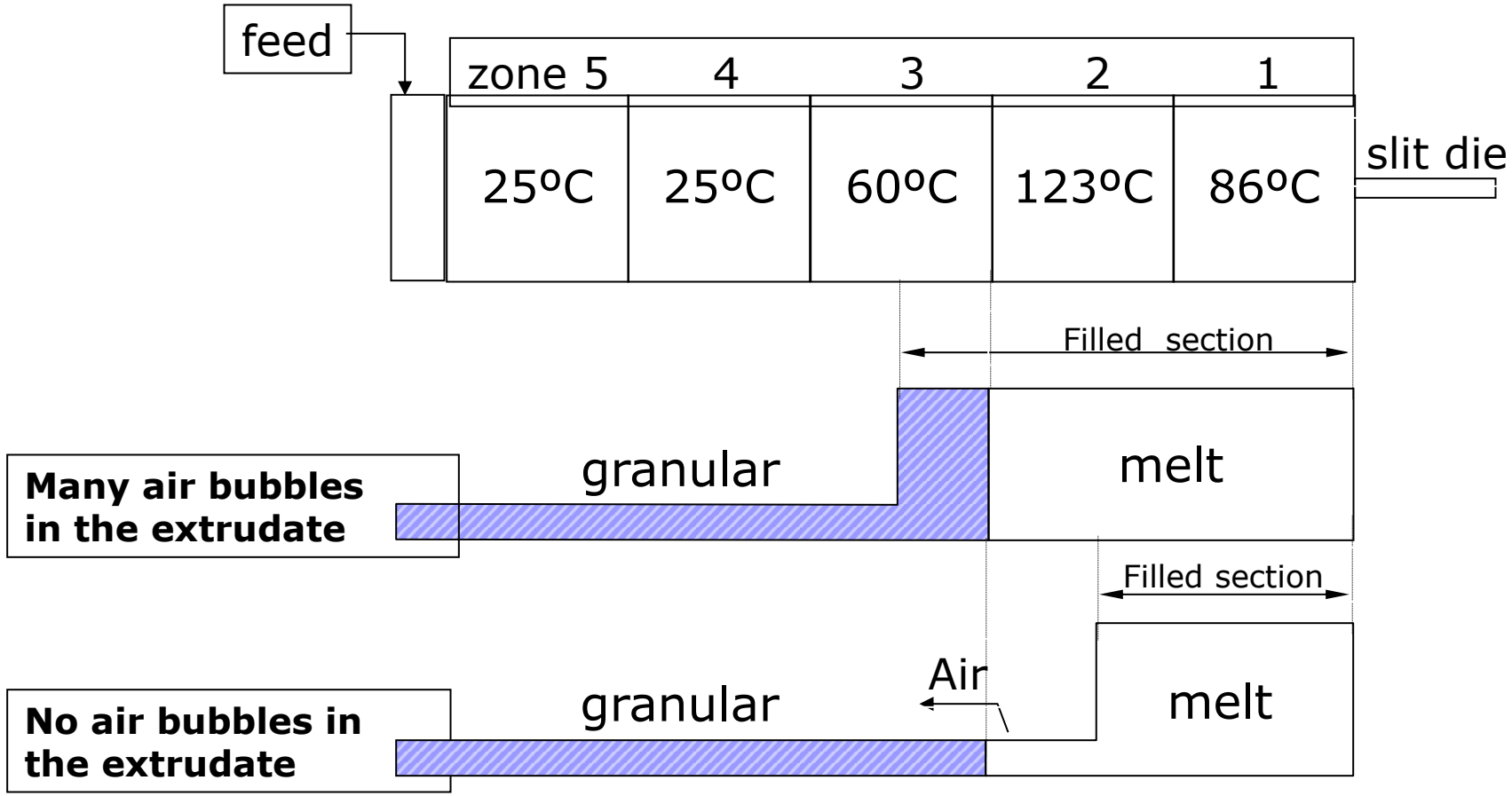

Porosity master curve

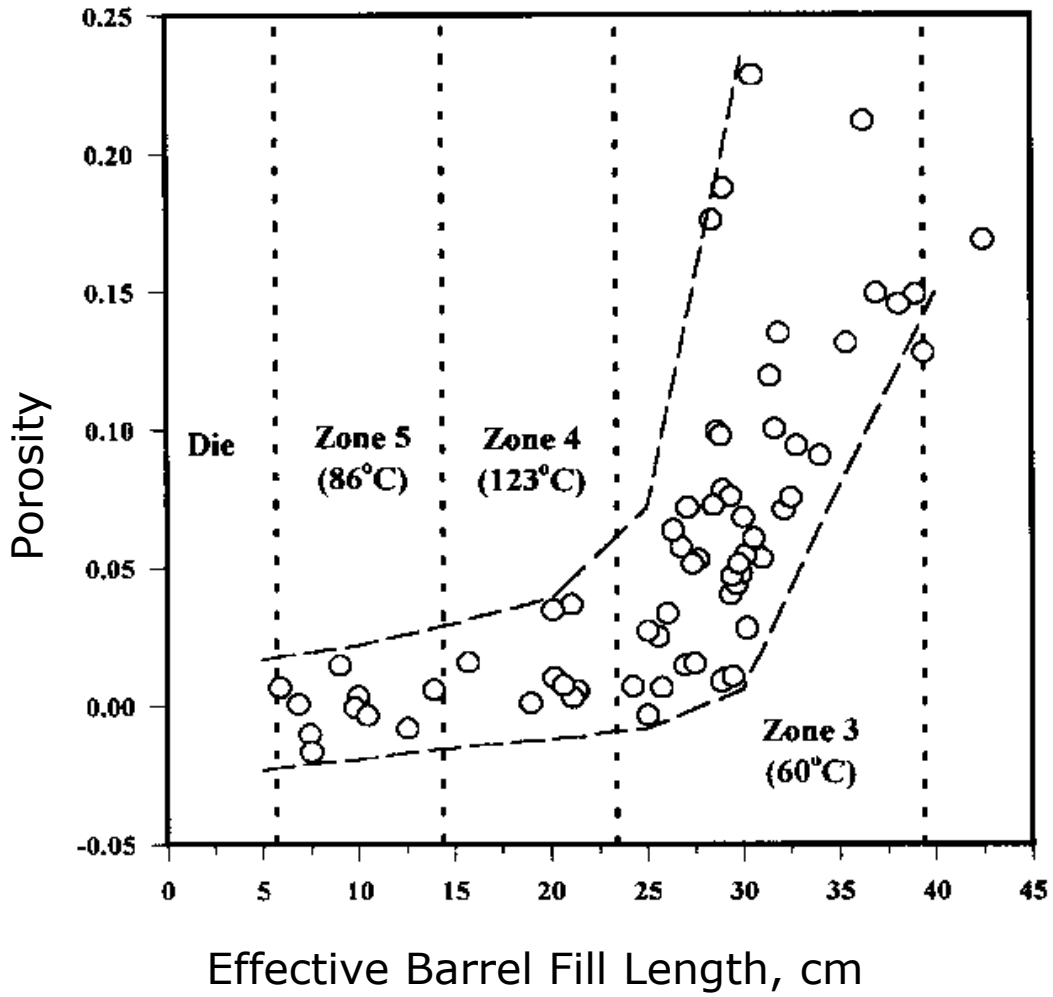

- All data points generate a **broad master curve**
- Two defined regions are observed:
  - at low EBFL, the porosity increases slightly
  - past a **critical EBFL**, the porosity increases exponentially.

Influence of the physical state of starch on air entrapment

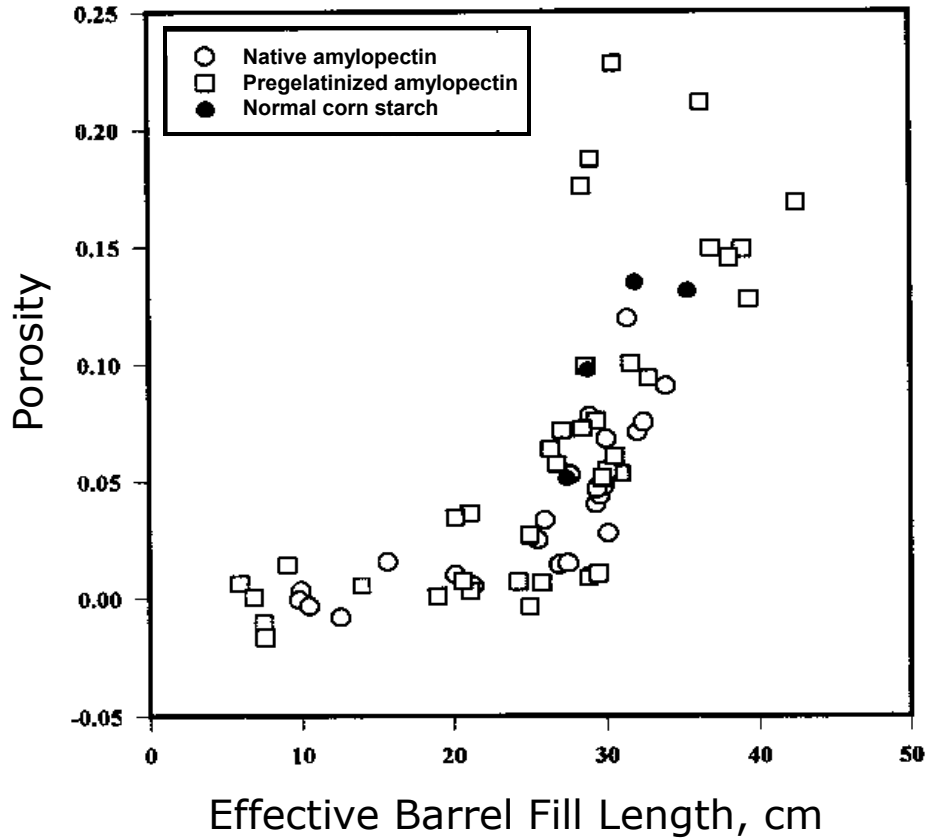

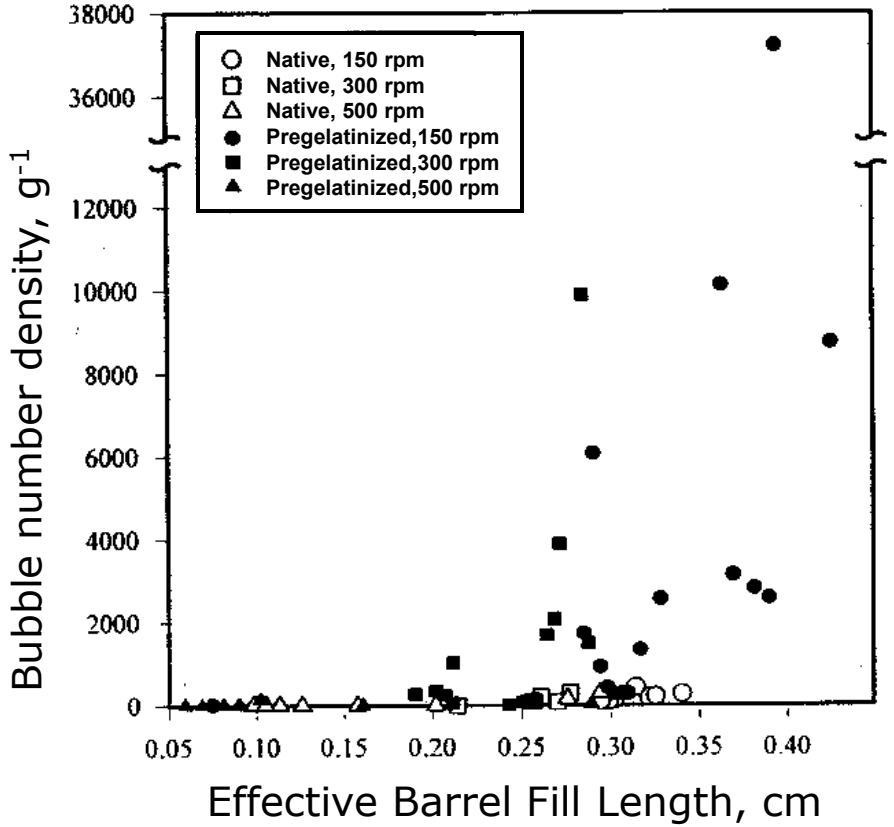

- The physical form and type of starch do not influence the porosity
- Pregelatinized amylopectin leads to much higher bubble number density values than native amylopectin

PURDUE UNIVERSITY

Effect of Specific Mechanical Energy on air entrapment

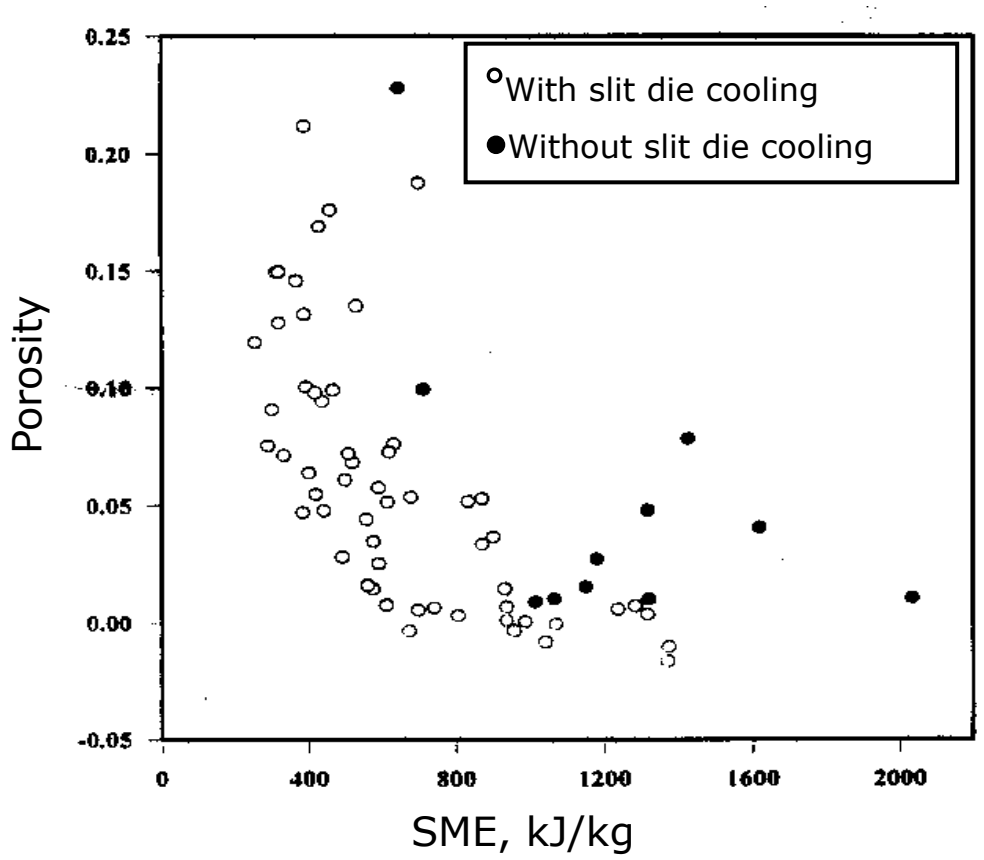

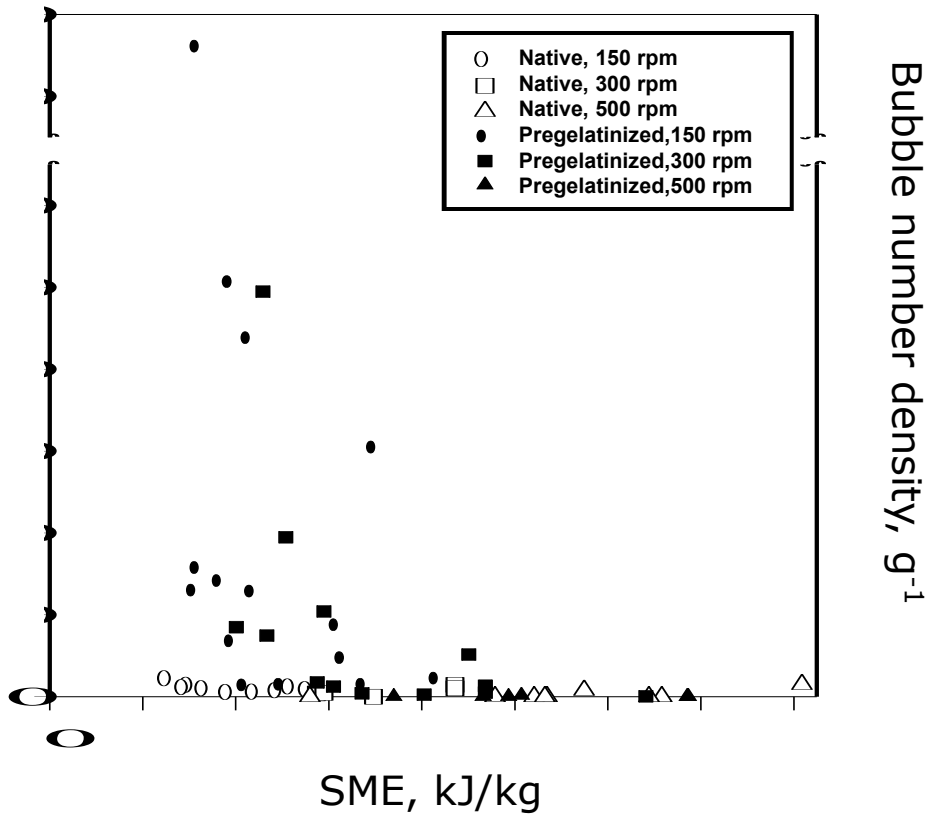

- Porosity decreases with SME
- Low SME (200-900kJ/kg) leads to high bubble number density, while high SME (900-1600kJ/kg) leads to low bubble number density

PURDUE UNIVERSITY

Influence of polymeric melt viscosity

Amioca (lower viscosity)

Hylon 7 (higher viscosity)

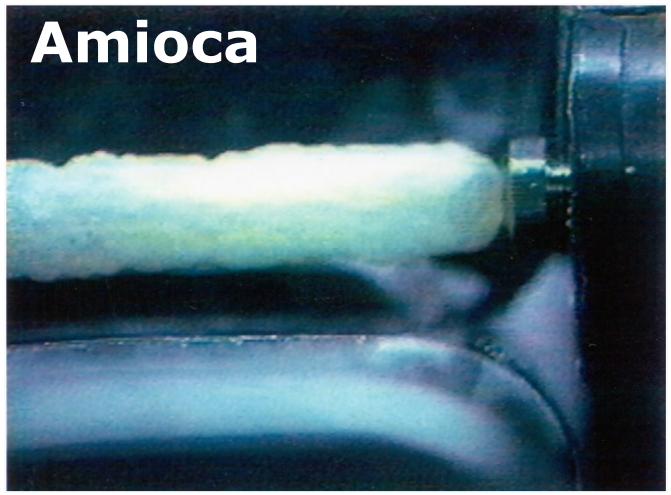

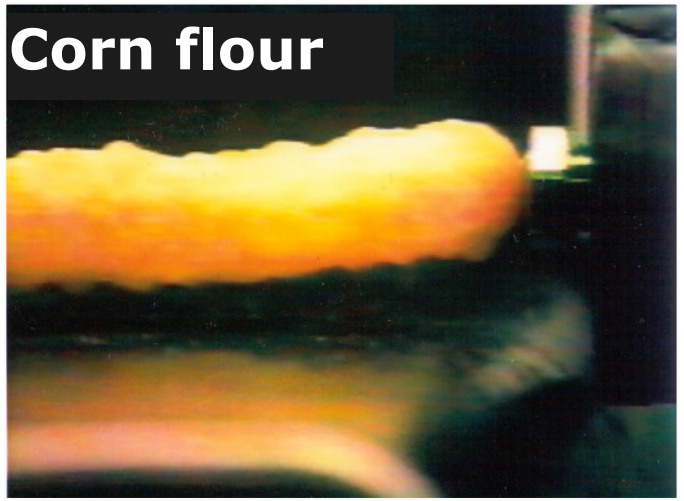

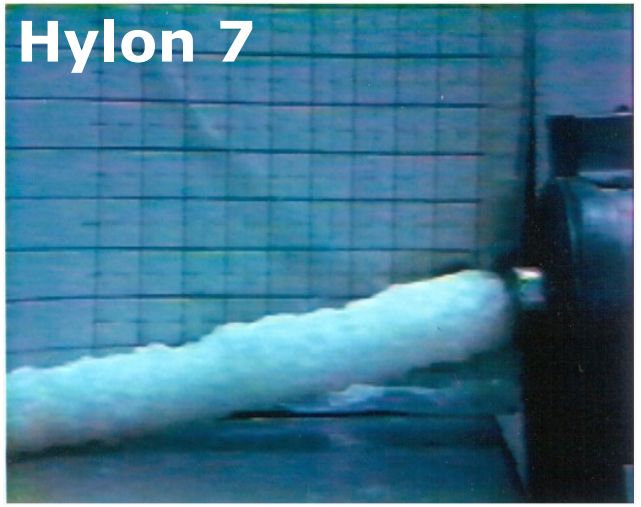

- **Extrudate swell -** the phenomenon that governs the diametral expansion of extrudates in the absence of blowing agents. It is caused by elastic recovery
- **Bubble growth** – in a high viscosity mass, it is mainly determined by the driving force and the resistance to deformation.
- **Bubble collapse** – determines the final extrudate expansion in high moisture and low viscosity materials.

PURDUE UNIVERSITY

Factors that control bubble growth-model based on steady shear viscosity

- Pressure difference is the driving force:

$$P_V - P_L = \frac{2\sigma}{R} + 4\eta_L\left(\frac{\dot{R}}{R}\right)$$

- Viscosity controls the rate of bubble growth:

  Very viscous materials:

$$\frac{\dot{R}}{R} = \frac{\Delta P}{4\eta_L}$$

  Power law fluids:

$$\frac{\dot{R}}{R} = \left(\frac{\Delta P}{4m}\right)^{\frac{1}{n}}$$

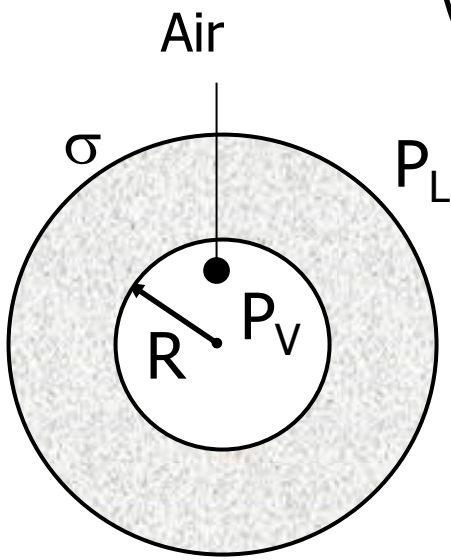

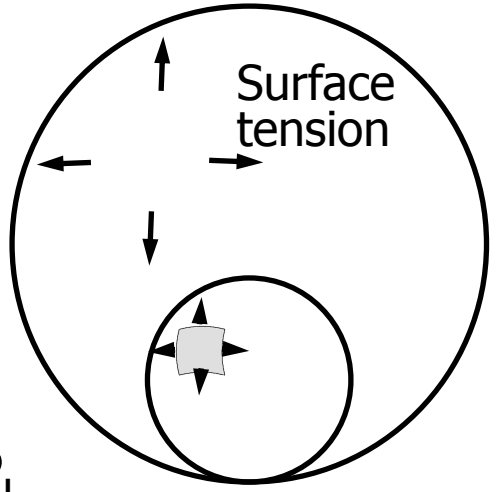

Biaxial extension during bubble growth

R: bubble radius
P_v: instantaneous bubble pressure
σ: surface tension

PURDUE UNIVERSITY

The bubble expansion model is experimentally tested:

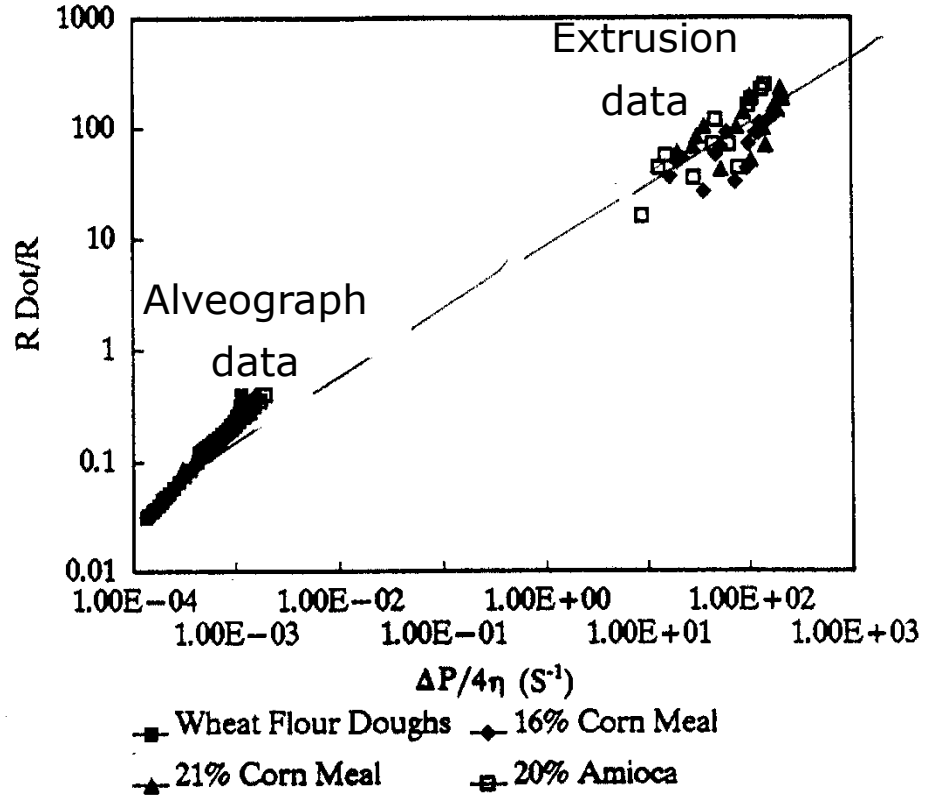

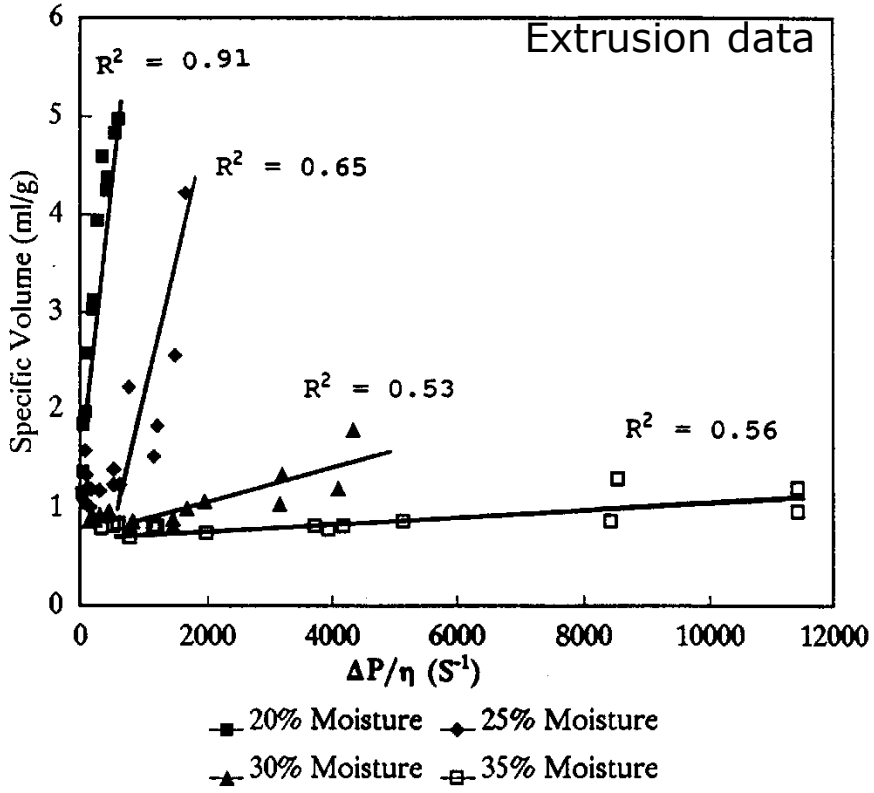

Conclusions on extrudate expansion

- Extrudate expansion is a result of structural order-disorder transformations, nucleation, extrudate swell, bubble growth and bubble collapse
- Air bubbles entrapped in the matrix can act as nuclei for further expansion of the matrix (by extrusion, microwave heating, etc.)
- A mechanism for air bubble nucleation was proposed
- Extrudate expansion is determined by the water vapor pressure and the rheological properties of the melt

PURDUE UNIVERSITY

Development of state diagrams for amorphous polymers

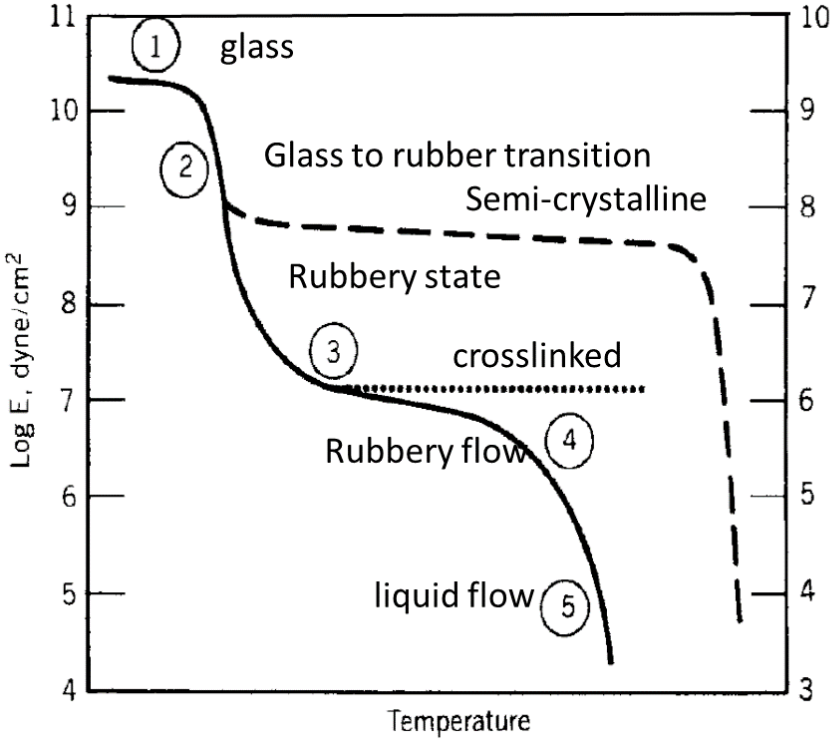

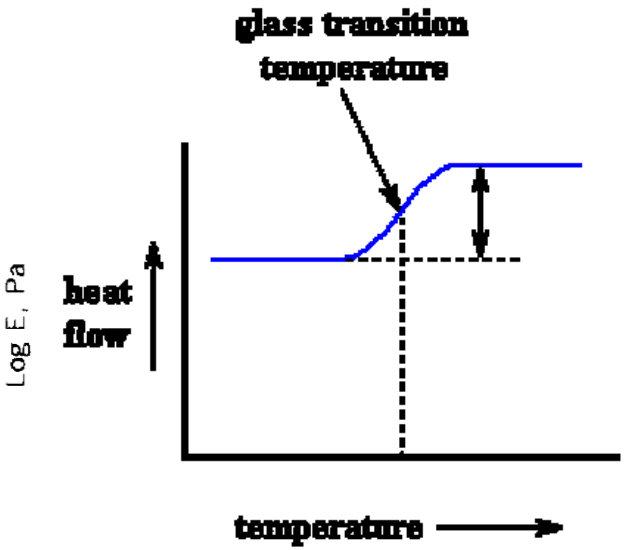

- Many important polymers **do not crystallize at all but form glasses in non-equilibrium states** at low temperatures. At higher temperatures they form viscous liquids.
- The transition that separates the glassy state from the viscous state is known as **the glass–rubber transition.**
- This transition has the properties of a **second-order transition** at very slow rates of heating or cooling.

Glass transition of gliadin as a function of moisture content using rheology and DSC

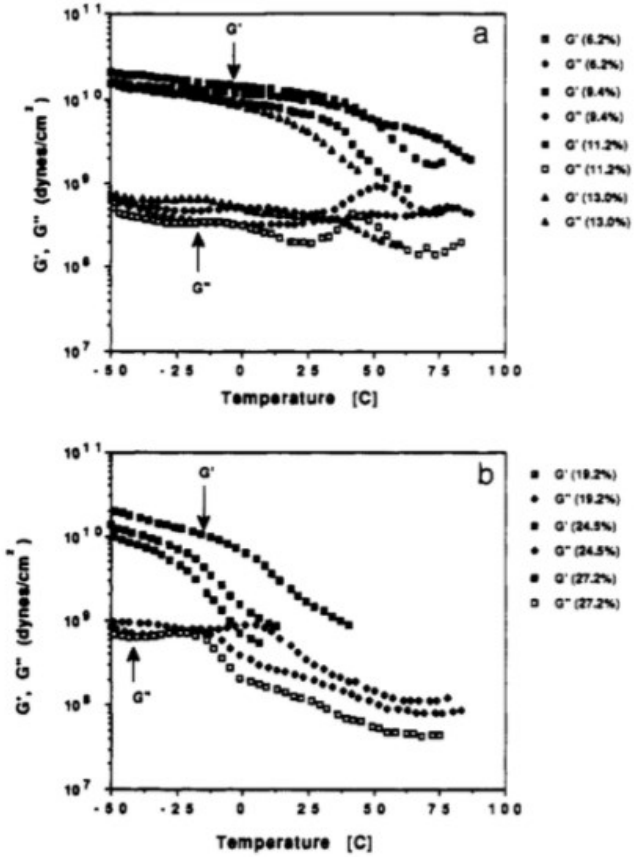

Figure 1. (a) Dynamic mechanical spectrometry curves of gliadin at 6.2, 9.4, 11.2, and 13.0% moisture. (b) Dynamic mechanical spectrometry curves of gliadin at 19.2, 24.5, and 27.2% moisture.

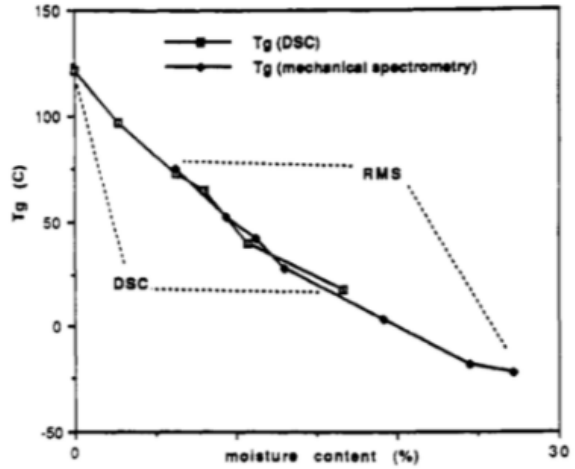

Figure 2. Glass transition temperatures of gliadin at different moisture contents using mechanical spectrometry (RMS) and differential scanning calorimetry.

Table I. Glass Transition Temperatures of Gliadin at Different Moisture Contents Determined by Dynamic Mechanical Spectrometry

equilibrium moisture content (%)	loss modulus (G'') maximum (°C)
6.2 ± 0.2	75.3 ± 2.7
9.4 ± 0.2	52.0 ± 2.0
11.2 ± 0.3	42.0 ± 1.0
13.0 ± 0.1	28.5 ± 0.5
19.2 ± 0.8	3.3 ± 1.7
24.5 ± 0.2	−18.0 ± 1.0
27.2 ± 0.4	−22.7 ± 1.7

Temperature sweep of gliadin with 25% moisture

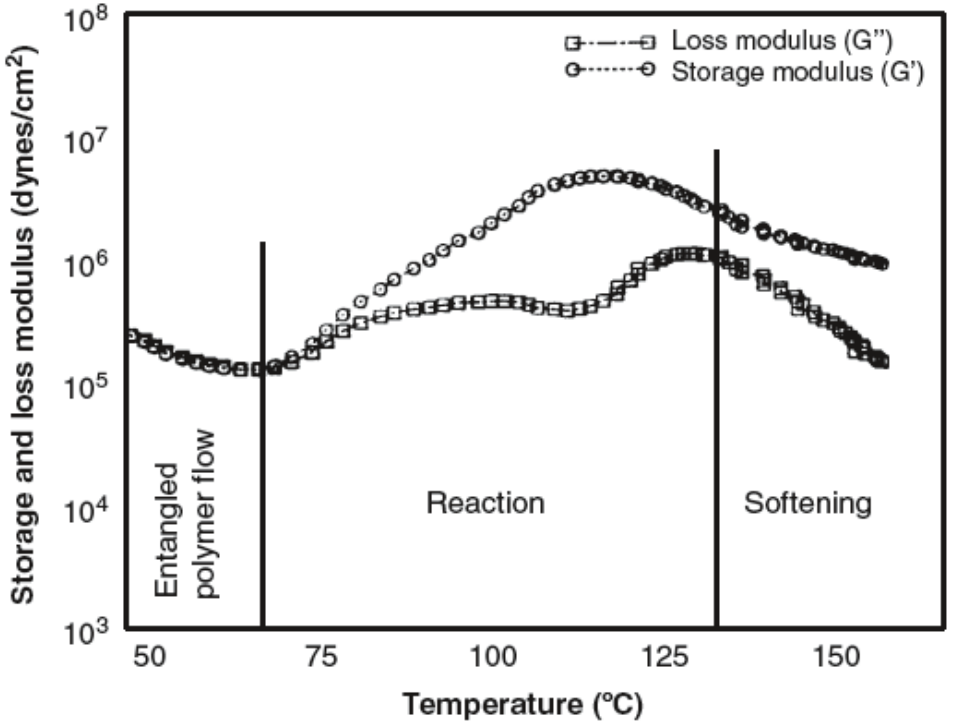

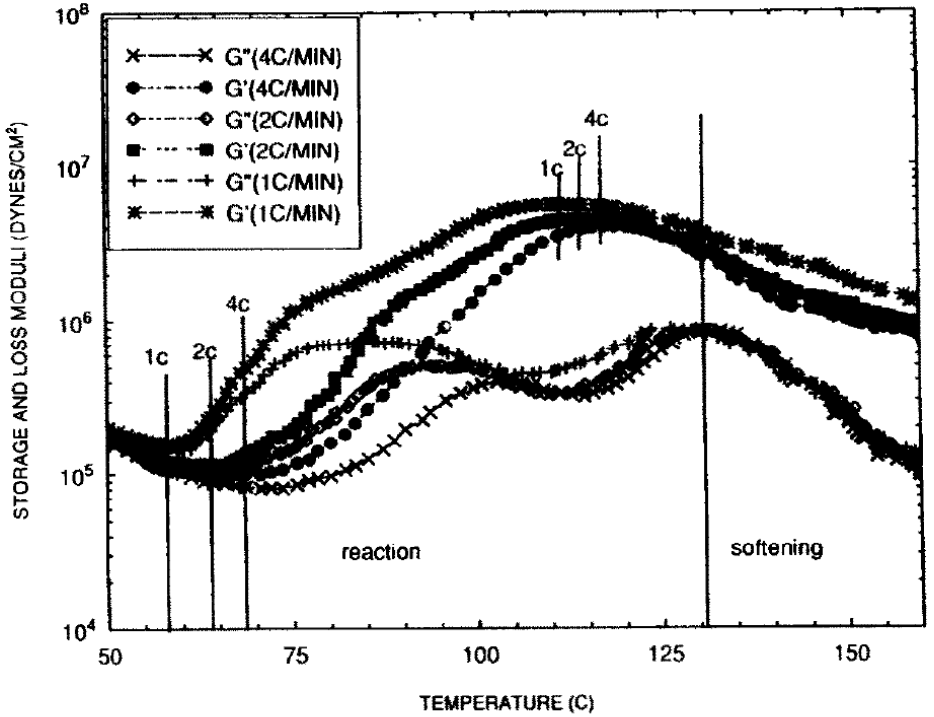

Fig. 2. Temperature sweep of gliadin with 25% moisture at different heating rates.

Frequency sweep of gliadin with 25% moisture

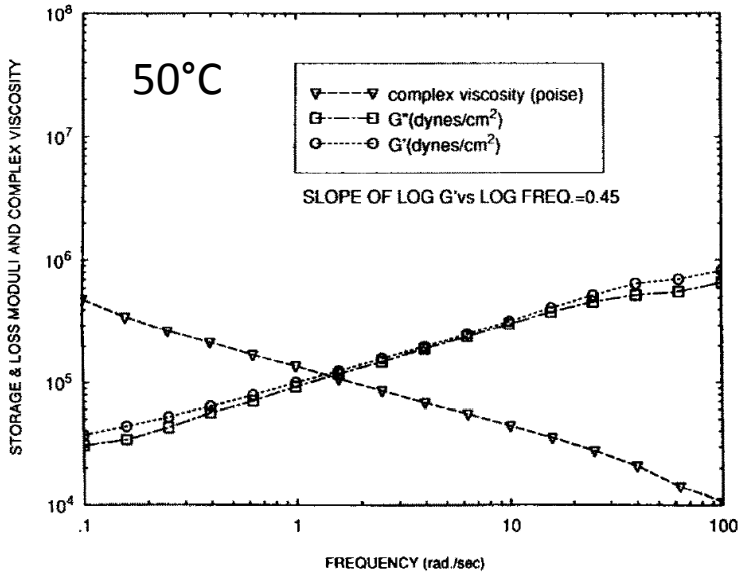

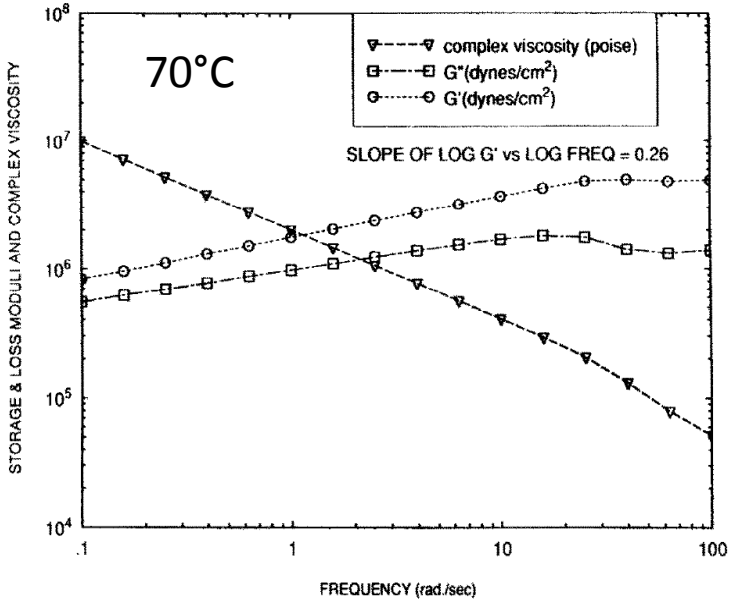

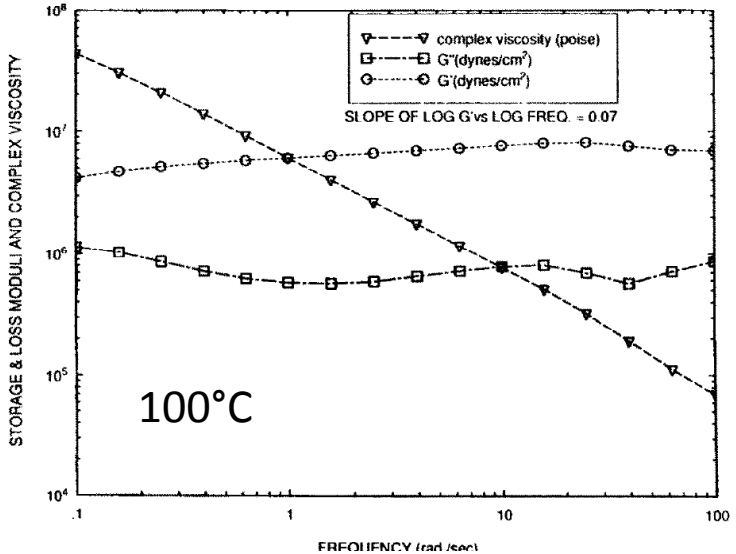

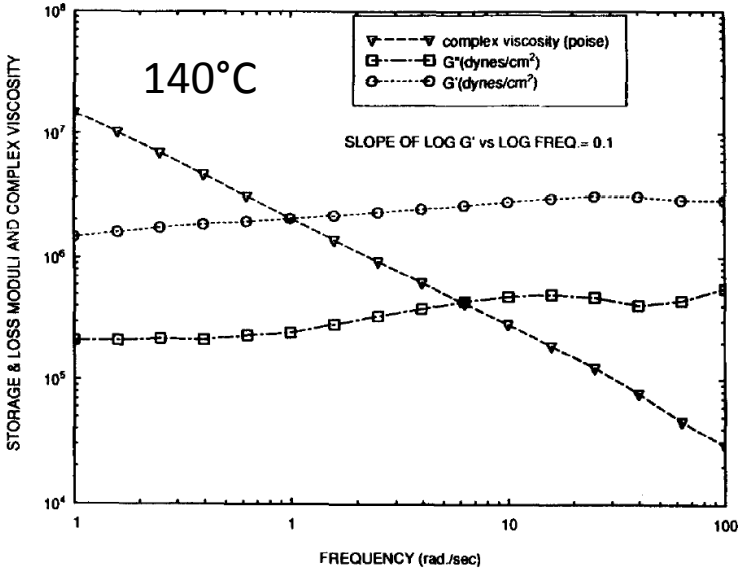

Estimation of the molecular weight between crosslinks and number of crosslink between molecules for gliadin

TABLE 1

Average Molecular Weight of Gliadin Chain Between Cross-links (M_c) and Number of Cross-links (N_c) in Molecular Weight of 50 000

Temperature (°C)	M_c	$\frac{1}{2} N_c$
70	7443·2	3·359
100	5354·1	4·669
140	14744·6	1·696
160	42645·7	0·586

$$M_c = \frac{\rho RT}{G'}$$

$$N_c = \frac{M_w^*}{2M_c}$$

State diagram for Gliadin, zein and gluten

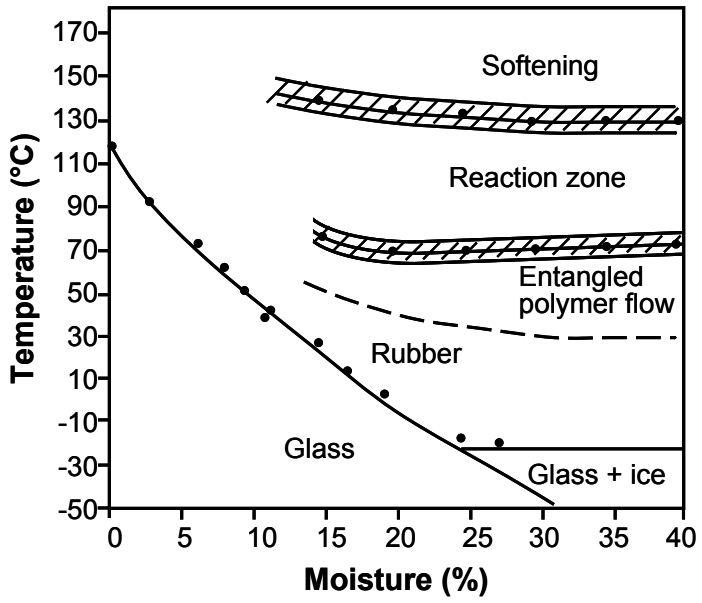

gliadin

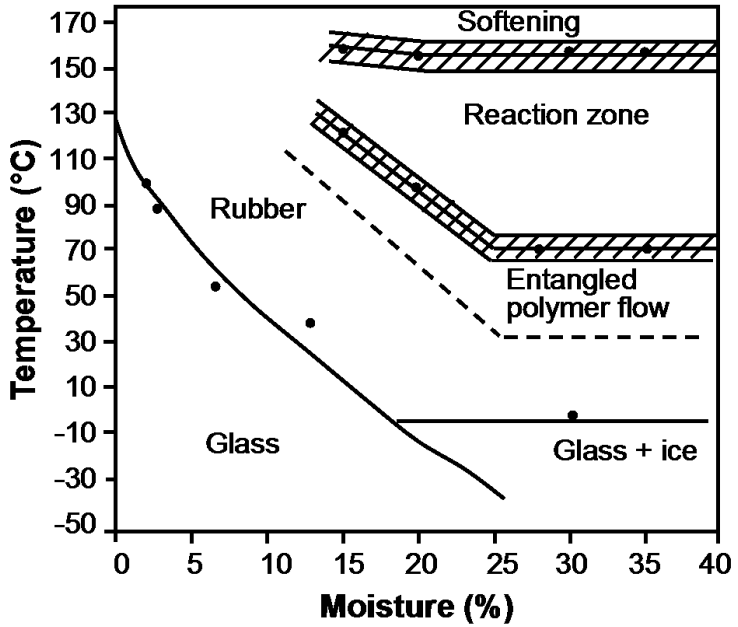

zein

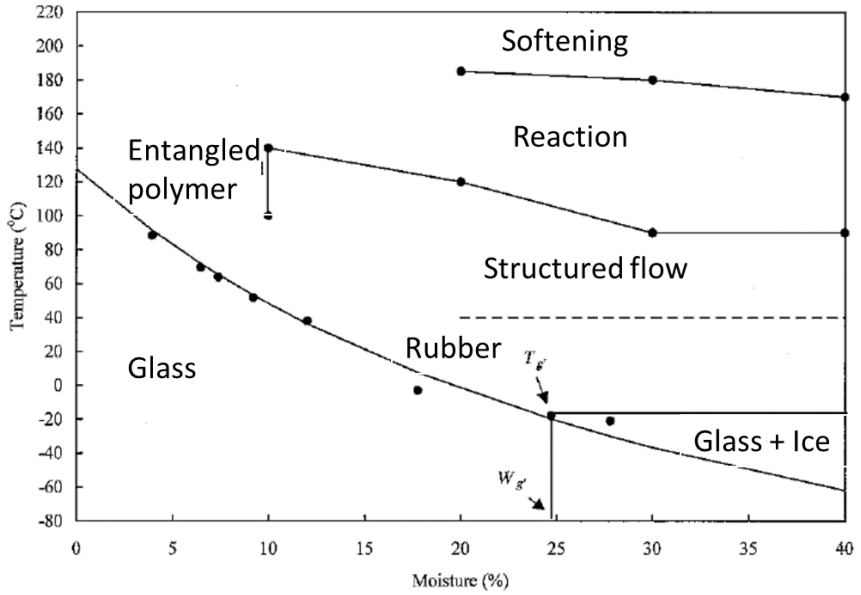

gluten

State diagrams for soy globulins

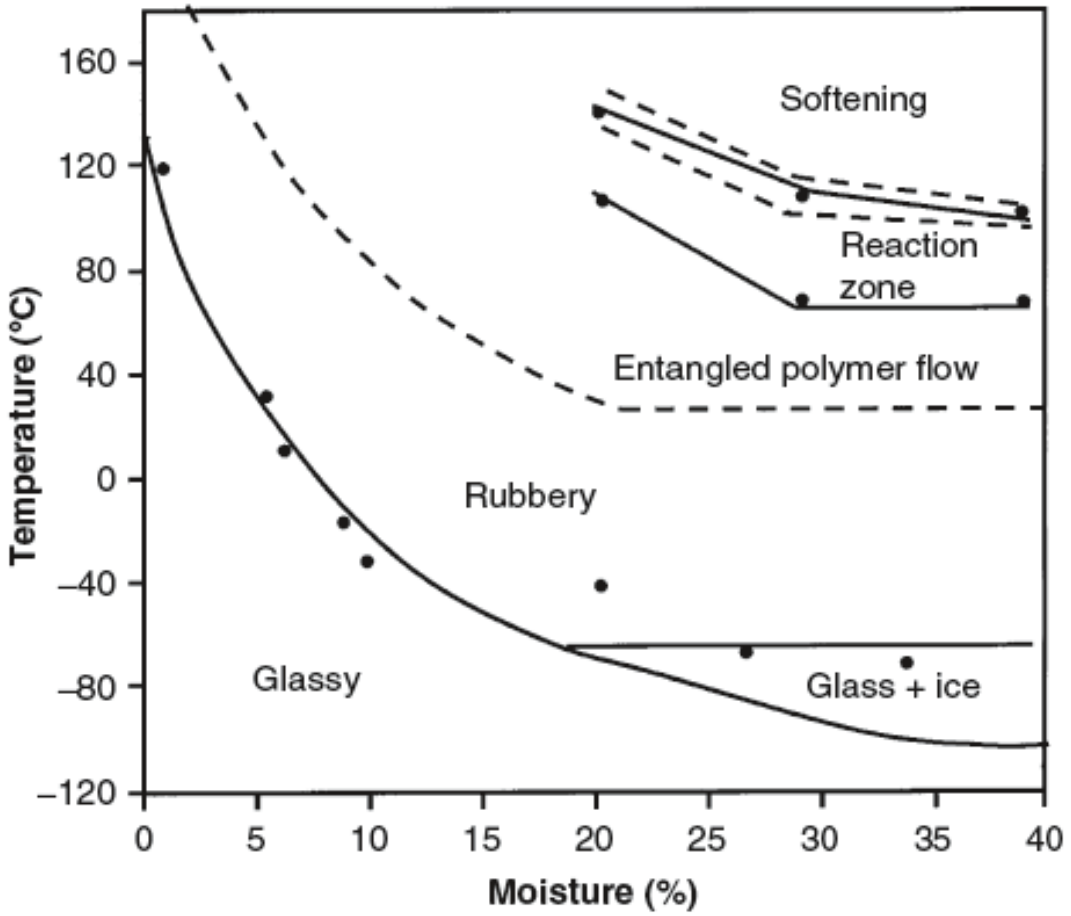

7S soy globulin

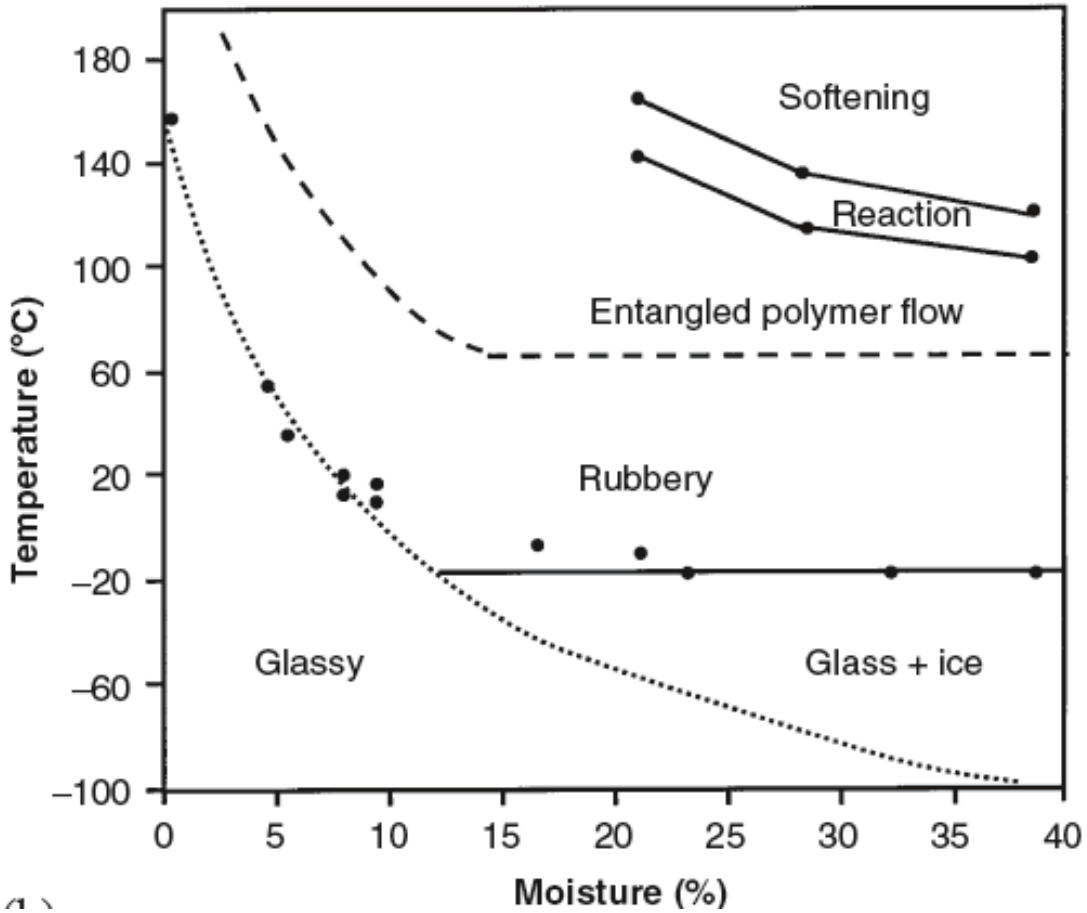

11S soy globulin

State diagram of cereal proteins during wetting, heating and cooling/drying stages of extrusion cooking

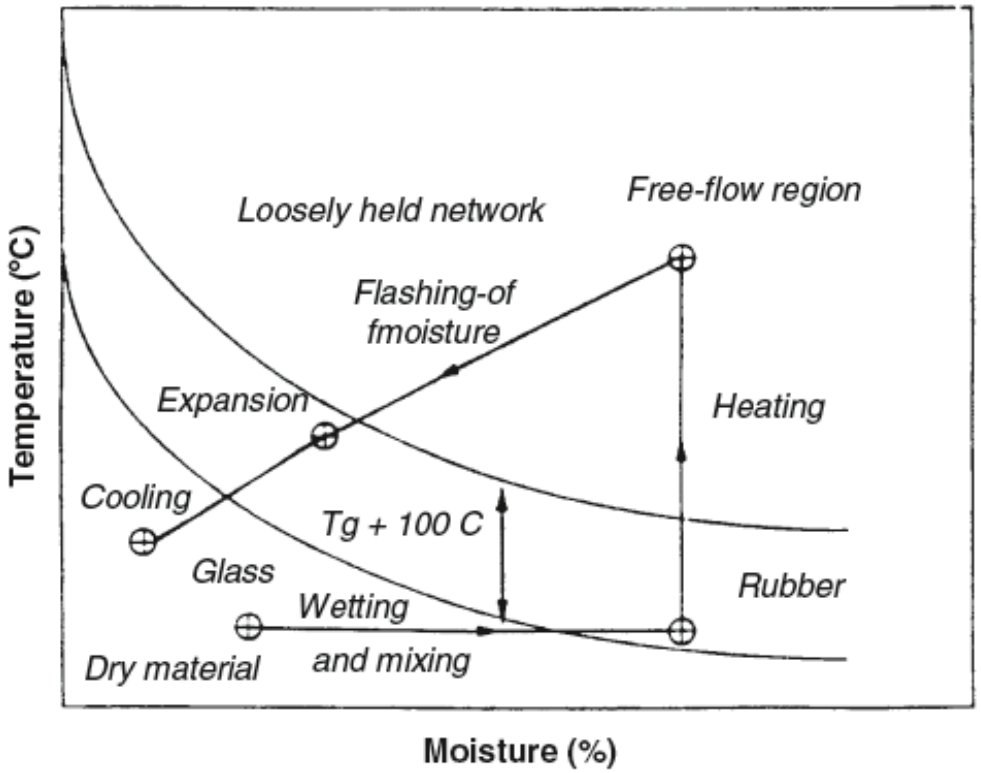

Cooking extrusion

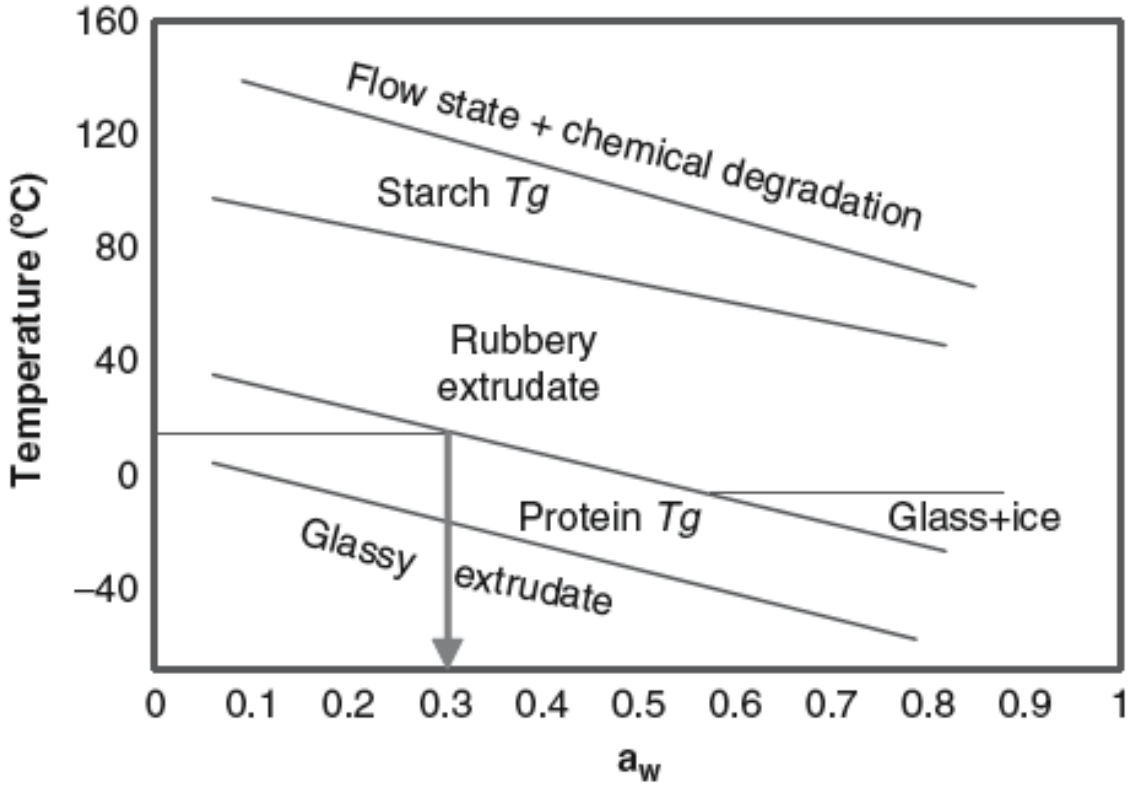

Meat-starch beef jerky analog extrusion

Glass transition and surface properties define Stickiness of Tortilla-application of impact of phase of behavior

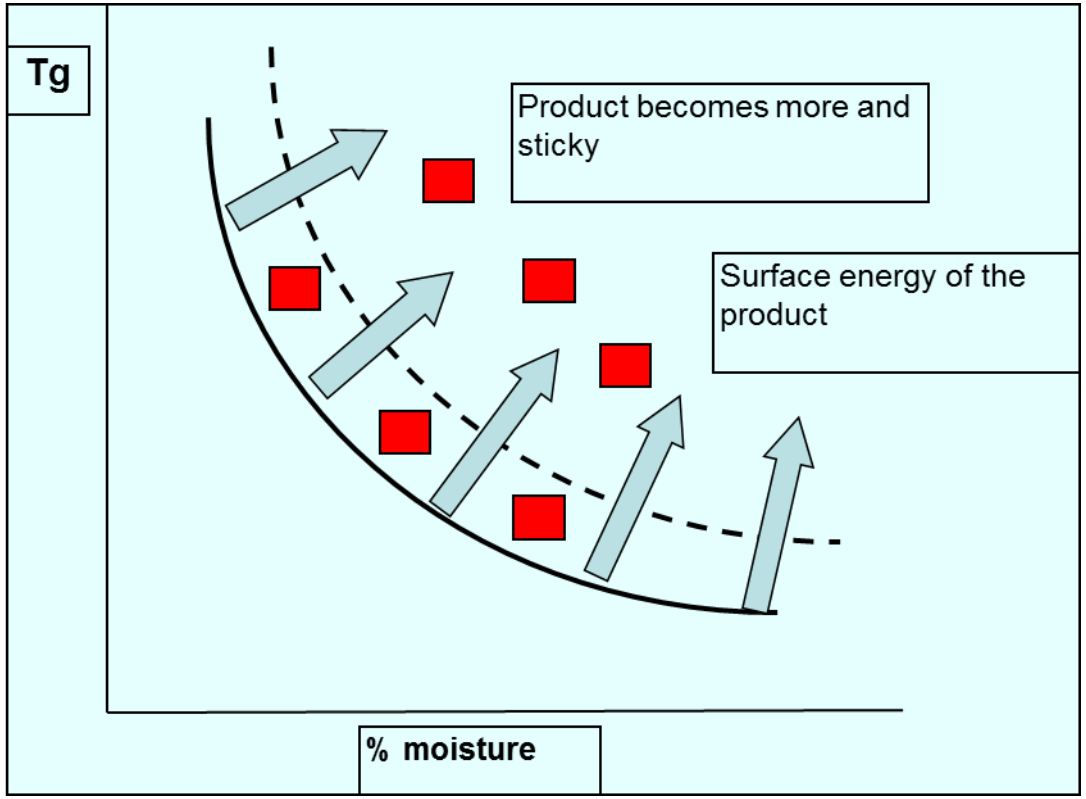

Stickiness is the result of changing phase behavior as a function of relative humidity and temperature and changes in the surface energy of the product

Effect of surface energy on contact angle

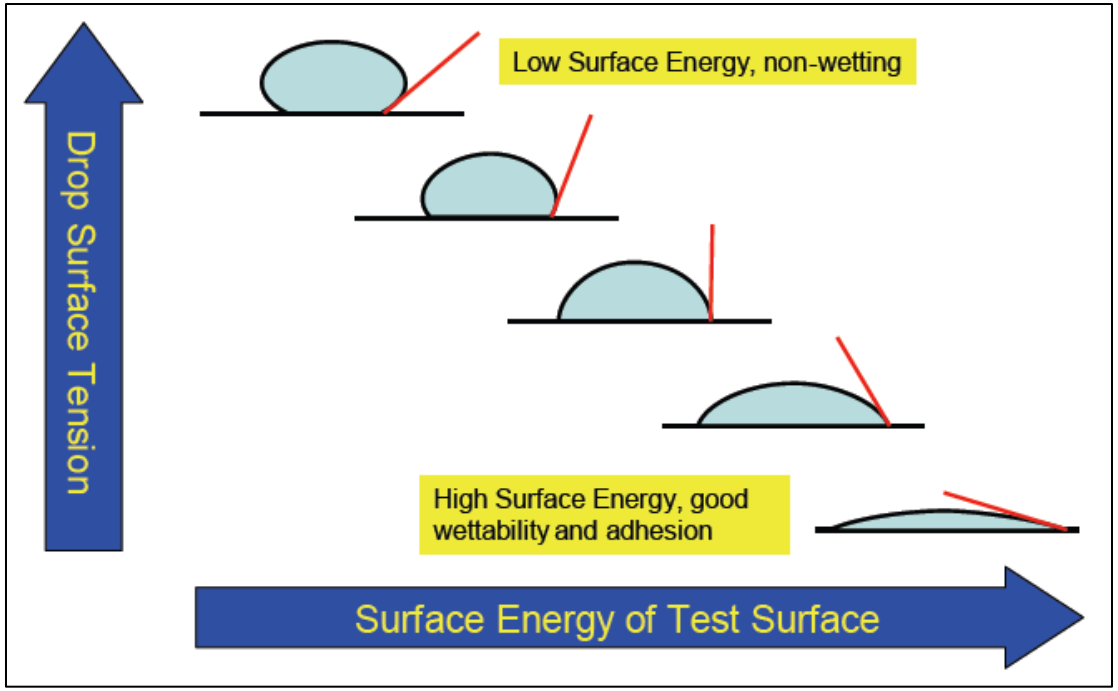

Source: AST Products Inc, MA

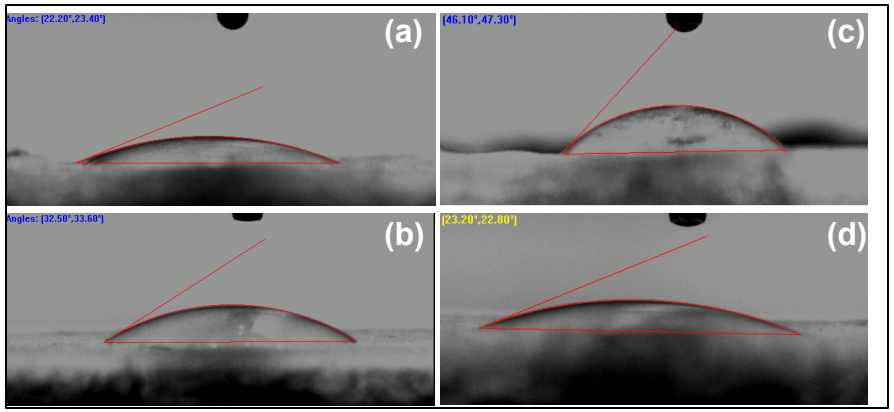

Contact angle of sticky & non-sticky tortilla measured in our laboratory

PURDUE UNIVERSITY

Variation in the instrumental stickiness with the surface energy

Dispersive surface energy (hydrophobic)

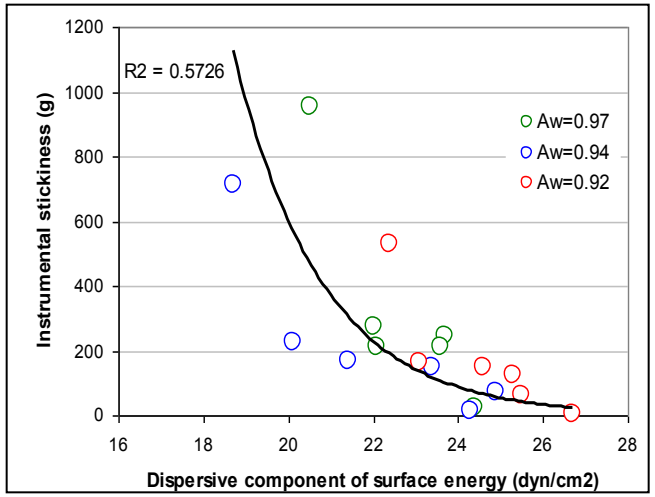

Polar surface energy (hydrophillic)

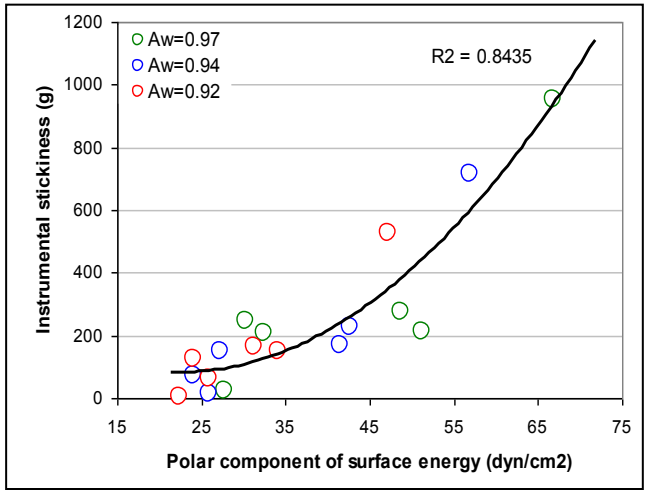

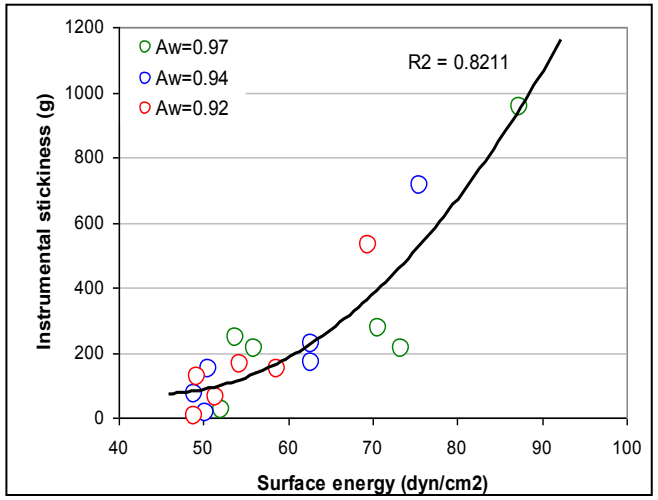

Total surface energy

PURDUE UNIVERSITY

A predictive model for Crispness of cellular foods

- Crispness is associated with cellular foods in the glassy state, and the crisp sensation is attributed to the cellular fracture of the glassy matrix.
- We have shown that the cellular fracture events are the stimulus for perception of the crispness sensation

PURDUE UNIVERSITY

Physical Properties of cellular foods that affect textural properties

[redacted]

Stages in the failure of a cellular material

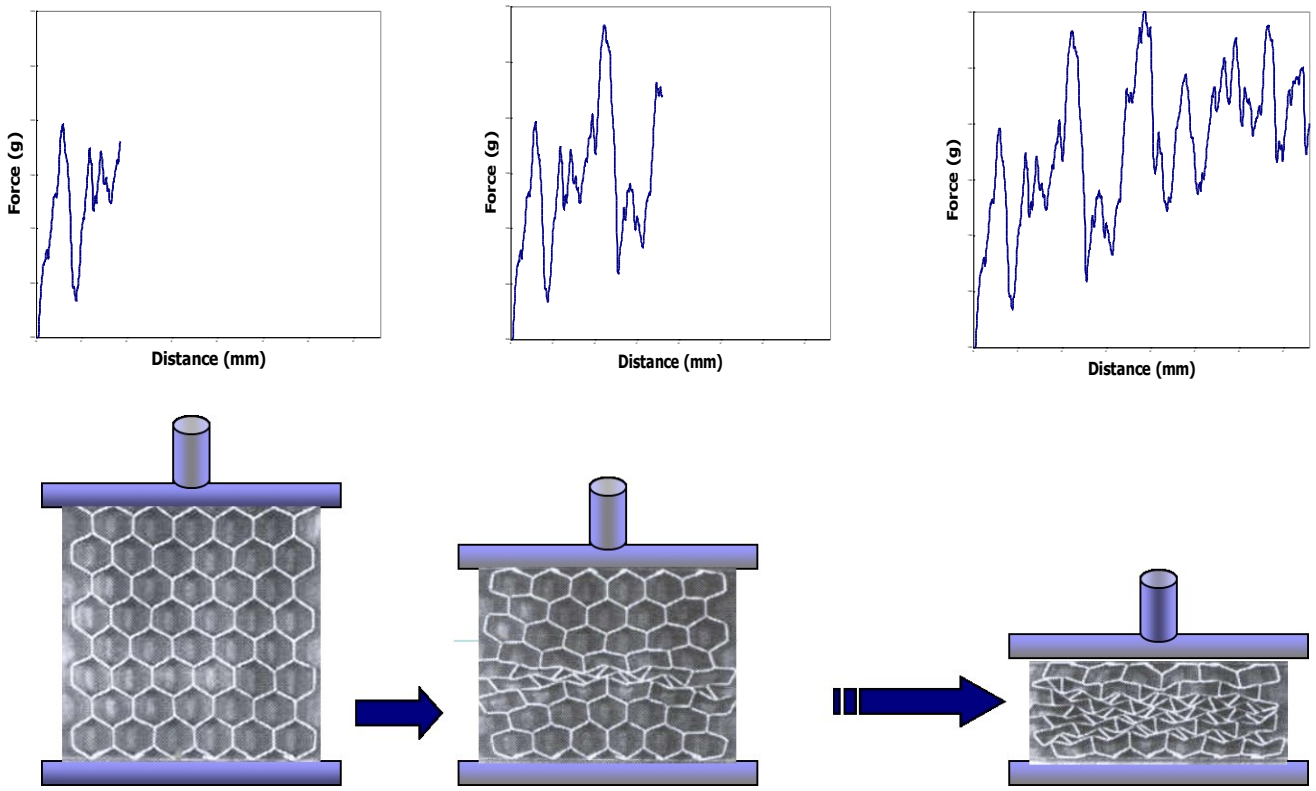

Measures of the jaggedness of force-deformation curve

- Number of peaks

Number of positive peaks greater than threshold force

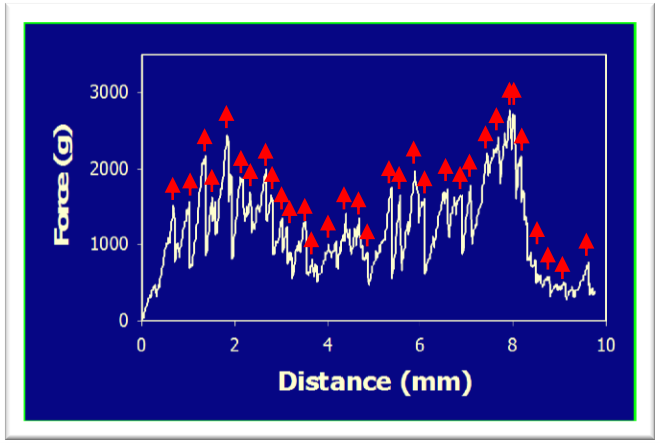

- Ratio of linear distance (RLD)

At constant smoothening ratio, RLD is higher for more crisp products.

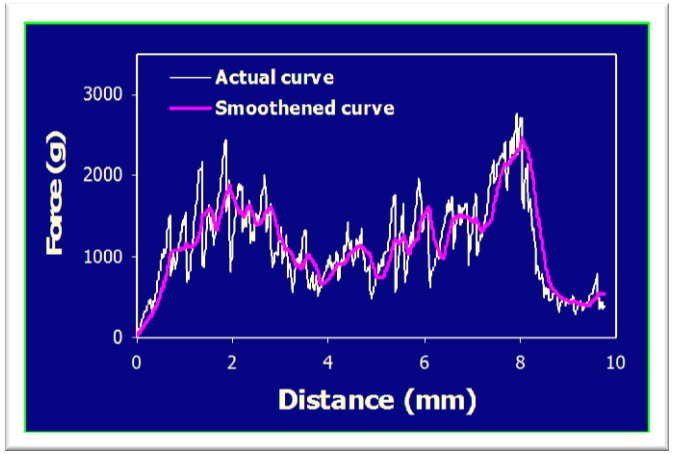

•Fractal analysis

Fractal dimensions were calculated according to Barrett and Peleg (1994).

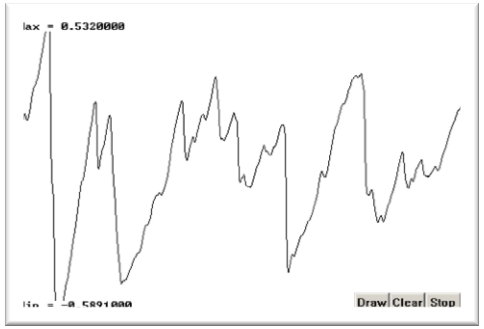

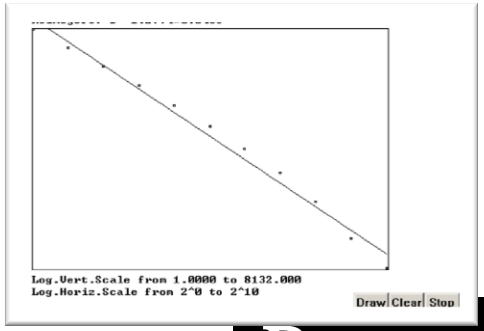

Sensory crispness correlates well with the average number of peaks (Np)

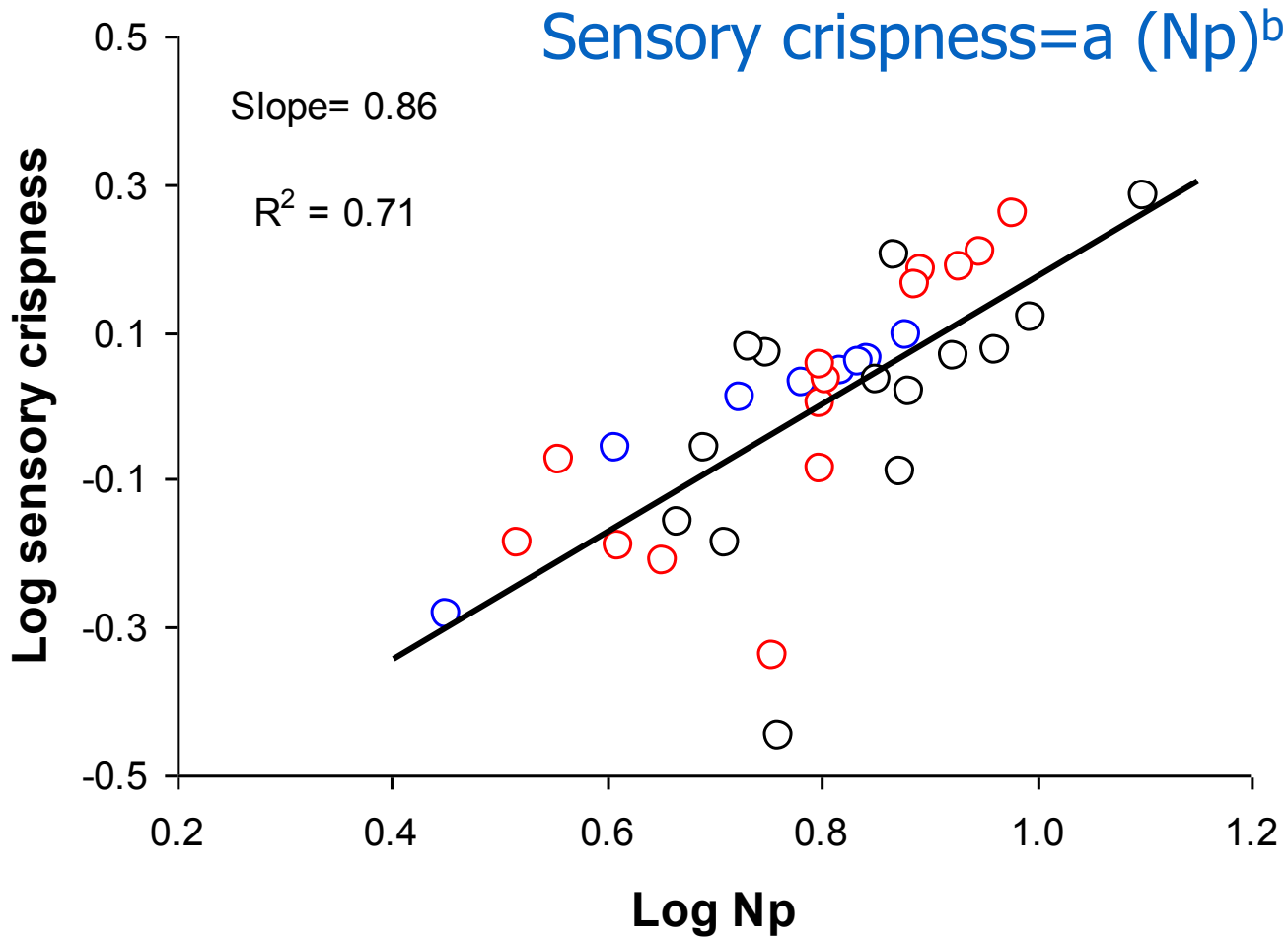

Microwave Expansion of Cereal Matrices

PURDUE
UNIVERSITY

Why microwave expansion?

- Third generation snacks can be obtained from extruded glassy, unexpanded half-products, which are further expanded by frying, baking or microwave heating

- Cereal flours are used as raw materials for the expanded snacks due to their unique functional properties

PURDUE UNIVERSITY

Microwave energy determines the expansion of glassy cereal pellets

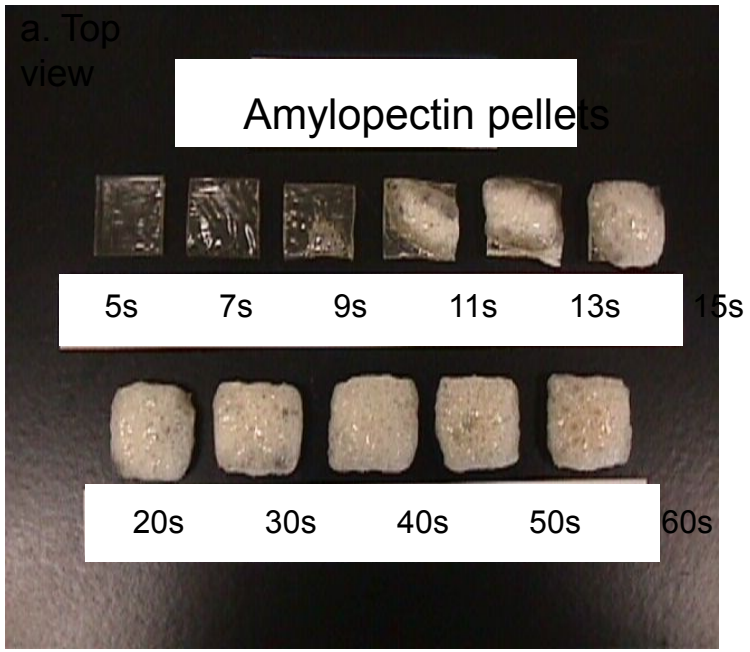

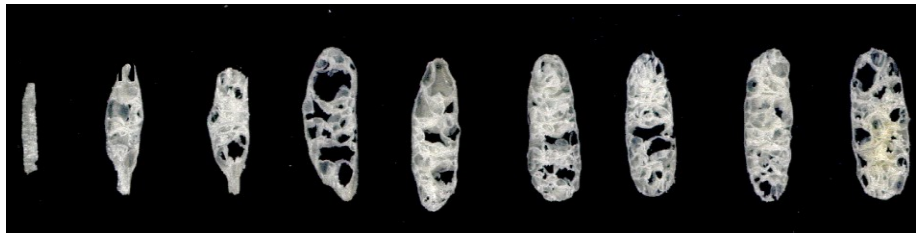

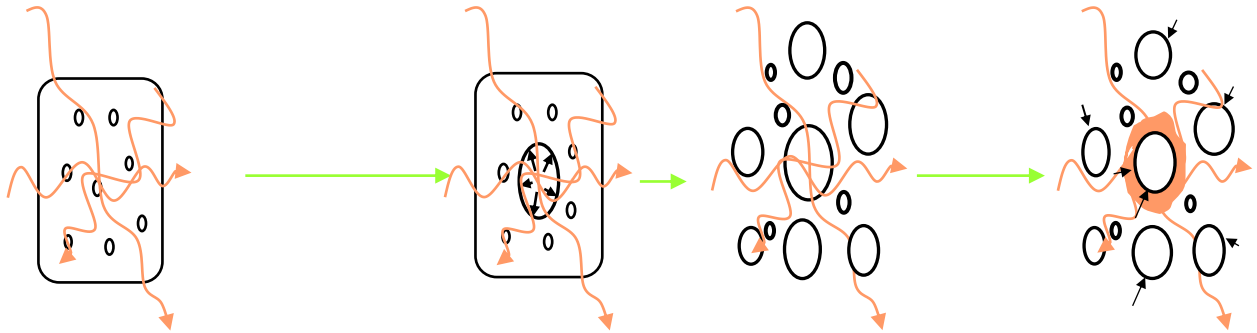

1. Water vaporizes, creating locally a high pressure; bubbles form at nuclei.

2. The glassy matrix undergoes a phase transition to a rubbery matrix where the bubbles grow; if the matrix is too soft, collapse occurs.

3. Under further heating, with moisture loss samples begin to burn.

PURDUE UNIVERSITY

Water is the driving force in microwave expansion of cereal pellets

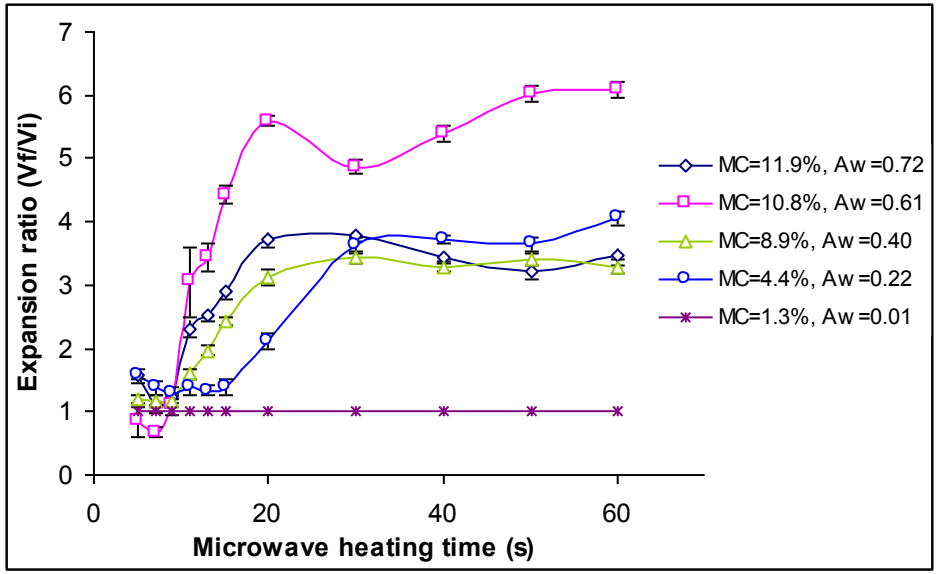

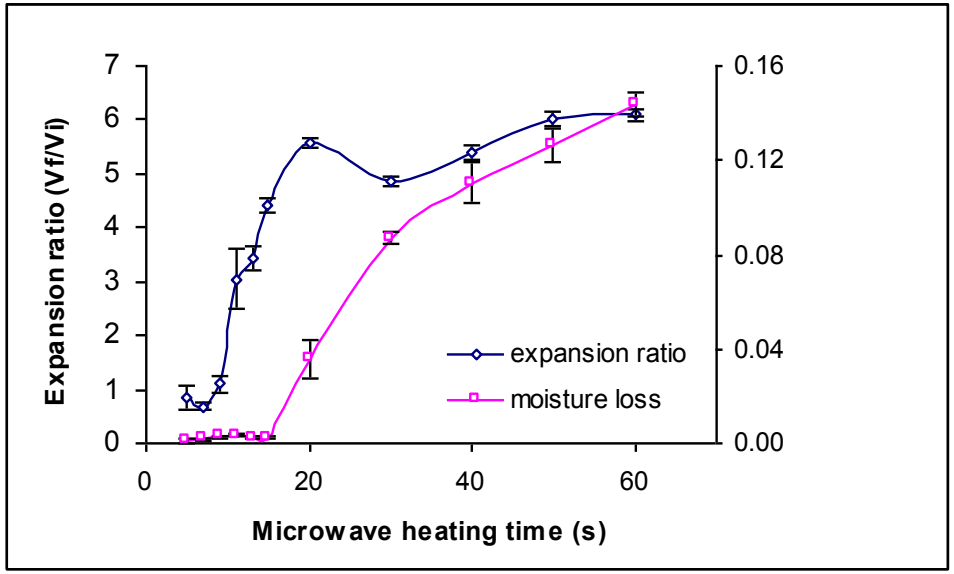

- no water → no expansion
- expansion increases with <u>increasing</u> the moisture content of the extruded pellets

- only a small amount of moisture can expand significantly the matrix (according to the gas law)

PURDUE UNIVERSITY

Path of microwave expansion on a state diagram

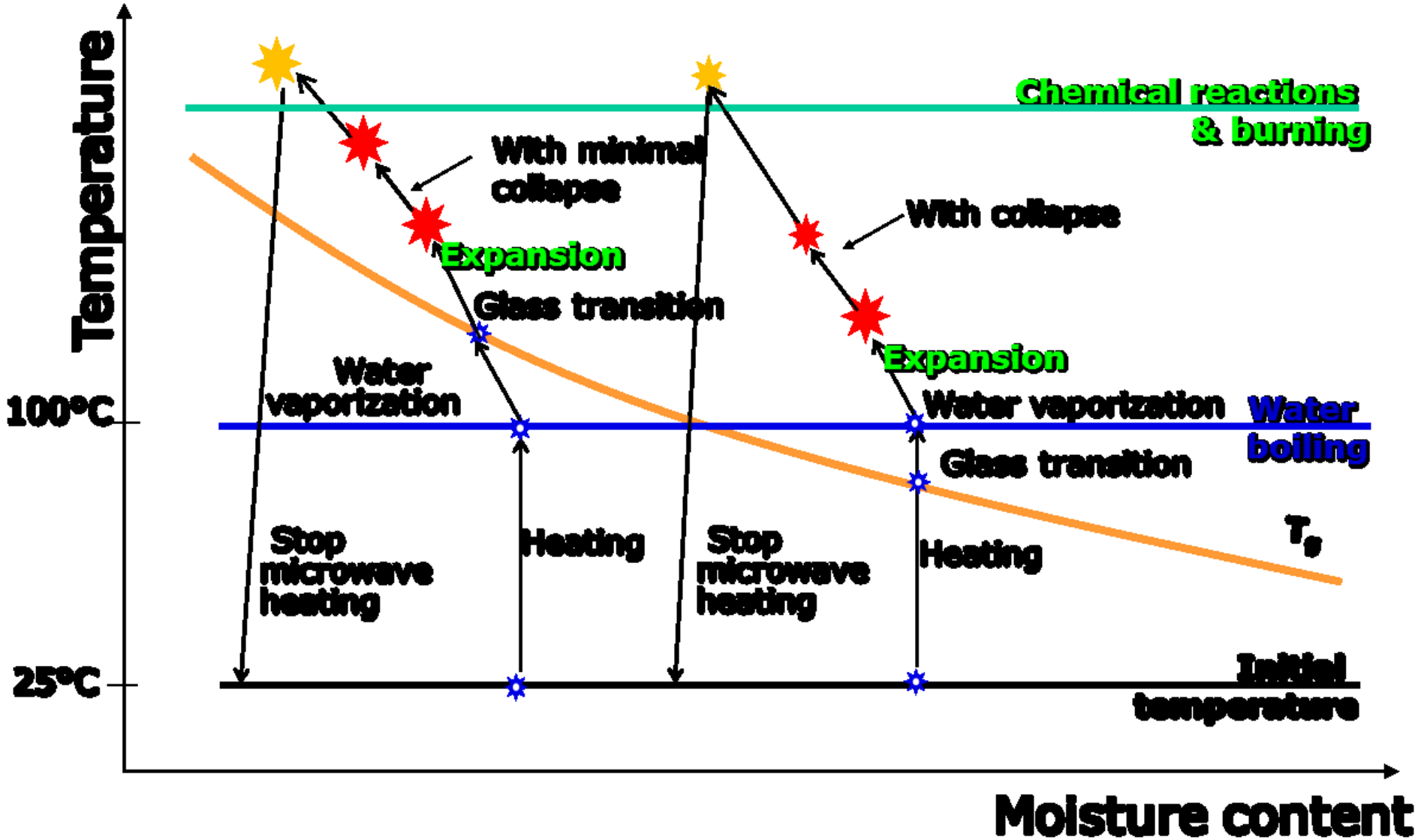

Effect of gums on the microstructure

- 1% Xanthan gum and 1% high viscosity CMC lead to a homogeneous microstructure and thinner cell walls than the reference (corn flour)

- Xanthan gum leads to smaller cells than the high viscosity CMC

Corn flour

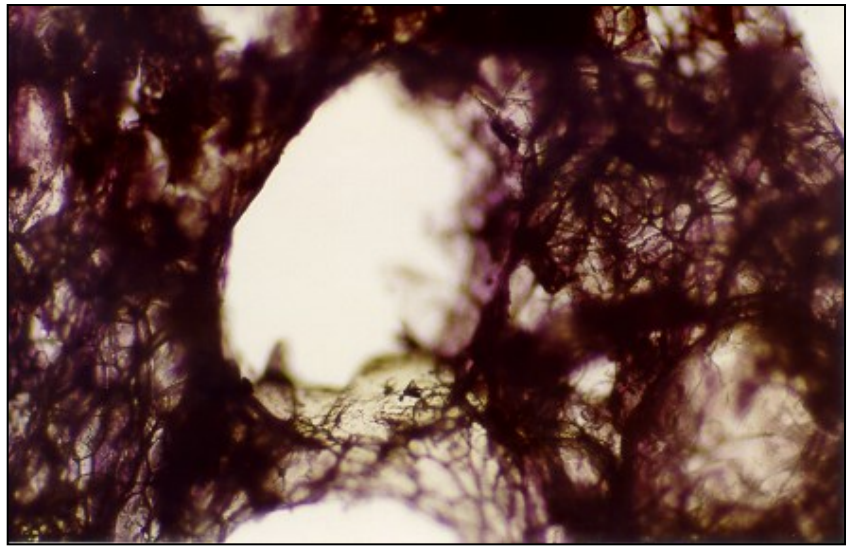

1% Xanthan gum

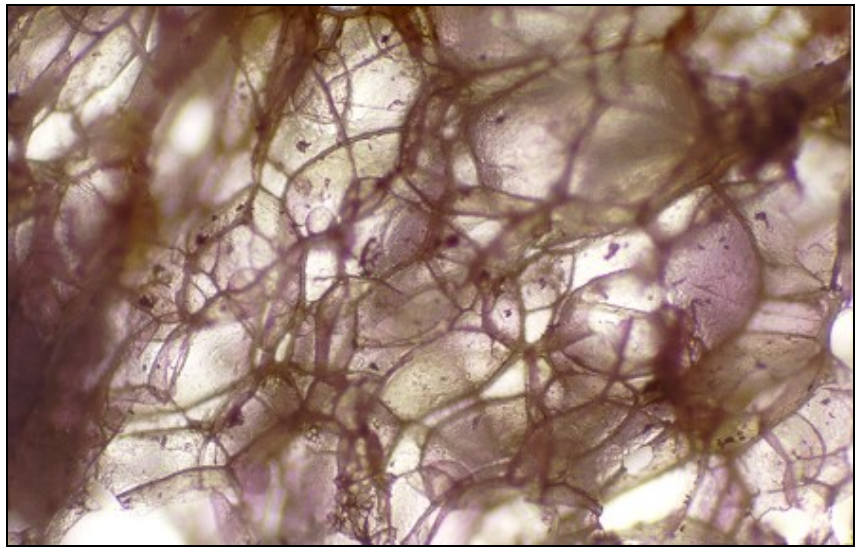

1%9H4F CMC

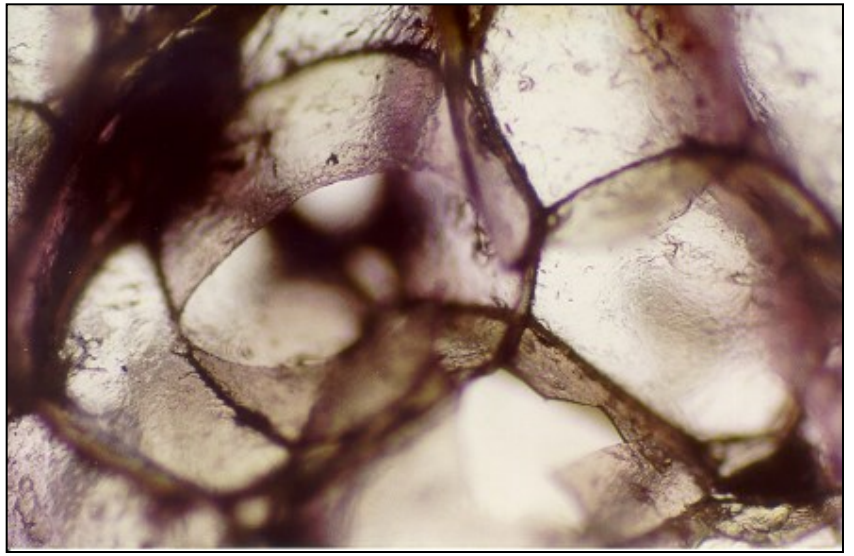

Conclusions on microwave expansion

- The microwave expansion of glassy cereal pellets is controlled by the moisture content and the phase transitions of the cereal matrix
- Increased moisture content leads to increased expansion, but also to a coarse structure, due to cell coalescence and rupture
- The addition of solid fat to the cereal matrix is able to improve significantly the expansion, structure and texture of the expanded products, while liquid fat has a negative influence on expansion
- 1% Xanthan gum or CMC can control the shape and microstructure of microwave expanded products

PURDUE UNIVERSITY

Restructuring for Food and Non-food uses using nanotechnology

Nanoparticulation of starch using desolvation

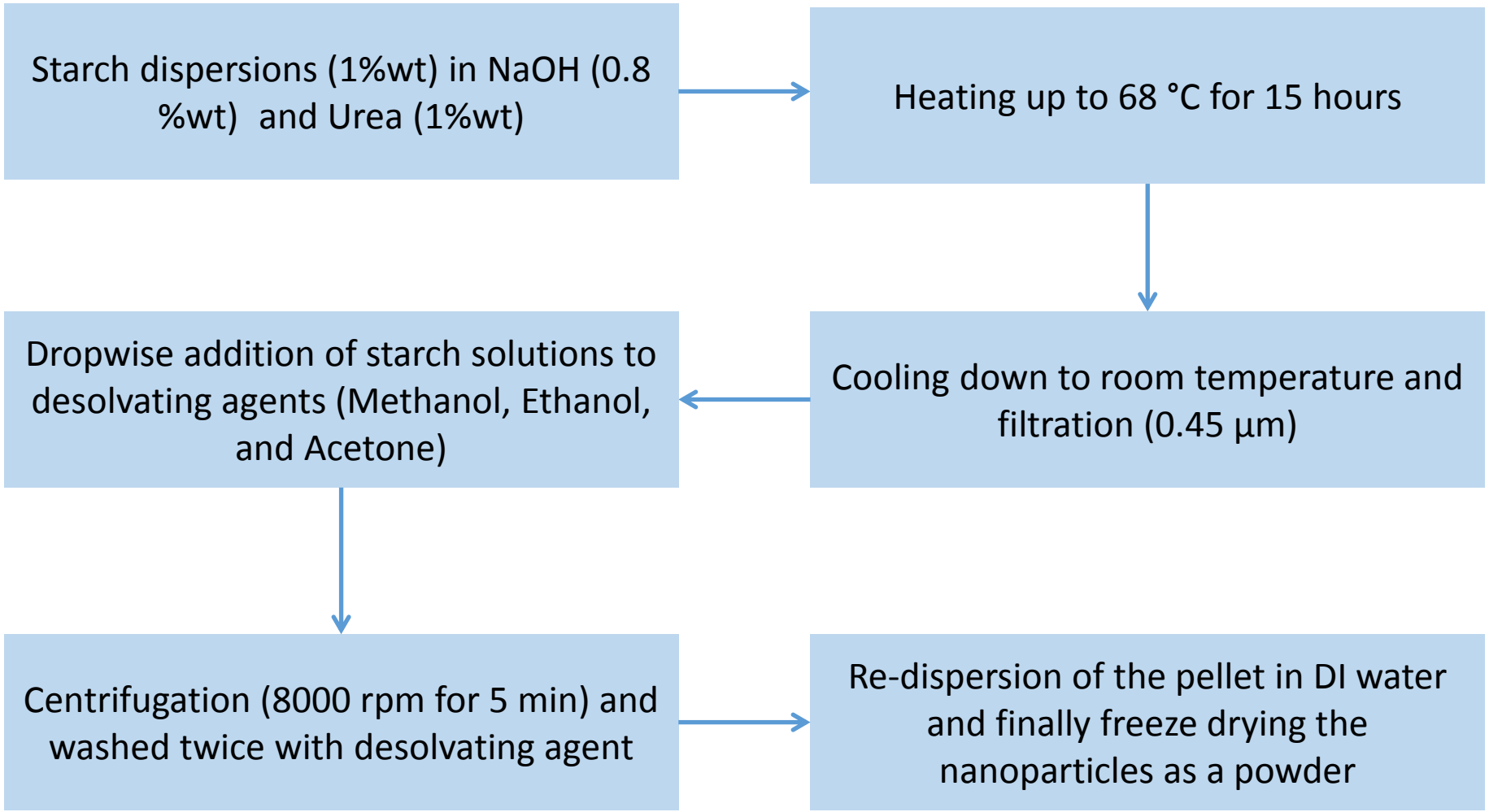

PURDUE UNIVERSITY

Particle size and zeta potential of starch NPs

Native NPs with Ethanol

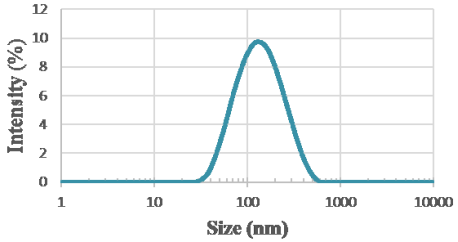

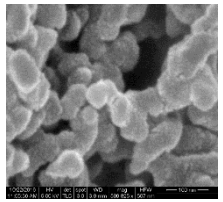

Native NPs with Methanol

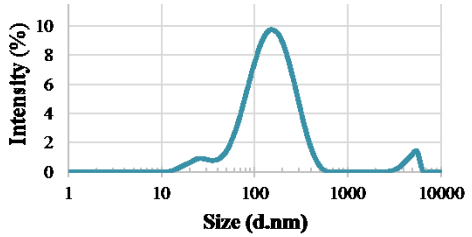

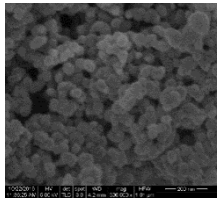

Native NPs with Acetone

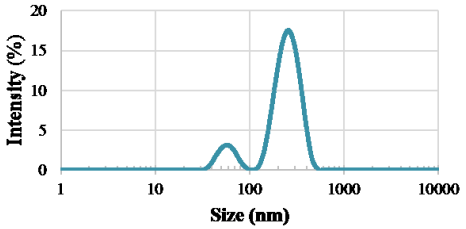

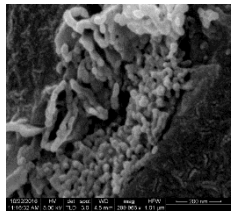

Amioca NPs with Ethanol

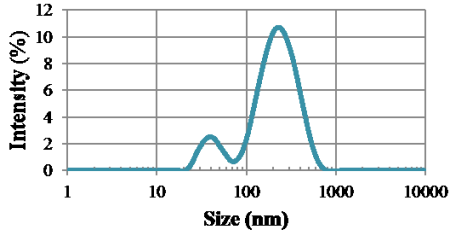

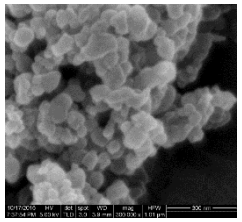

Hylon V NPs with Ethanol

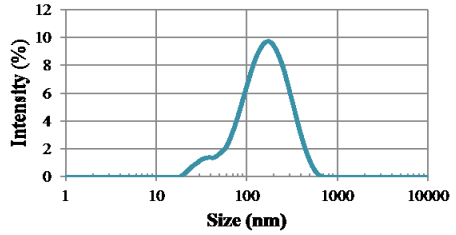

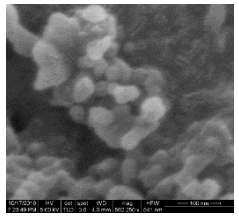

Corn starch type	Desolvating agent	Size (nm)	Polydispersity index	Zeta potential (mV)
Native	Ethanol	**112.8±2.0**	**0.278±0.007**	**-14.7±5.5**
	Methanol	**118.6±5.2**	**0.336±0.056**	**-6.2±3.0**
	Acetone	**319.4±51**	**0.382±0.022**	**-32.8±4.8**
Amioca	Ethanol	**174.0±40**	**0.491±0.048**	**-11.1±4.0**
	Methanol	**145.9±3.0**	**0.400±0.041**	**-10.4±2.2**
	Acetone	**253.3±68**	**0.396±0.090**	**-18.3±5.6**
Hylon V	Ethanol	**119.9±1.8**	**0.346±0.039**	**-11.6±4.1**
	Methanol	**181.2±18**	**0.440±0.055**	**-15.0±2.9**
	Acetone	**295.8±47**	**0.558±0.083**	**-25.0±5.3**
Hylon VII	Ethanol	**189.4±5.6**	**0.334±0.031**	**-14.0±1.0**
	Methanol	**500.7±160**	**0.678±0.145**	**-12.7±3.3**
	Acetone	**294.5±36**	**0.371±0.068**	**-36.1±7.0**

Hylon VII NPs with Ethanol

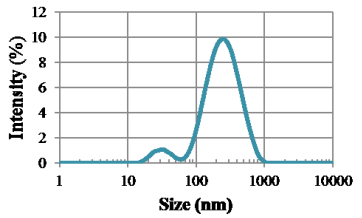

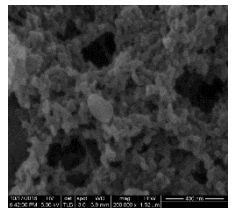

Alginate/BSA nanotubes

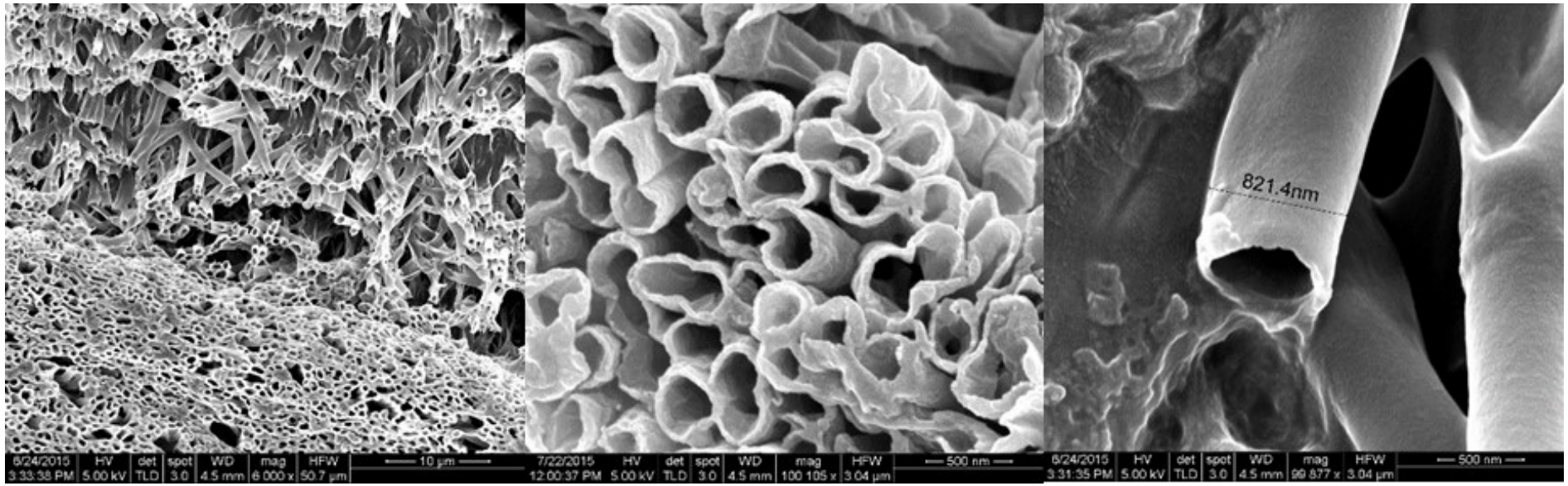

Layer-by-layer fabrication of GRAS nanotubes include alginate and BSA on polycarbonate template. SEM images of alginate/BSA nanotubes with diameter of 800 nm (left and right), and 400 nm (center) (Maldonado et al., 2017)

Using Quantum dots as imaging tools for cereal proteins in bread

- Quantum dots nano-crystals were used to understand the molecular organization of food proteins in flat bread in order to assess their impact on morphological and structure characteristics.
- The protocols in sample preparation and labeling process were developed

(Courtesy of N. Sozer)

The peaks' whiteness height is due to quantum dot fluorescence intensity

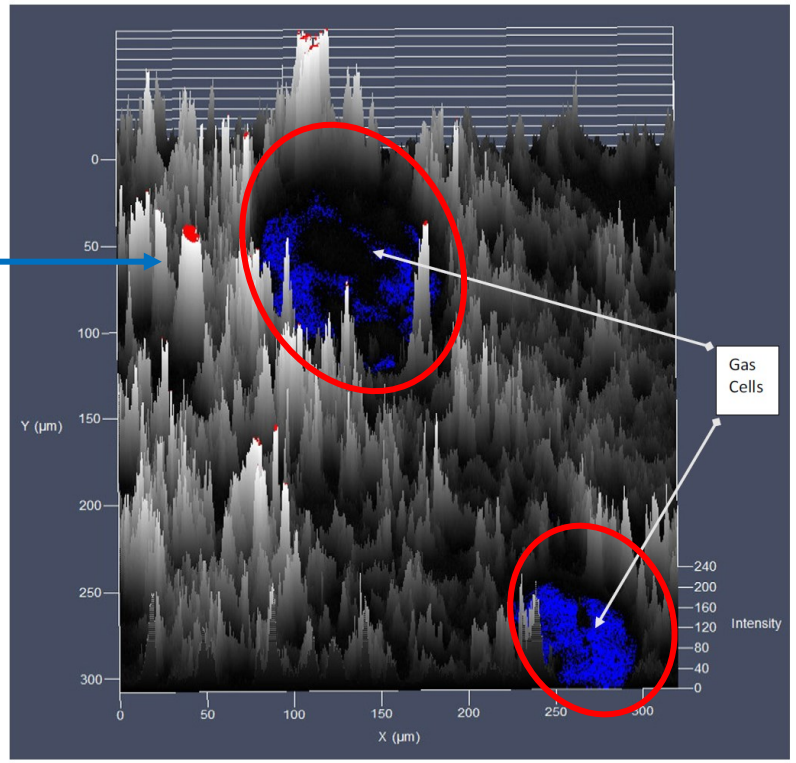

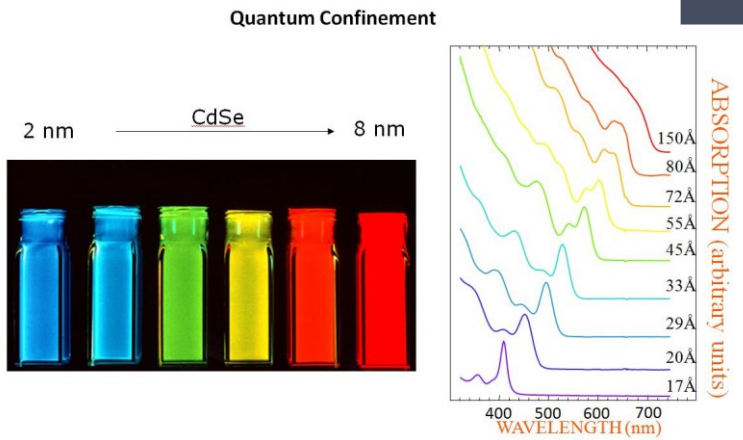

Distribution of gliadin in dough using QDs and CLSM in reflection, transmission, and the overlay of transmission and reflection.

Microstructure of dough sections at i) arrival time, ii) peak time, iii) departure time, and iv) 10min after departure time. A (left), protein molecules bound to quantum dots.

the red zones are anti-gliadin bound to quantum dots representing gliadin and the black zones are non-gliadin zones;

B (middle), starch granules under polarized light; the bright shapes represent starch and the gray zones represent largely the protein

C (right), overlay of A and B showing the distribution of gliadin in the dough matrix in red and around starch. (Bozkurt et al., 2014).

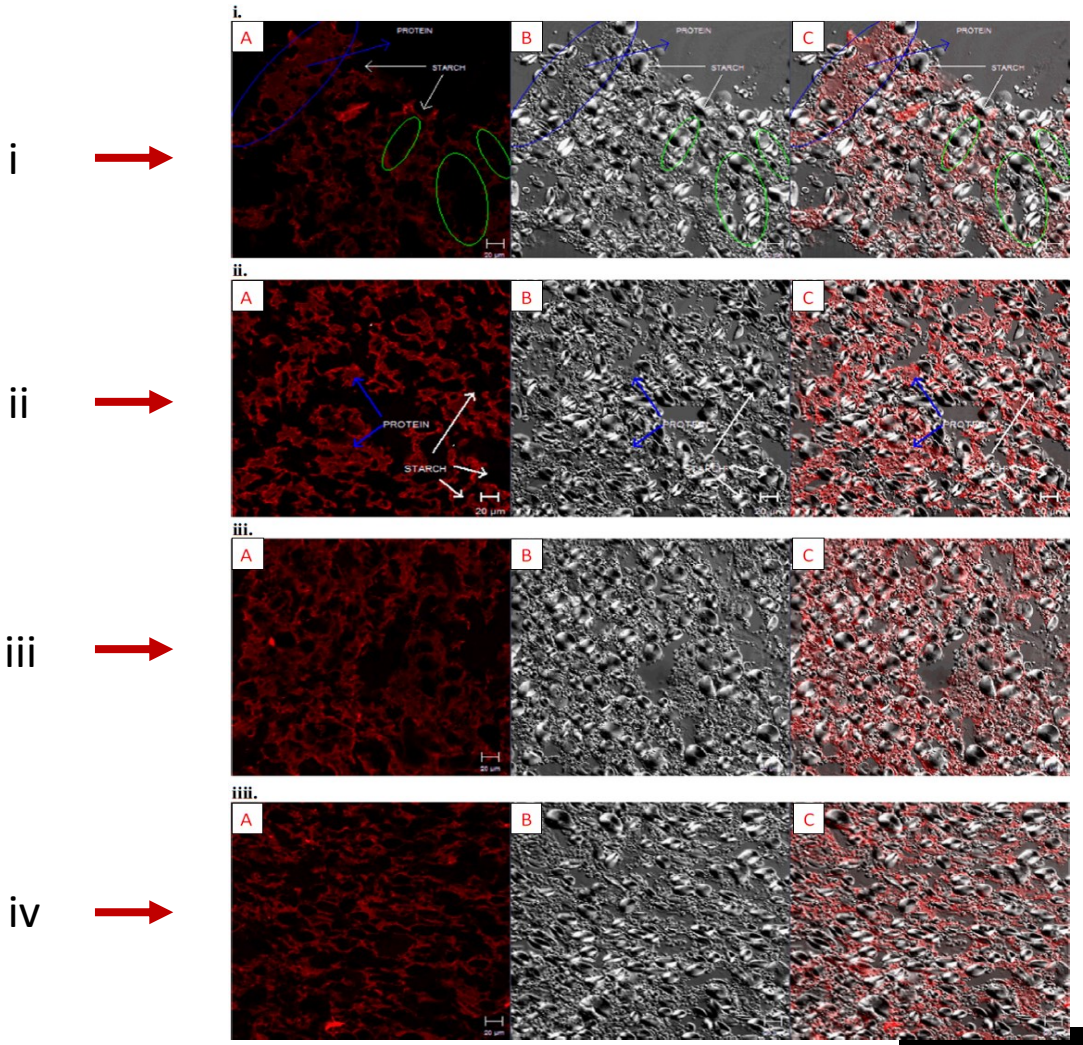

Application of nanotechnology in fabrication of zein based *biosensors*

- **<u>Fabrication of zein nanophotonic platform</u>**
  - Surface-enhanced Raman spectroscopy (**SERS**) is a technique for molecular detection and characterization that relies on the enhanced Raman scattering of molecules that are adsorbed on, or near, **SERS**-active surfaces, such as nanostructured gold or silver.
  - Combination of Raman spectroscopy and signal enhancement by nanophotonic structures can help us to fabricate more reliable nanobiosensors.

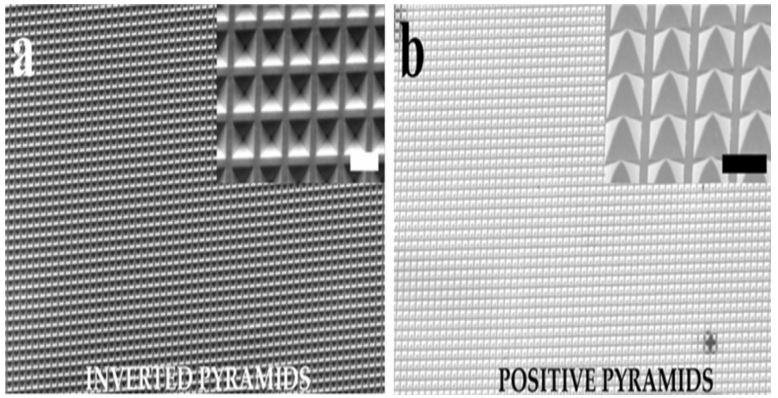

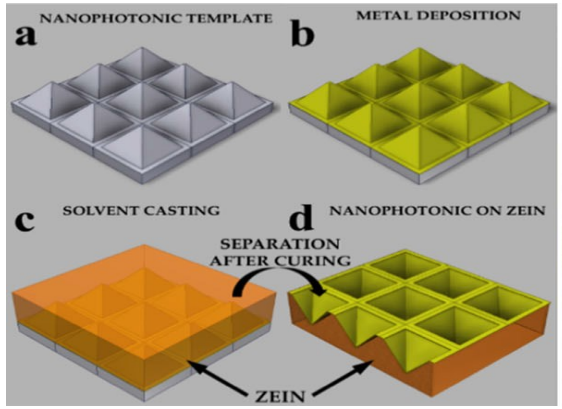

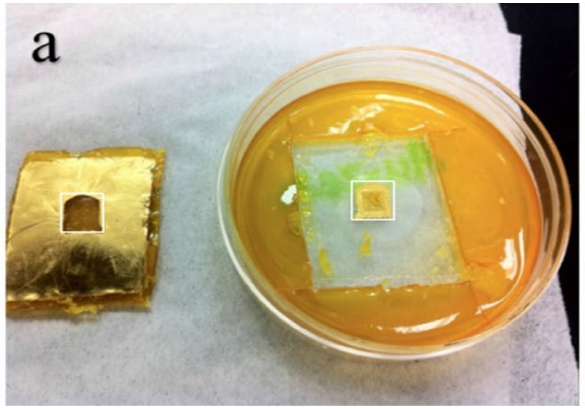

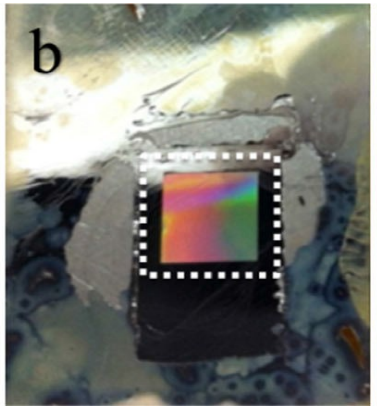

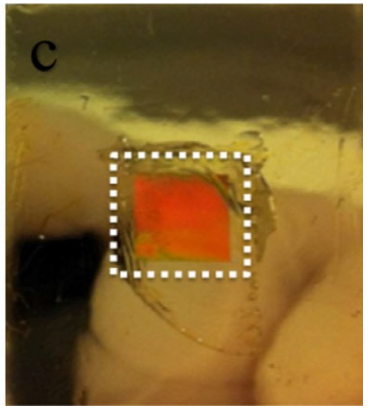

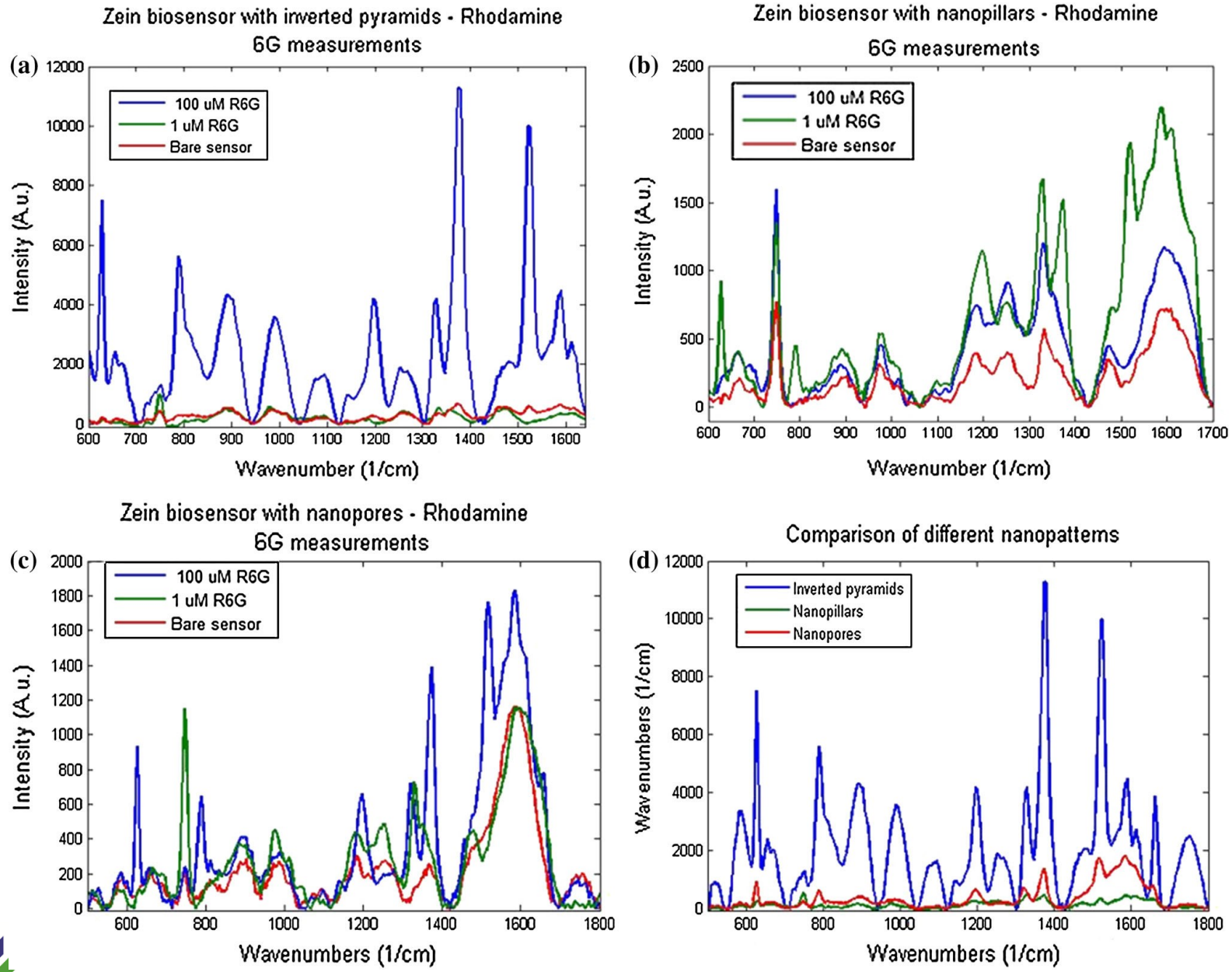

Different concentrations of Rhodamine 6G on a) 200 nm gold-coated inverted pyramid sensor on zein, b) 80 nm gold-coated nanopore sensor on zein, and c) 80 nm gold-coated nanopillar sensor on zein and d) the comparison of 100 µM concentration of these sensors (Gezer et al. 2016a).

PURDUE UNIVERSITY

- Fabrication of biodegradable platform coated with gold nanopattern along with SERS can be developed to detect the Ara h1 protein. Principal component analysis is employed for both detection and quantification purposes. The first step to prepare zein gold coated platforms for this application is functionalization of the surface of the platform with the monoclonal antibodies of Ara h1, 2F7.

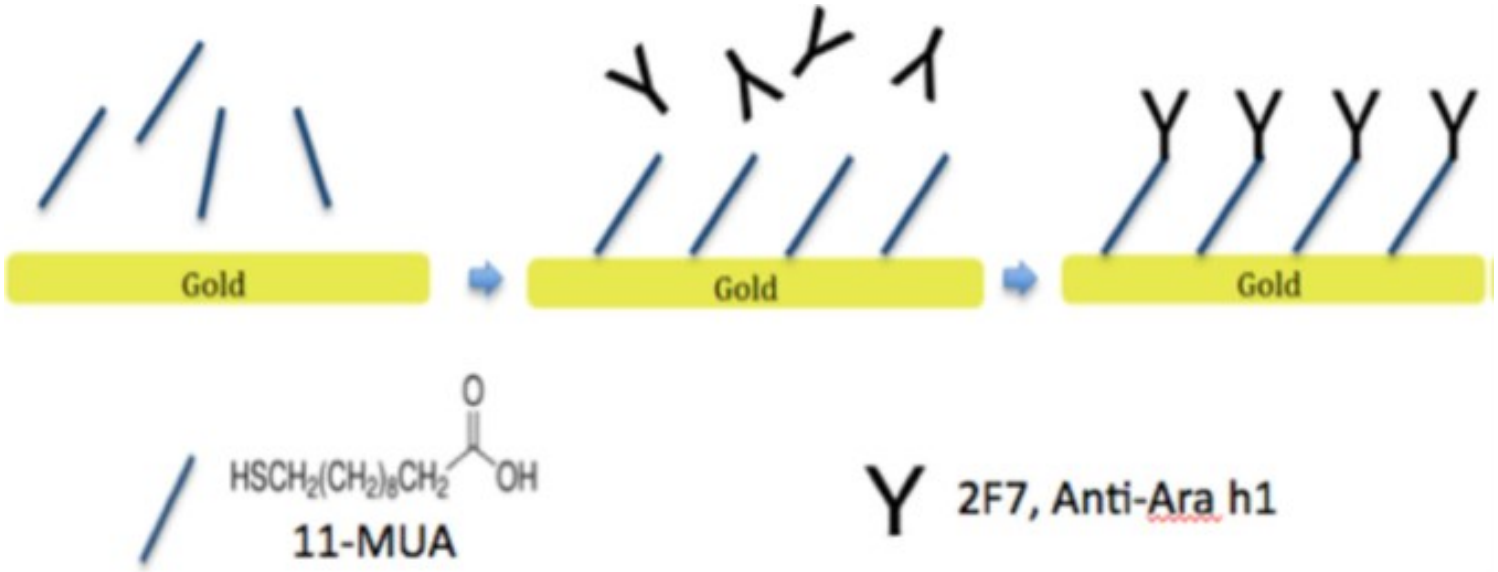

Schematic illustration of the functionalization of the gold surface (Gezer, Liu, Kokini, 2016).

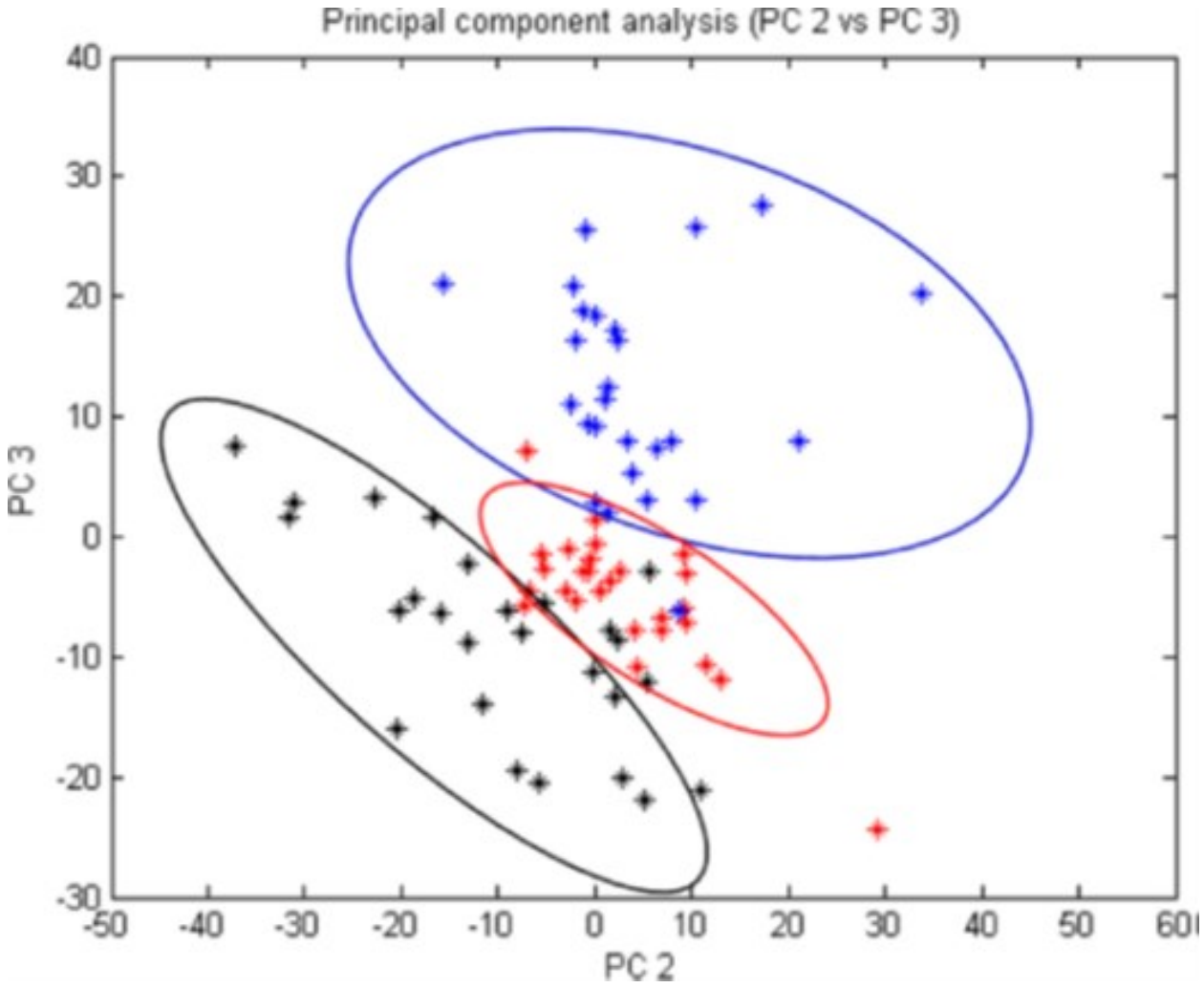

Principal component analysis (PC2 vs PC3) of baseline-corrected Raman spectra for background zein-SERS sensor (black), antibody-functionalized zein-SERS sensor (blue) and Ara h1 protein captured by antibody-functionalized zein-SERS sensor (red) (Gizer, Liu, Kokini, 2016).

PURDUE UNIVERSITY

Zein-based acrylamide biosensor

- Gold-coated zein-SERS platform is utilized to detect acrylamide.

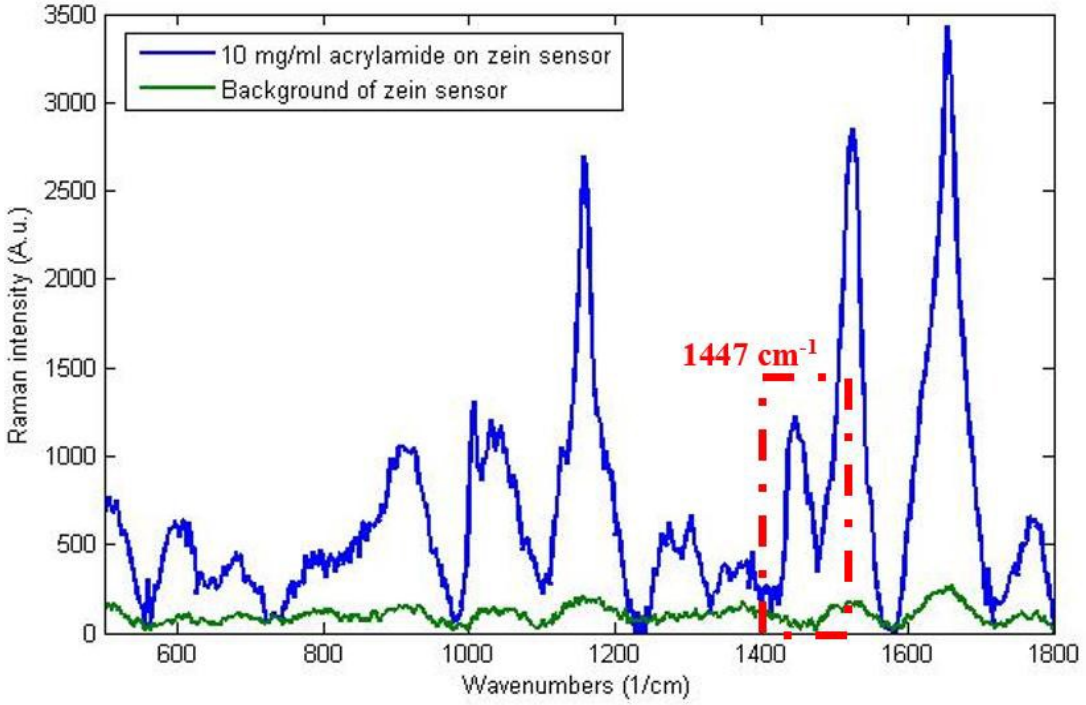

Comparison of the background signature of zein-SERS sensor (green) with acrylamide on top of the sensor (blue). Red dotted square indicates the peak at the wavenumber of 1447 cm^{-1}, which does not exists in the background, but exists in acrylamide signature. (A.u.: arbitrary units) (Gizer et al., 2016c).

PURDUE UNIVERSITY

Thank you…

Zein-based SERS biosensor production

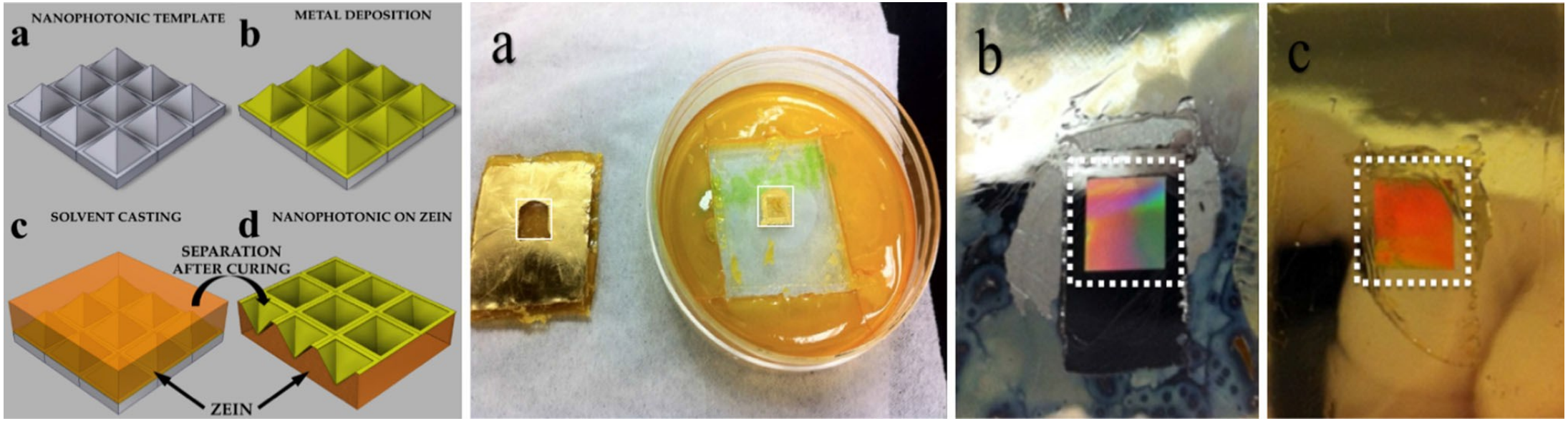

Left: Schematic diagram of the direct transfer of three dimensional metallic nanophotonic structures onto zein, a corn plant based biopolymer. A template made of either PET or with nanophotonic structures (a) is deposited with 200 nanometers of noble metal using E-Beam Evaporation (b). Zein solution is solvent-casted over the metal-coated template (c), and after fully solidifying; the zein film with three-dimensional metallic nanophotonic structures is separated from the template (d). Right: The transfer of noble metal onto zein film. Unsuccessful transfer evident by the squared area having the patterns (a) did not transfer onto zein film (on the right), successful transfer of silver (b) and gold (c) (Gezer et al., 2016a).

PURDUE UNIVERSITY

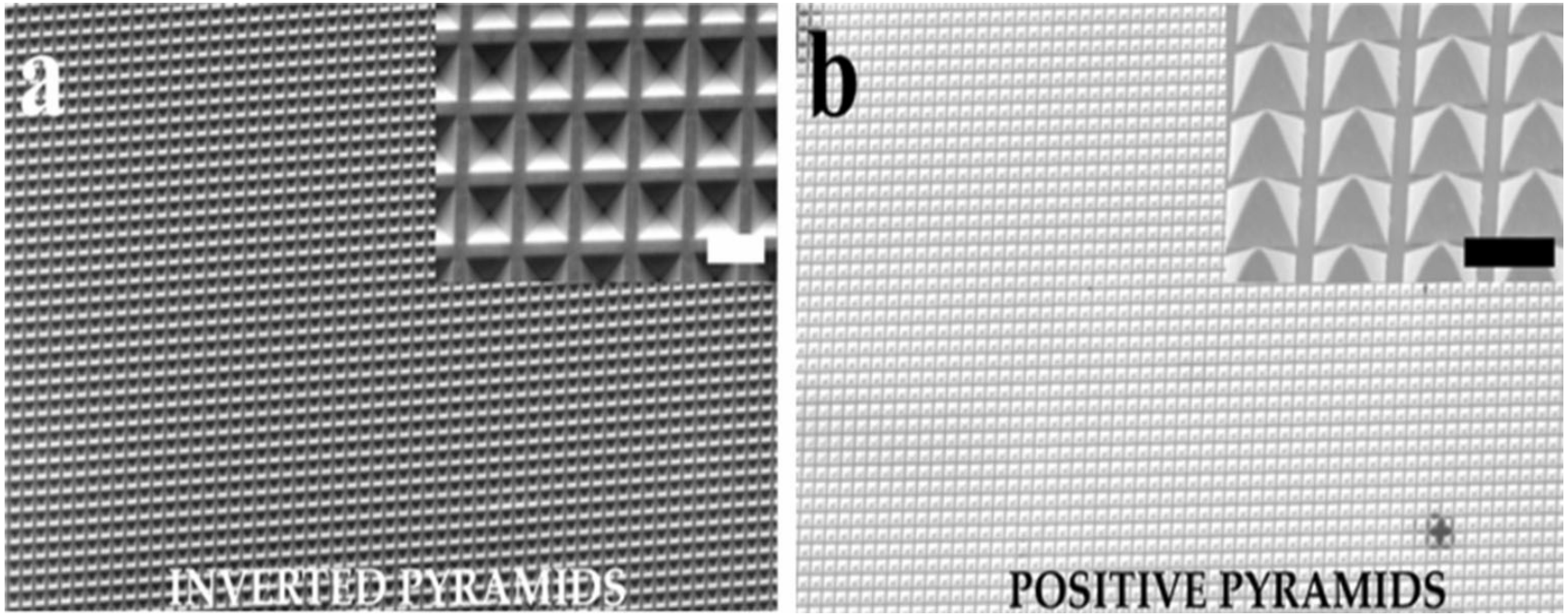

Scanning electron microscopy images of a) top-down view of the inverted pyramid nanophotonic structures and b) positive pyramid nanophotonic structures transferred onto zein (scale bars 2 μm) (Gezer et al. 2016a).

Factors that influence nucleation and extrudate expansion

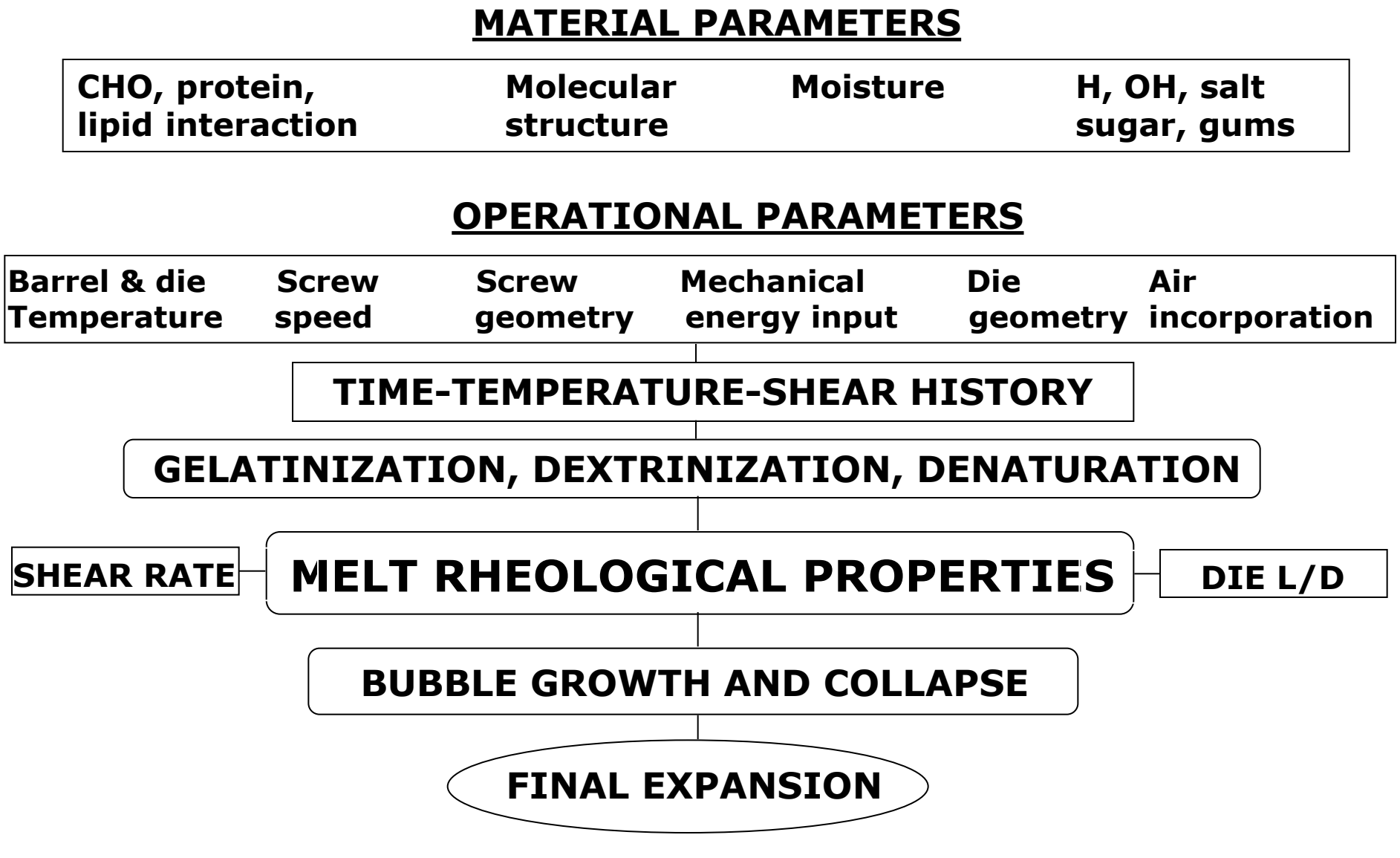

Air bubble nucleation

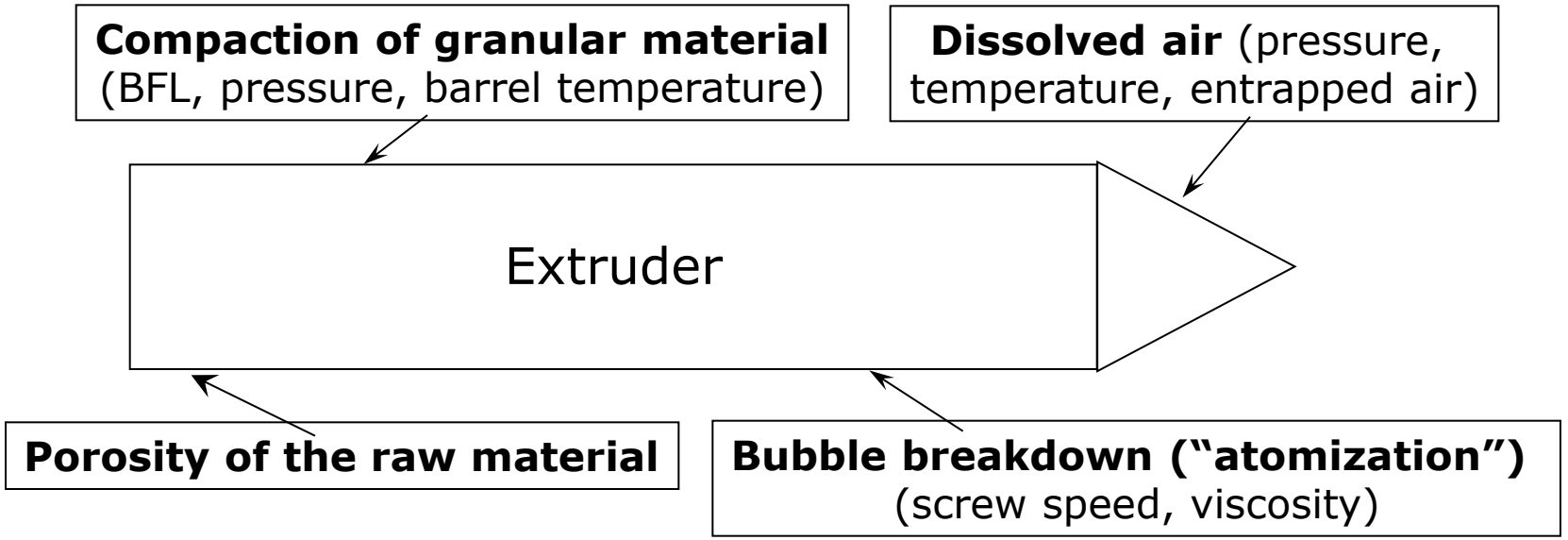

- **The total air volume entrapped (porosity)** is determined by the barrel fill length, the barrel temperature profile and their interaction

- **The factors that affect bubble size** are the original pore size distribution of the granular material and the bubble breakdown in the extruder barrel due to high shear conditions

PURDUE UNIVERSITY

Bubble size distribution
effect of screw configuration

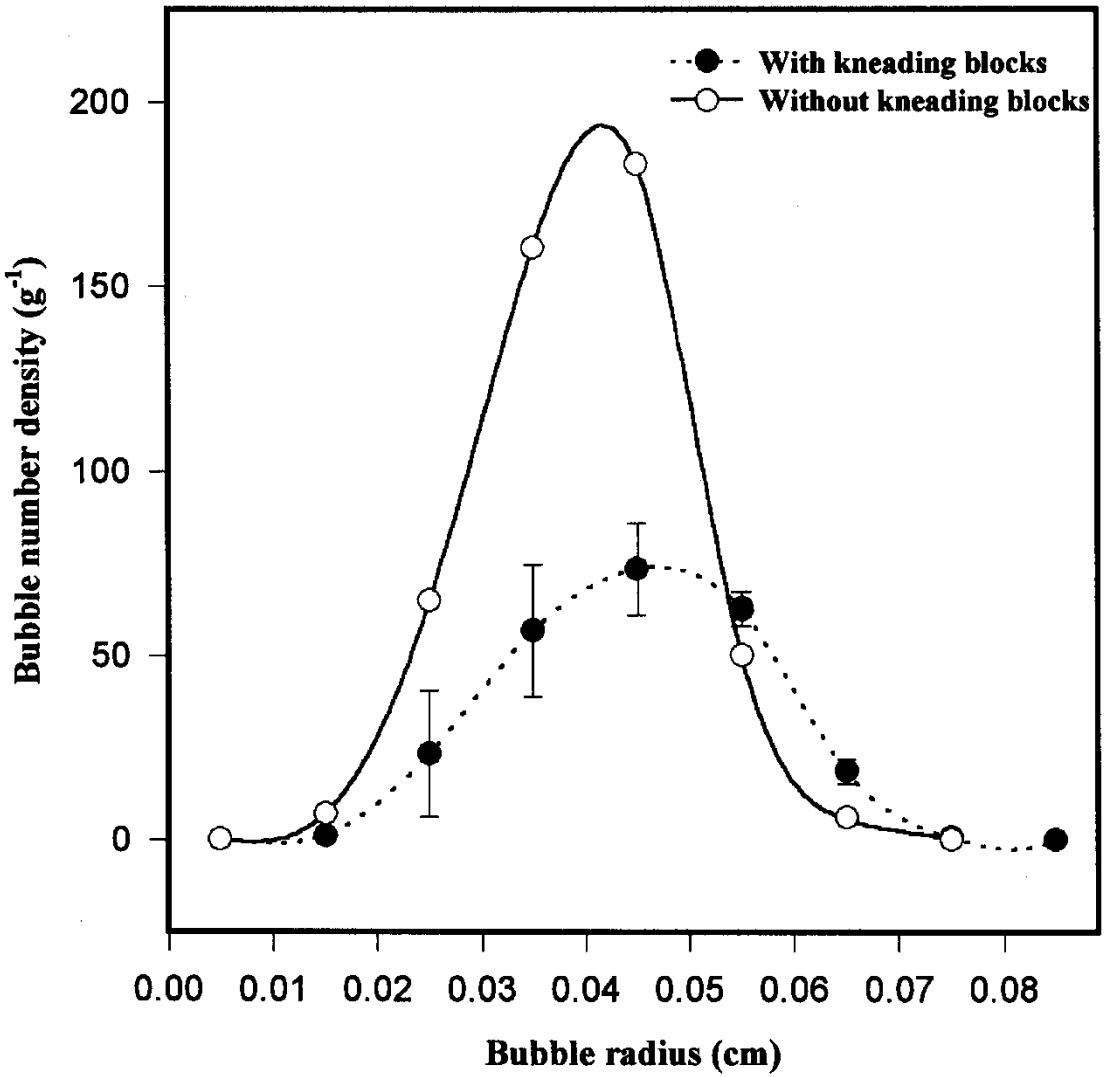

Native amylopectin, rpm=150, 3.3g/s, m.c.=32%

PURDUE UNIVERSITY

Bubble size distribution
effect of screw speed and mass flow rate

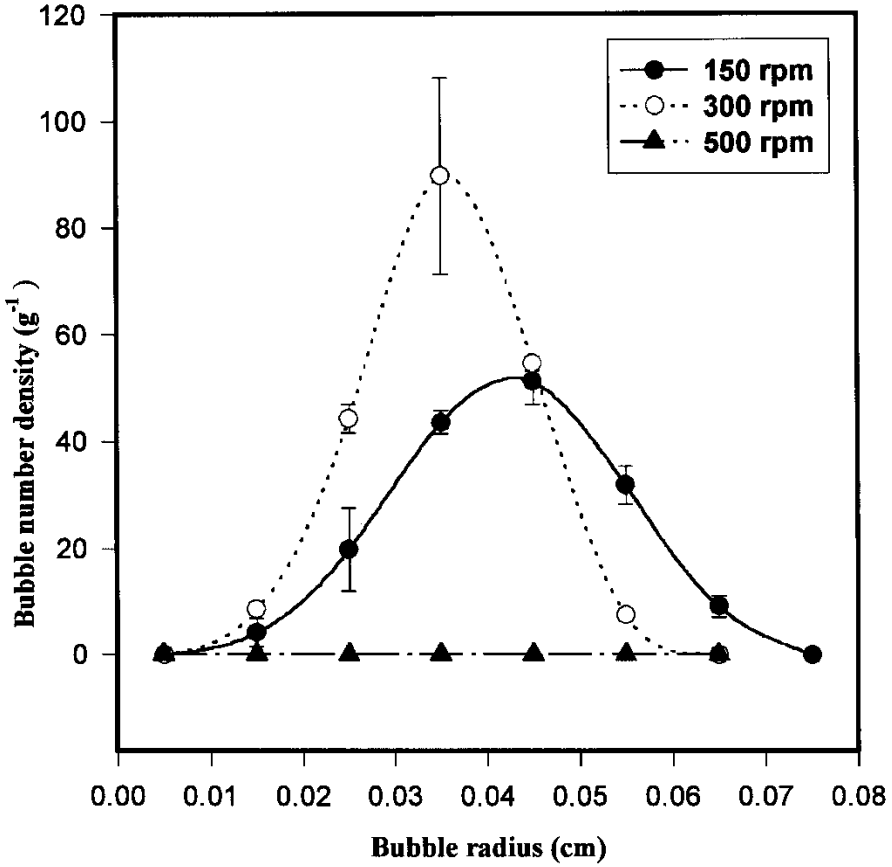

Native amylopectin, 1.67g/s, m.c.=32%,

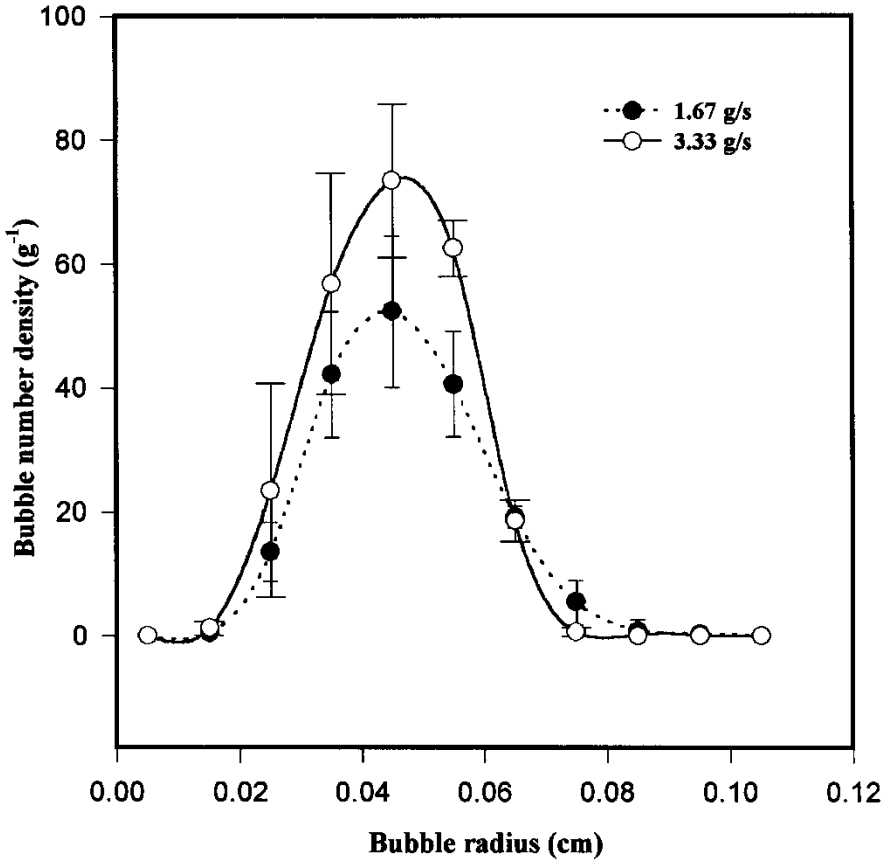

Native amylopectin, rpm=150, m.c.=35%

Bubble size distribution
effect of type of starch and moisture content

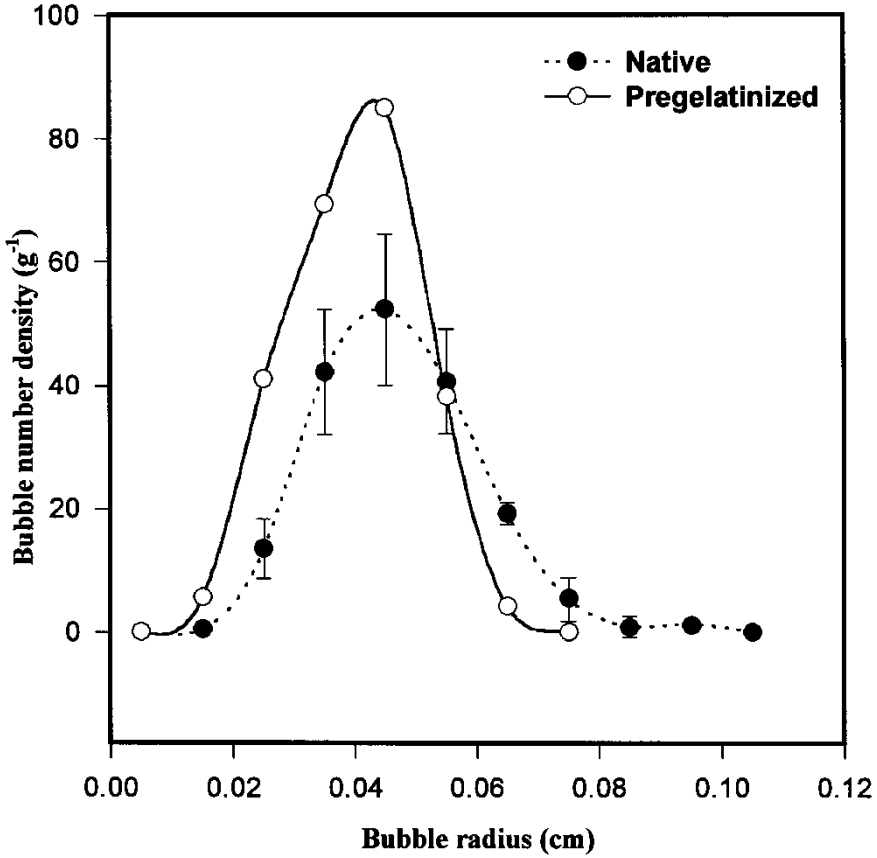

rpm=150, 1.67g/s, m.c.=35%

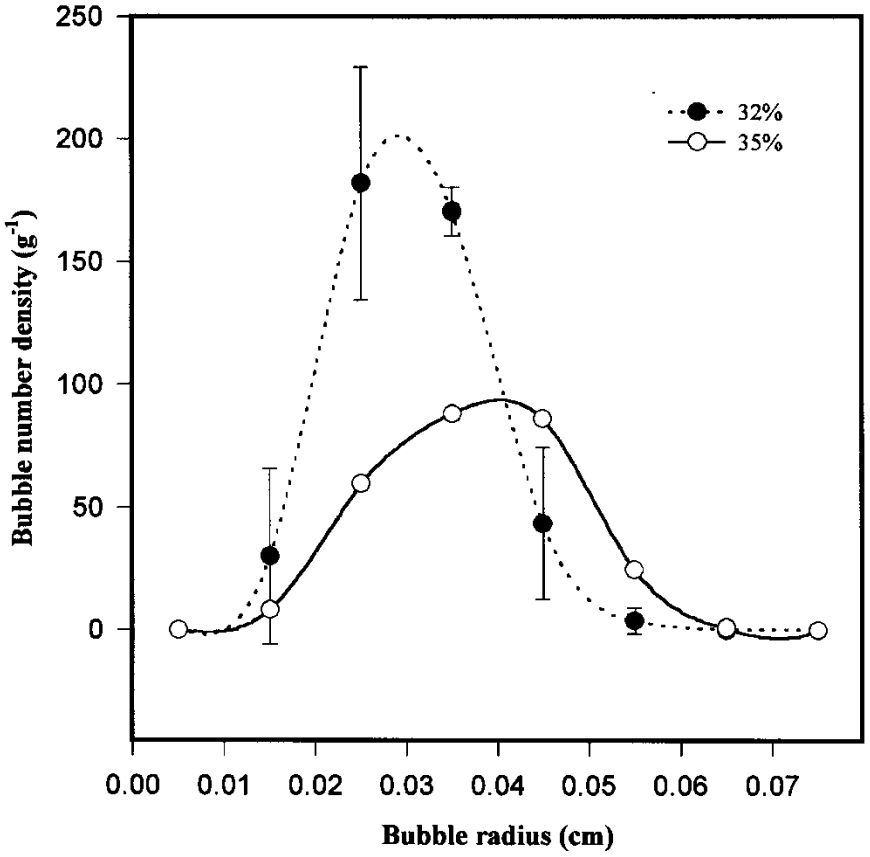

rpm=150, 1.67g/s

PURDUE UNIVERSITY

Relationship between porosity and bubble number density

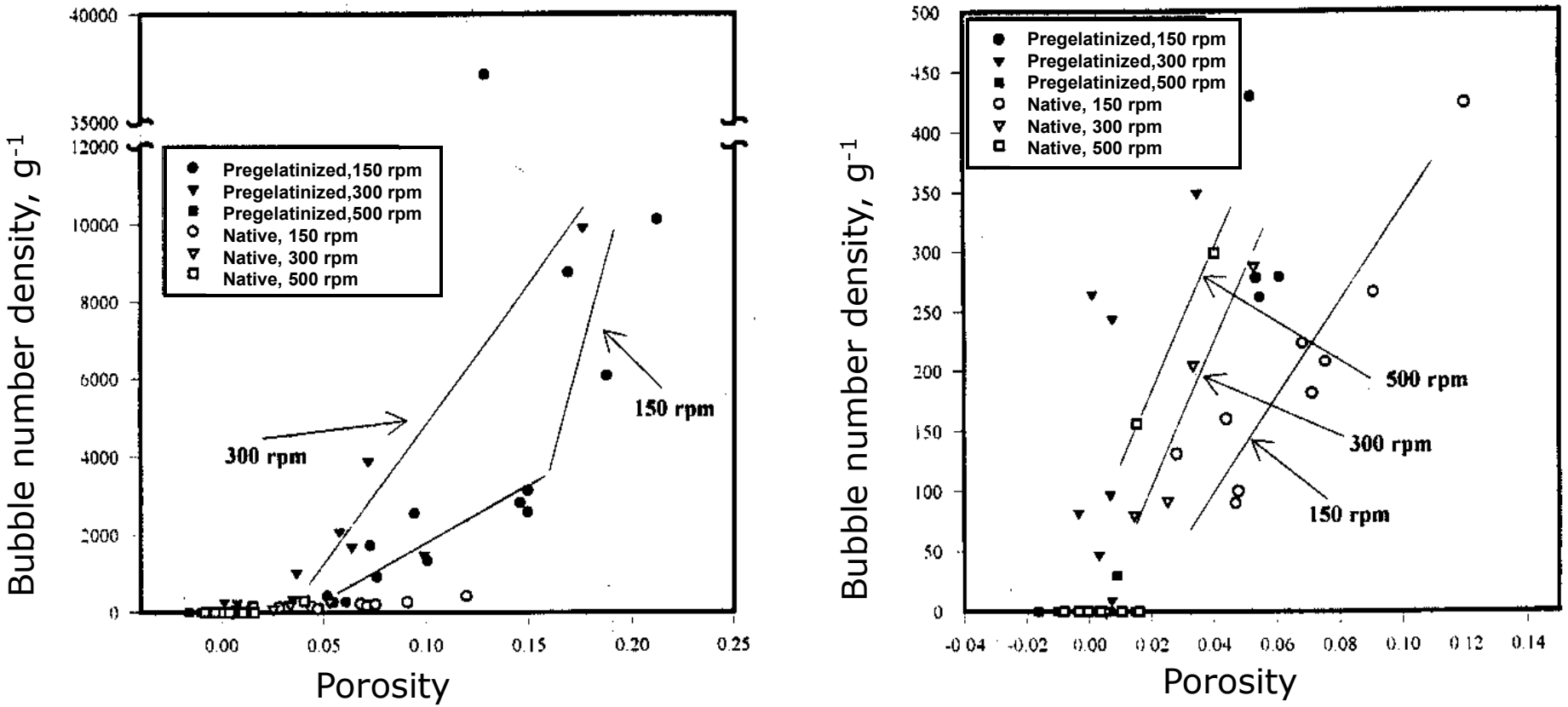

For the same porosity, pregelatinized amylopectin gives higher bubble number densities than the native amylopectin

- An increase in screw speed seems to increase bubble breakdown (atomization)

Breakup of entrapped air during extrusion

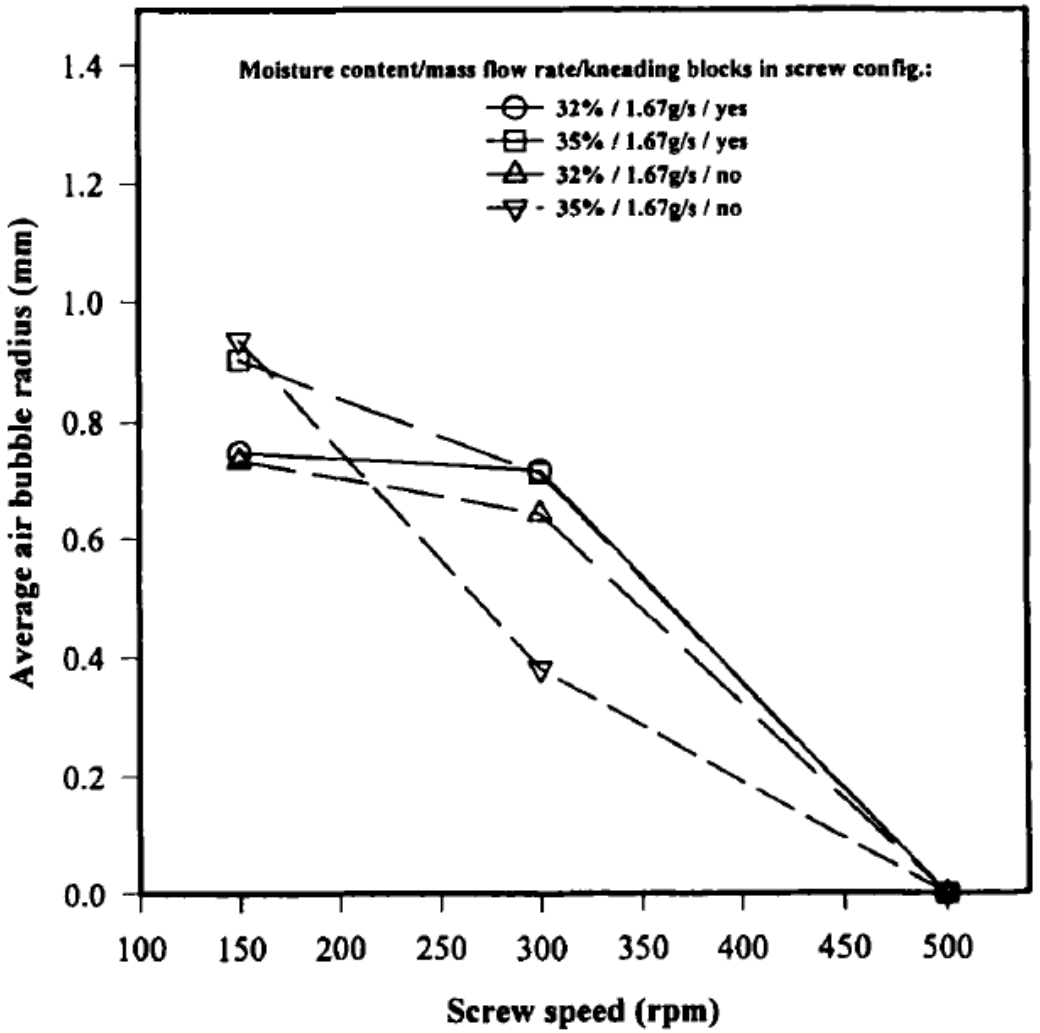

An increase in the shear field due to increase in screw speed caused breakup of entrapped air bubbles in the unexpanded extrudate

(Cisneros and Kokini, 2002)

PURDUE UNIVERSITY

Bubble growth rate and diametral expansion are influenced by extrusion parameters

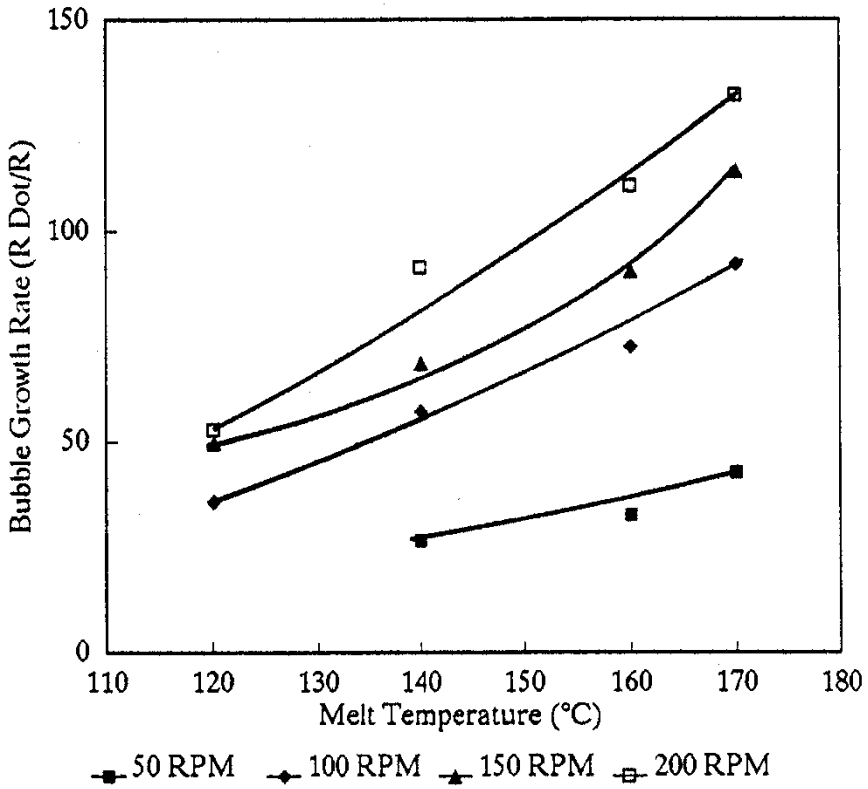

Corn meal extrudate, 16% moisture

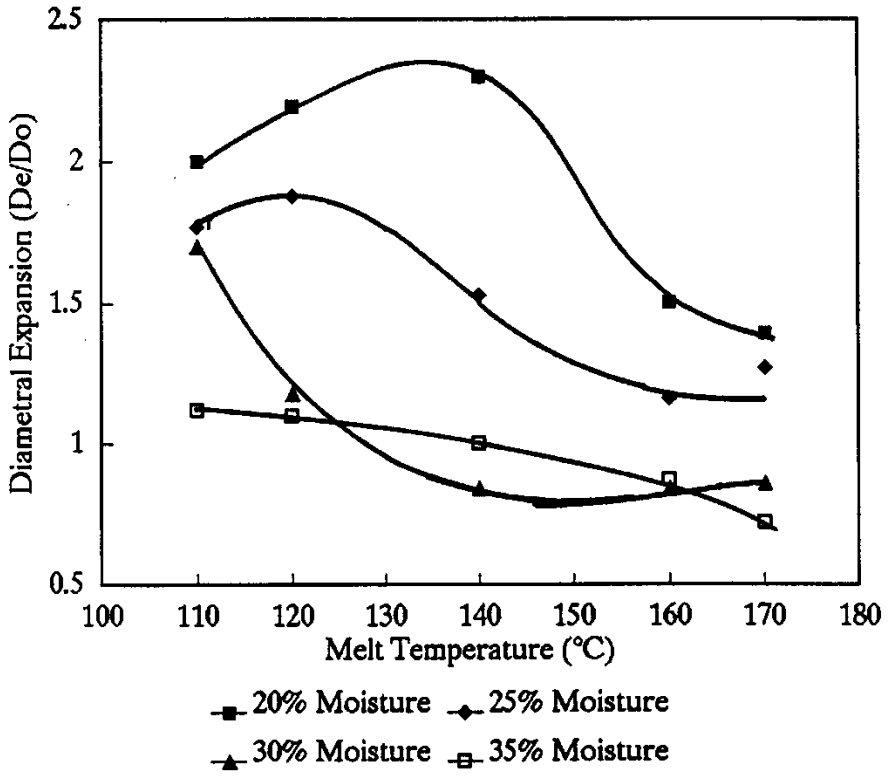

Amylopectin extrudate, 200 rpm

PURDUE UNIVERSITY

Influence of melt viscosity on extrudate expansion

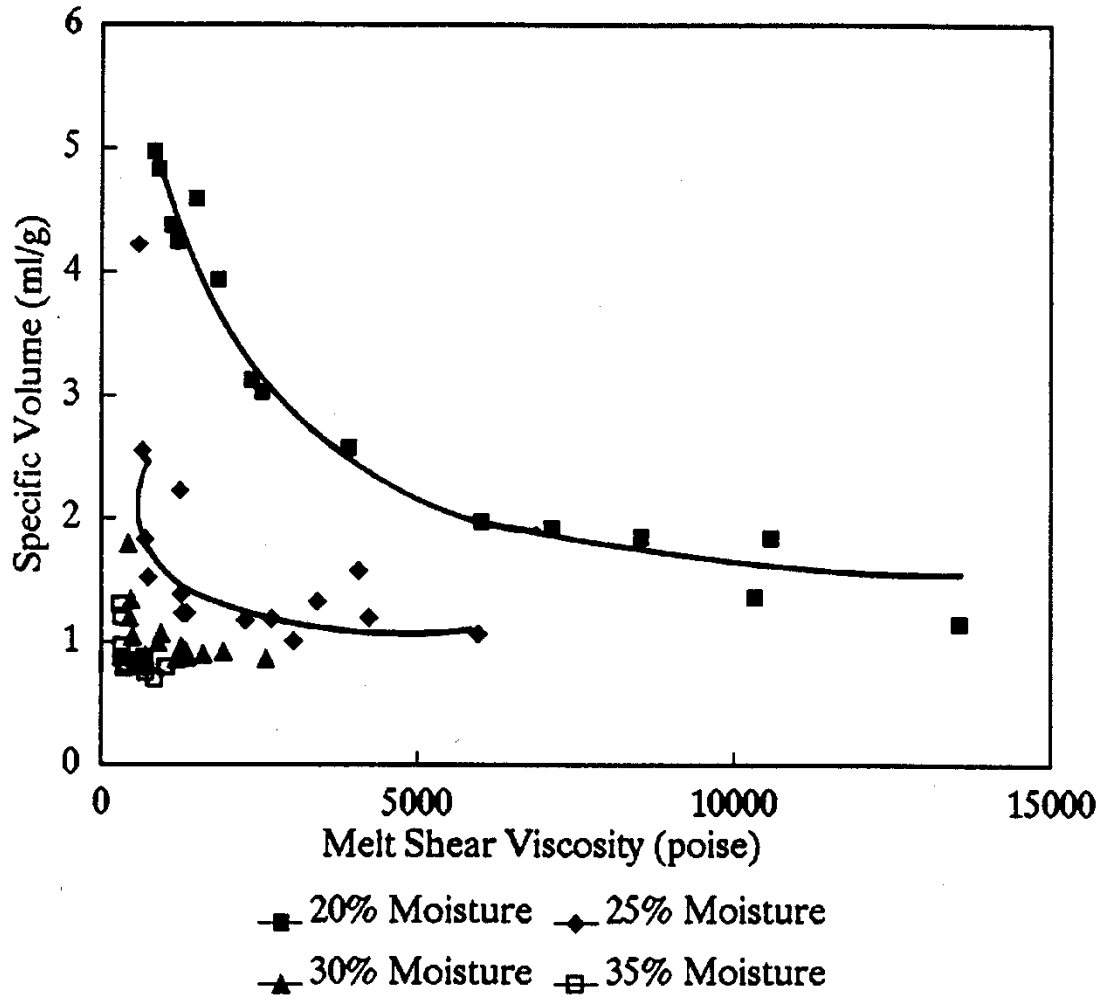

PURDUE UNIVERSITY

Influence of melt elasticity on extrudate expansion

According to Lai (1991):

$$N_1 = k_1 \dot{\gamma}^{k_2} e^{\frac{\Delta H}{RT}} e^{k_3 C}$$

N_1 - first normal stress difference

$\dot{\gamma}$ - shear rate

T - material temperature, K

C - material moisture content, %

k_1, k_2, k_3 - constants

Prediction vs. experimental:

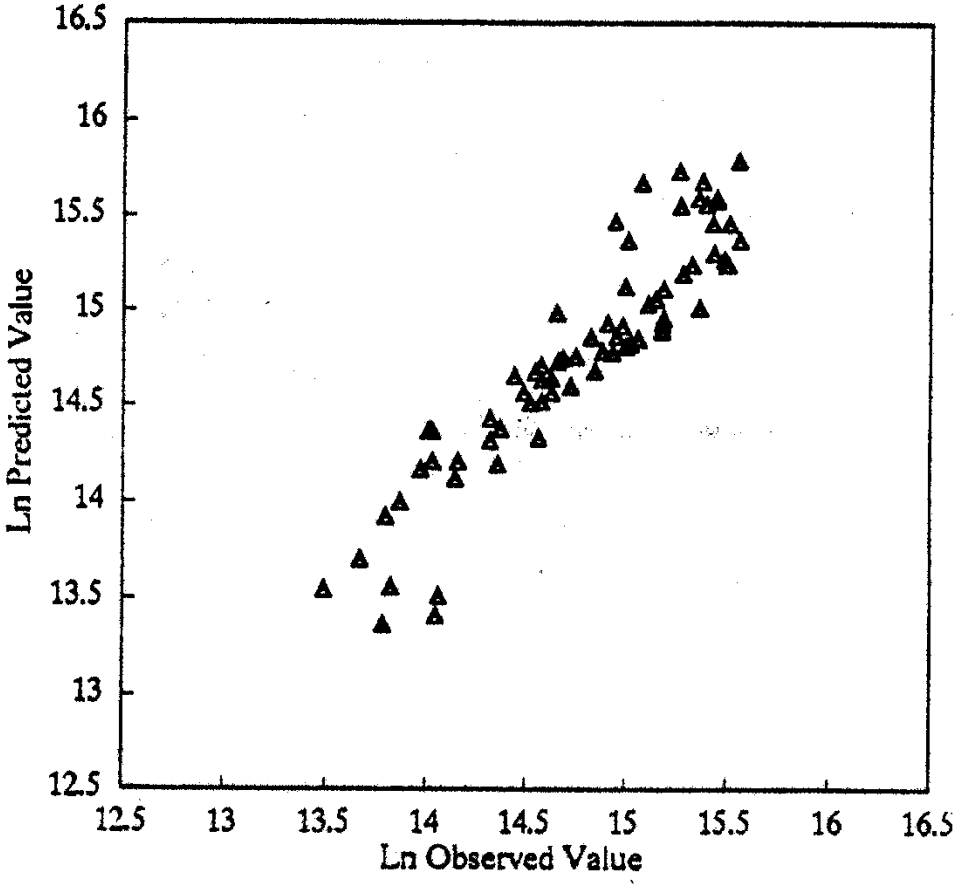

First normal stress difference and recoverable shear strain

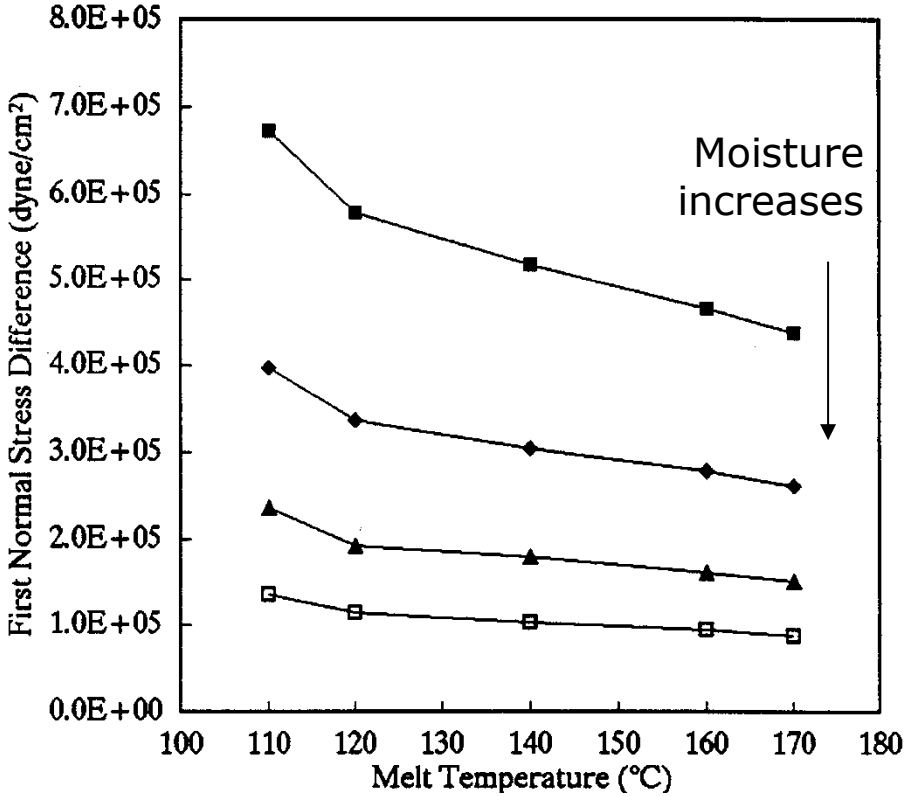

First normal stress difference of amylopectin as function of C and T

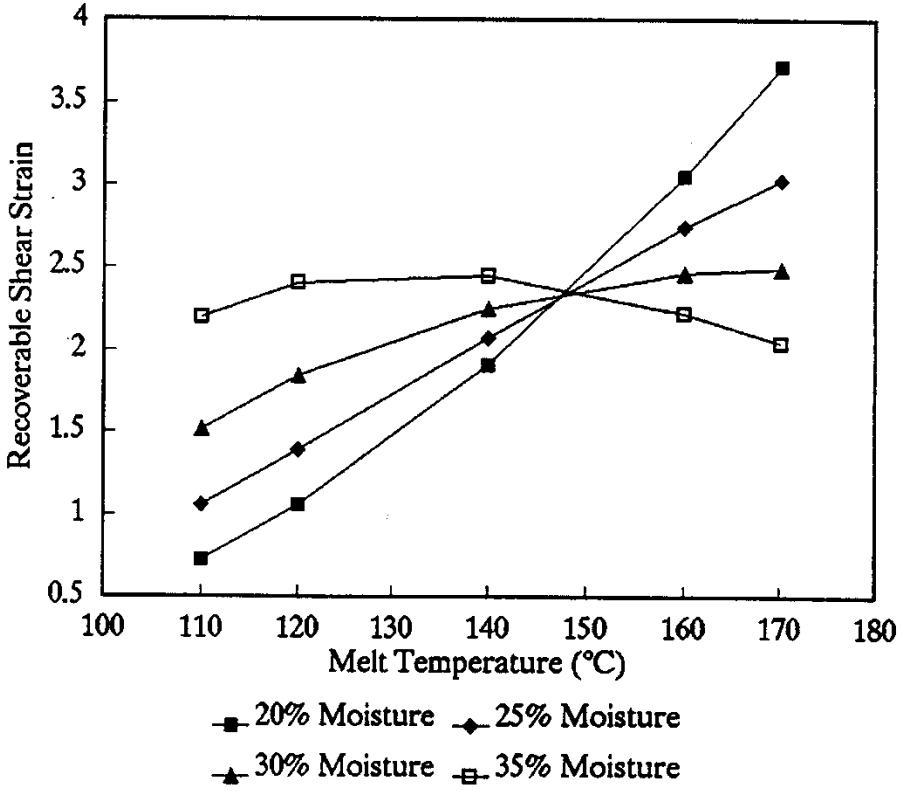

Recoverable shear strain of amylopectin as function of C and T

Bubble growth rate and diametral expansion are influenced by extrusion parameters

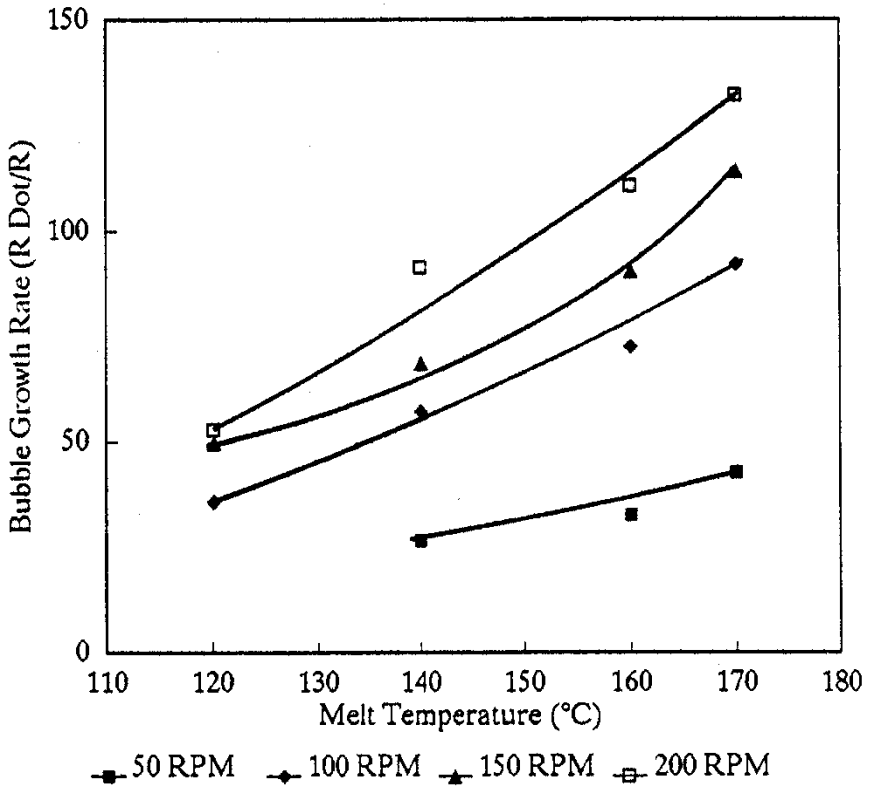

Corn meal extrudate, 16% moisture

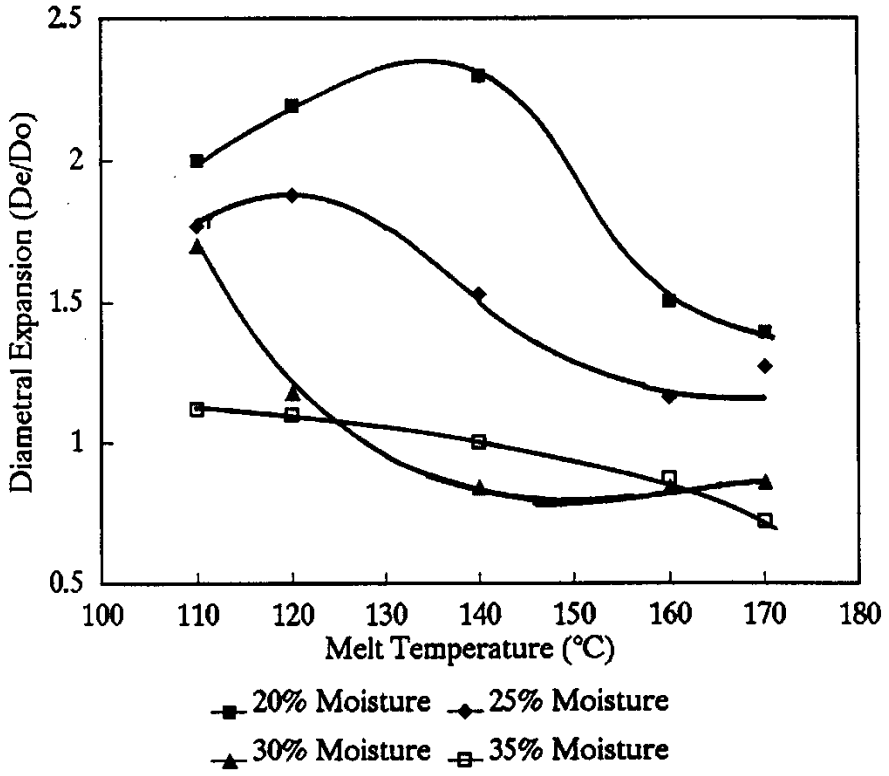

Amylopectin extrudate, 200 rpm

PURDUE UNIVERSITY

Influence of melt viscosity on extrudate expansion

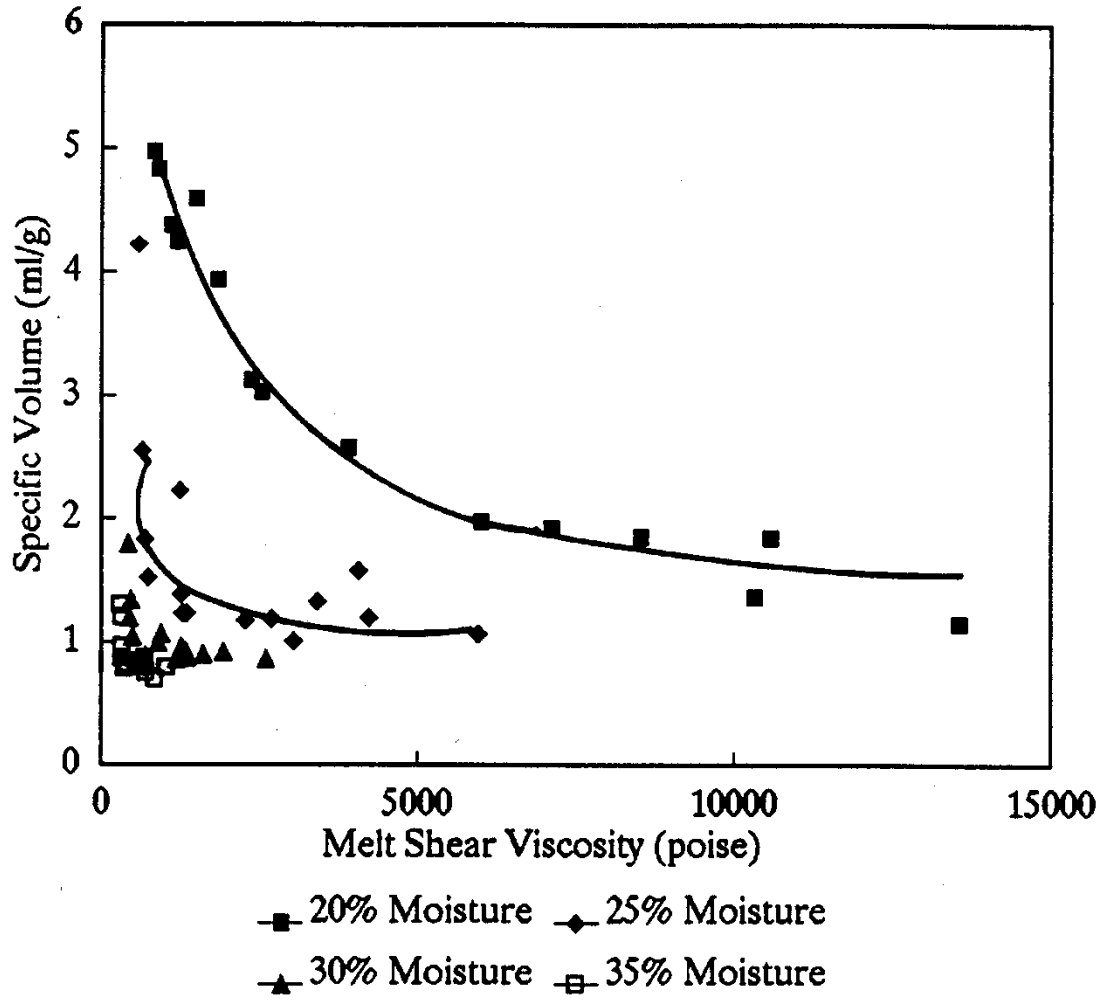

PURDUE UNIVERSITY

Influence of melt elasticity on extrudate expansion

According to Lai (1991):

$$N_1 = k_1 \dot{\gamma}^{k_2} e^{\frac{\Delta H}{RT}} e^{k_3 C}$$

N_1 - first normal stress difference

$\dot{\gamma}$ - shear rate

T - material temperature, K

C - material moisture content, %

k_1, k_2, k_3 - constants

Prediction vs. experimental:

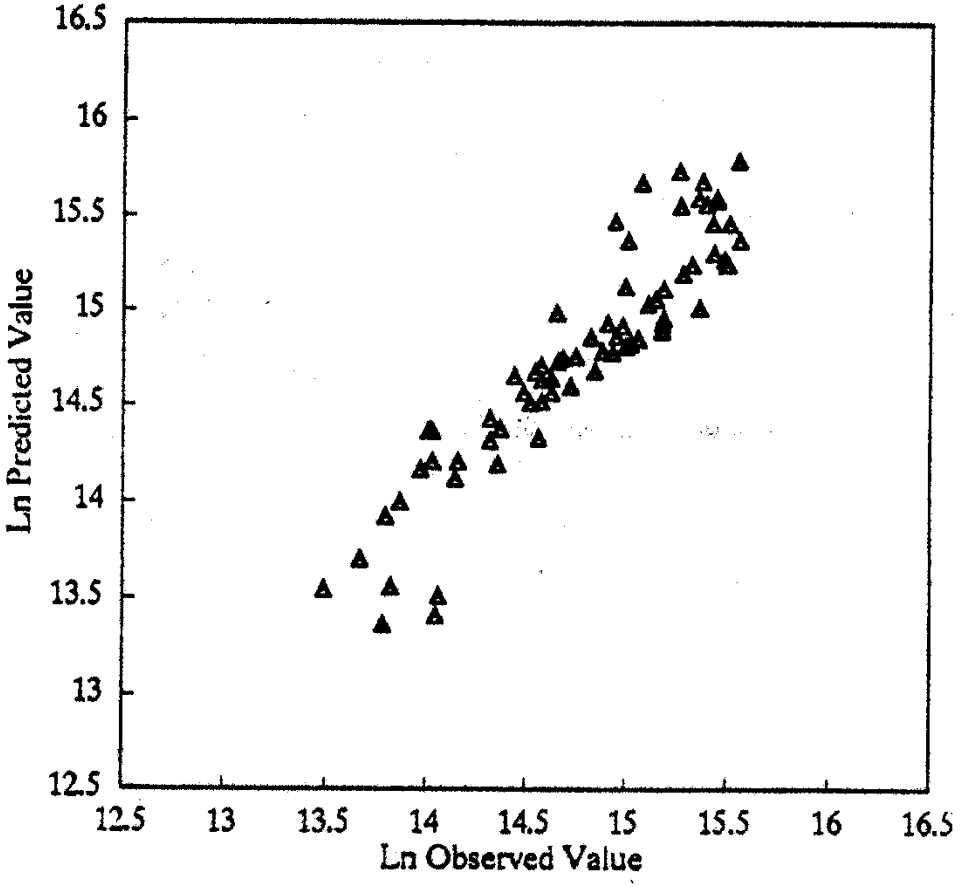

First normal stress difference and recoverable shear strain

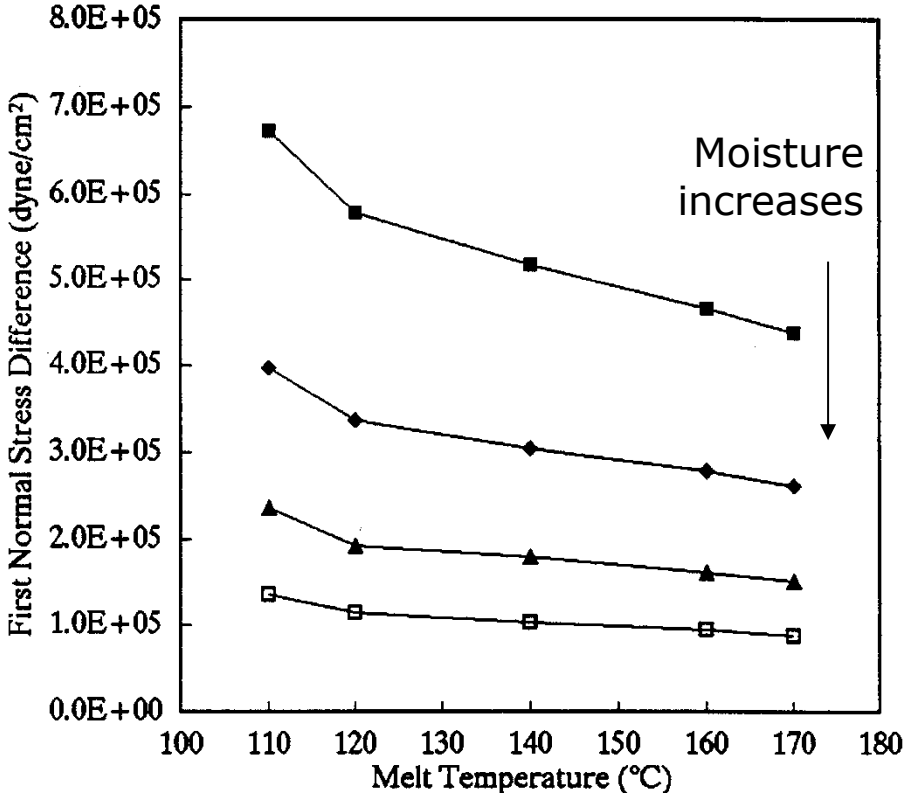

First normal stress difference of amylopectin as function of C and T

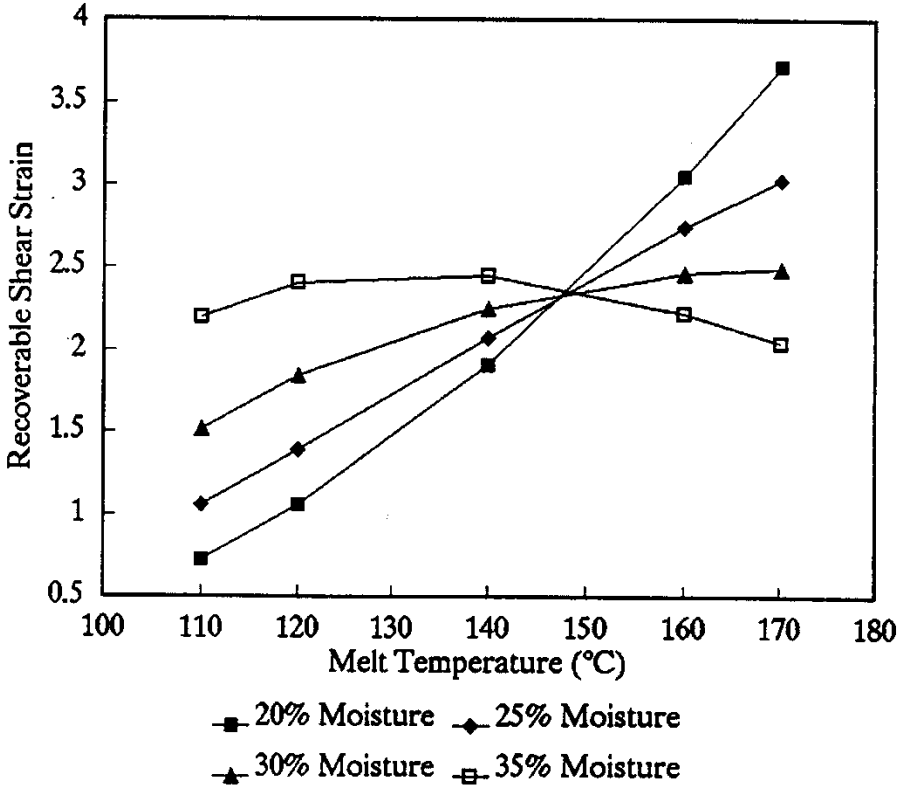

Recoverable shear strain of amylopectin as function of C and T

State diagrams

- Amorphous materials undergo transition from a solid glassy state to rubberlike state at the glass transition temperature (Tg).
- State diagrams allow the prediction of material phases that can be expected during engineering processes as a function of plasticizer content and shear/temperature
- The state diagrams for biological and synthetic materials describe the moisture content and temperature region at which the material will undergo appropriate reactions.

PURDUE UNIVERSITY

Quantification of networking properties through Rubber Elasticity Theory

- Molecular weight between entanglements (Me) or crosslinks (Mc), and slope and magnitude of the storage modulus (G′) are the most commonly used rheological measures for quantifying the network formation in biopolymers.
- When a polymer undergoes crosslinking, network density increases, Me (or Mc) decreases, G′ increases and becomes frequency independent.

$$Mc = \frac{c^{1/3}\rho^{2/3}RT}{G'} \qquad Nc = \frac{Mw}{2Mc}$$

Nc: number of crosslinks per molecule
Mw: Molecular weight
C: concentration
ρ: density
R: gas constant
T: temperature

PURDUE UNIVERSITY

Bubble growth is controlled by the driving force and material viscosity

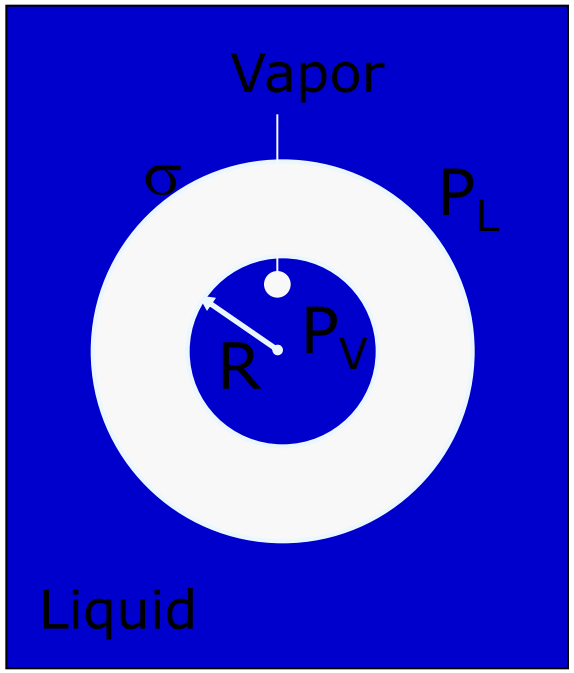

$$P_V - P_L = \frac{2\sigma}{R} + 4\eta_L\left(\frac{\dot{R}}{R}\right)$$

- For very viscous materials: $\frac{\dot{R}}{R} = \frac{\Delta P}{4\eta_L}$
- For power law fluids: $\frac{\dot{R}}{R} = \left(\frac{\Delta P}{4m}\right)^{\frac{1}{n}}$

PURDUE UNIVERSITY

Effect of Water Activity on Polar Component of Surface Energy

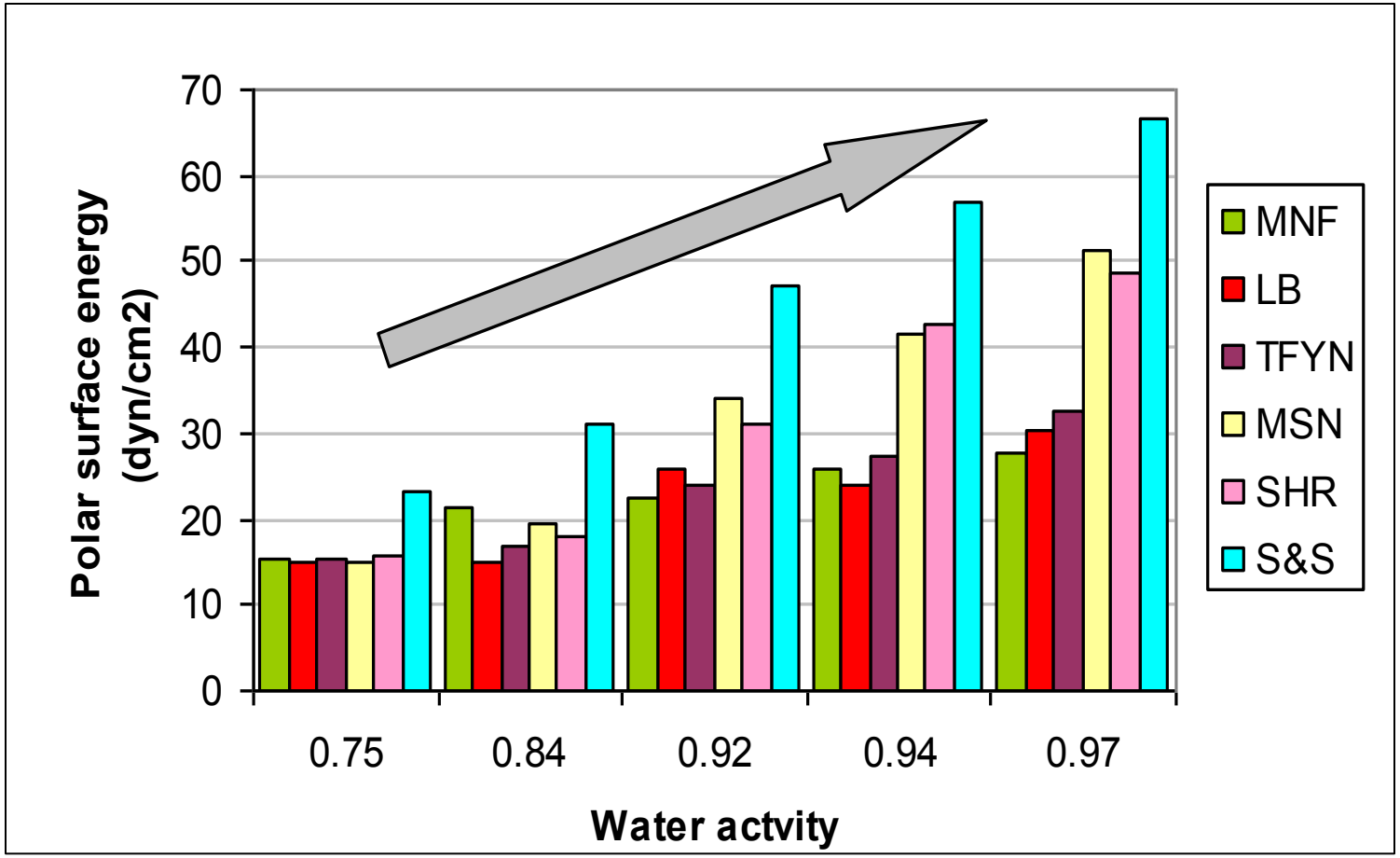

MNF: Manny's Fajita Tortilla
TFYN: Toufayan Plain Wrap
SHR: Sahara Wrap

LB: La Bandarita Tortilla
MSN: Mission Tortilla
S&S: Stop & Shop Tortilla

PURDUE UNIVERSITY

Effect of Water Activity on Dispersive Component of Surface Energy

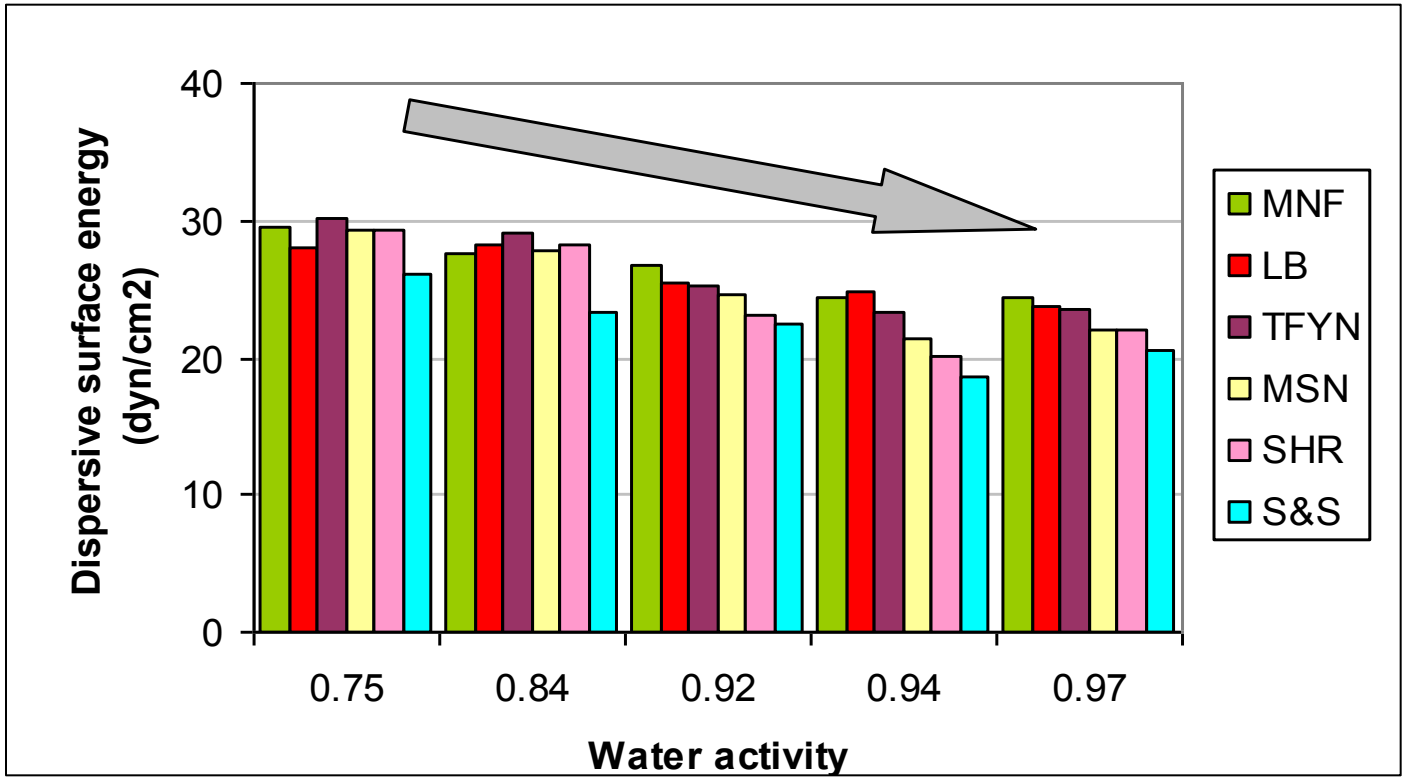

MNF: Manny's Fajita Tortilla
TFYN: Toufayan Plain Wrap
SHR: Sahara Wrap

LB: La Bandarita Tortilla
MSN: Mission Tortilla
S&S: Stop & Shop Tortilla

PURDUE UNIVERSITY

Effect of Water Activity on Total Surface Energy

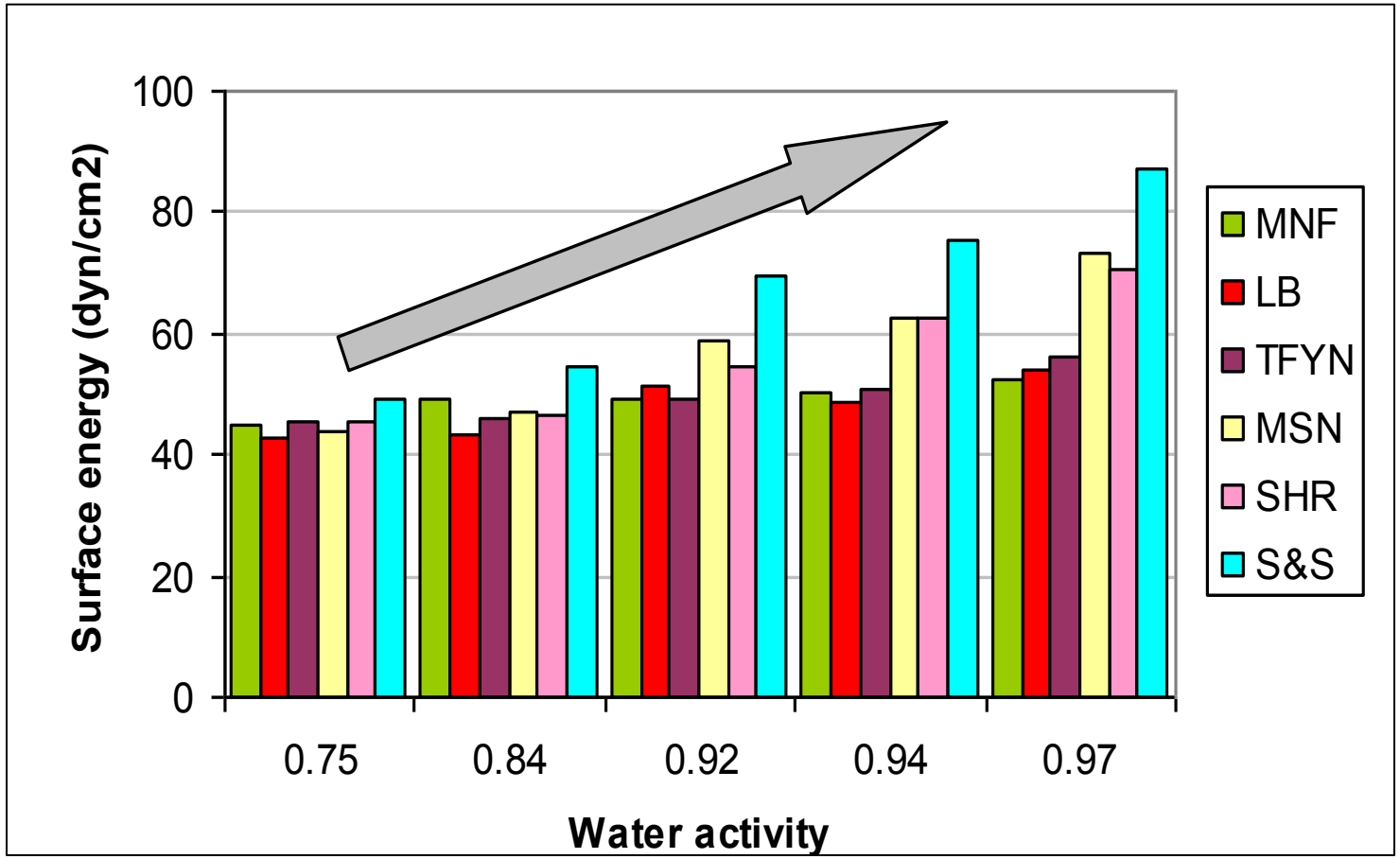

MNF: Manny's Fajita Tortilla
TFYN: Toufayan Plain Wrap
SHR: Sahara Wrap

LB: La Bandarita Tortilla
MSN: Mission Tortilla
S&S: Stop & Shop Tortilla

PURDUE UNIVERSITY

Predicting the Rheology of Glassy and Rubbery Phases

- Molecular weight between cross-links (*Mc*) versus time for (a) 7S and (b) 11S globulin fractions

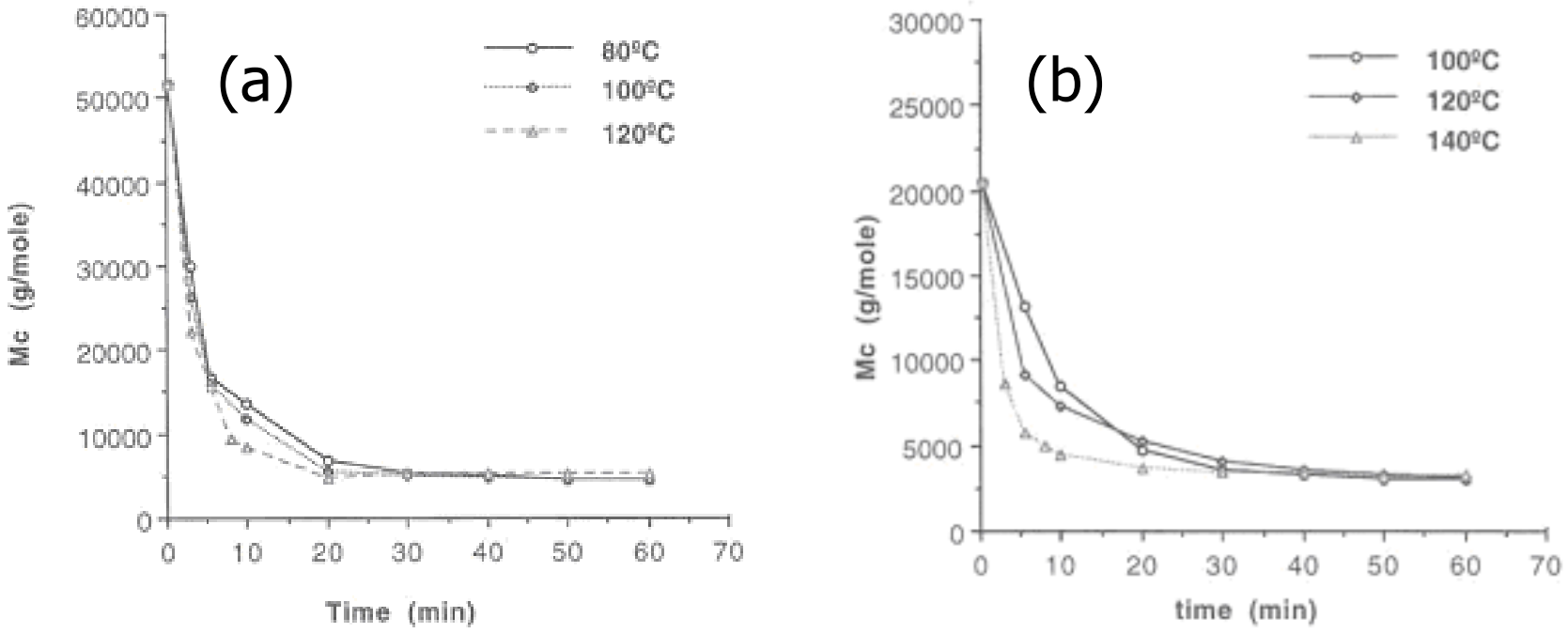

PURDUE UNIVERSITY

Kinetics of crosslinking

- The linear relationship between $\ln[(M_c-M_e)/(M_{c,0}-M_e)]$ and time indicates a first order crosslinking process.

$$\ln\left[\frac{M_c - M_e}{M_{c,0} - M_e}\right] = -kt$$

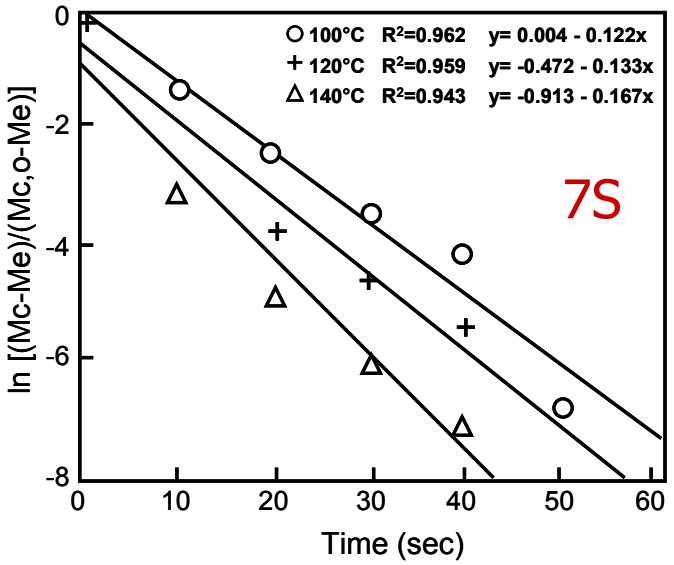

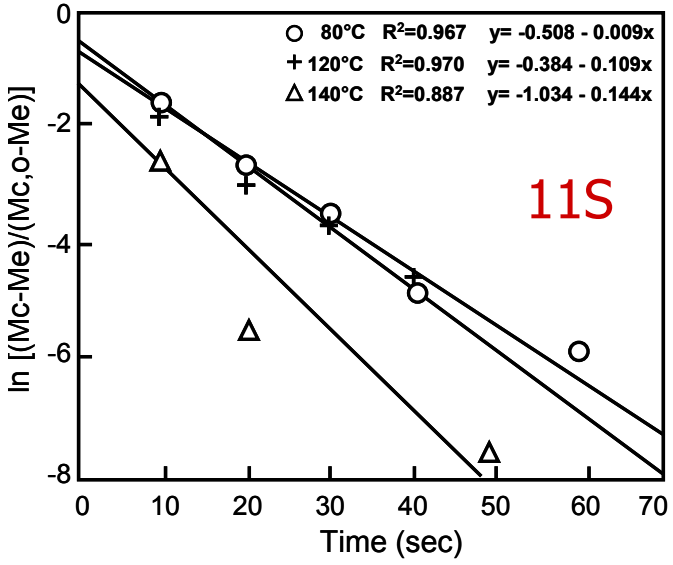

PURDUE UNIVERSITY

Influence of moisture on microwave expansion

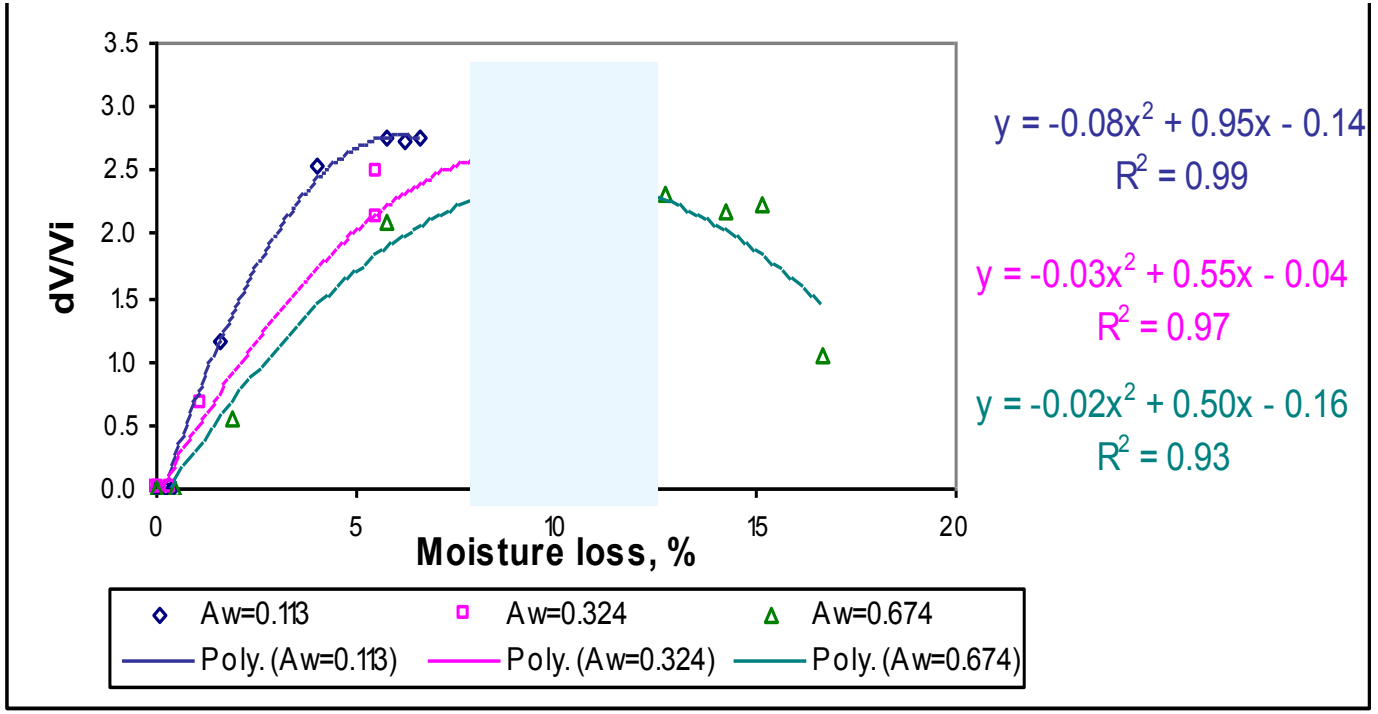

- Expansion – moisture dependency follows a second order degree polynomial

- At high moisture contents of the pellets, maximum expansion is followed by collapse.

PURDUE UNIVERSITY

Influence of solid fat on expansion

✓ The addition of more than 2% **solid** fat determines a significant increase of expansion

Aw = 0.61

5s **9s** **15s** **30s**

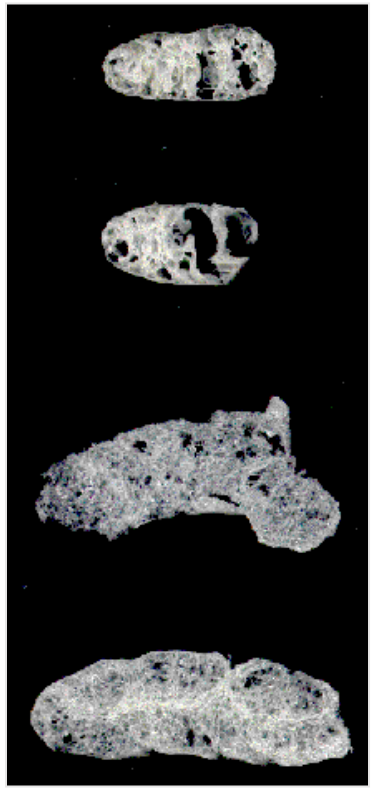

Reference

Reference + 2% fat

Reference + 6% fat

Reference +10% fat

✓ **Liquid fat** has a negative effect on expansion properties

PURDUE UNIVERSITY

Effect of solid fat content on expansion

- ✓ Maximum expansion is obtained for 5-8% solid fat

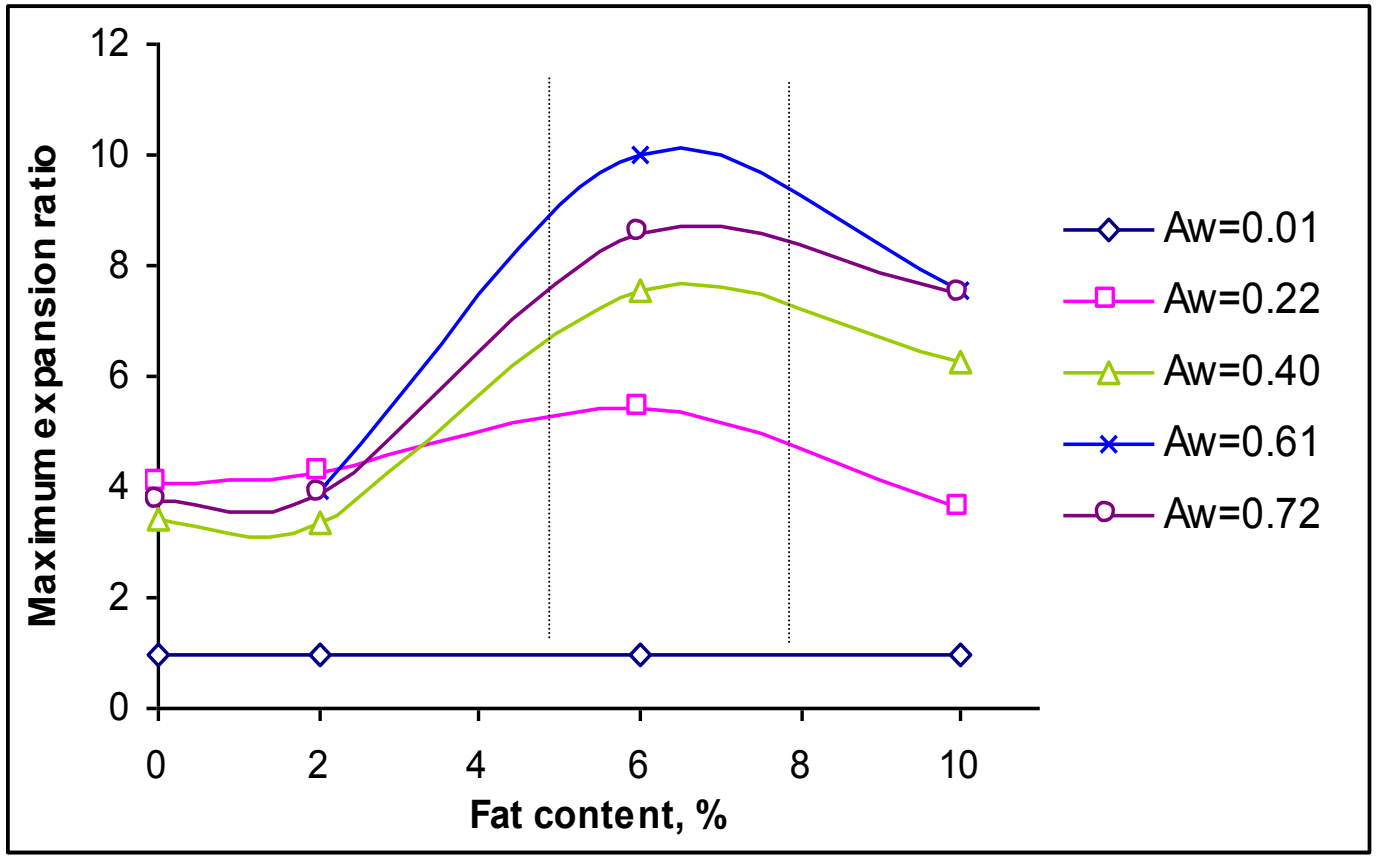

The addition of gums controls the shape during microwave expansion

- **In presence of Xanthan gum and CMC, the shape of the expanded products becomes more regular and the appearance smoother than for the reference**

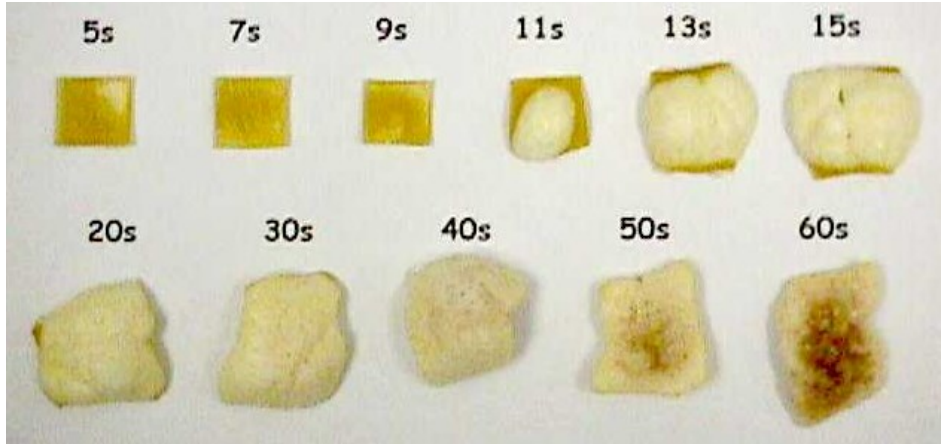

Shape evolution during microwave expansion of corn flour pellets

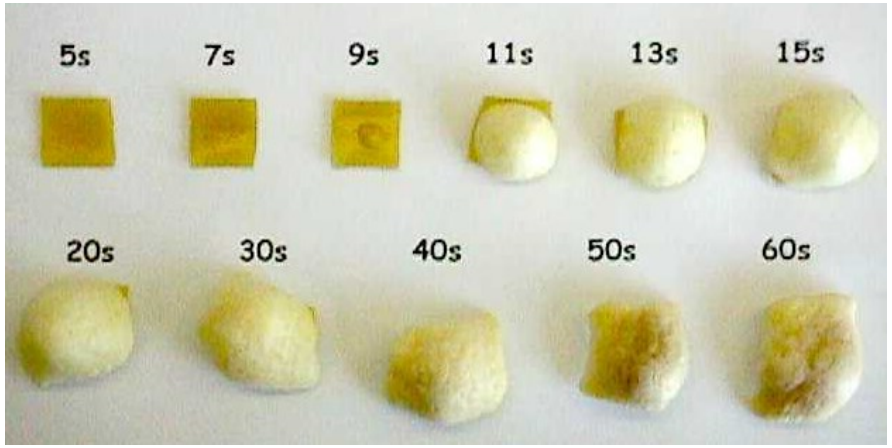

Shape evolution during microwave expansion of corn flour pellets with 1%XG

PURDUE UNIVERSITY

Moisture Sorption Isotherm

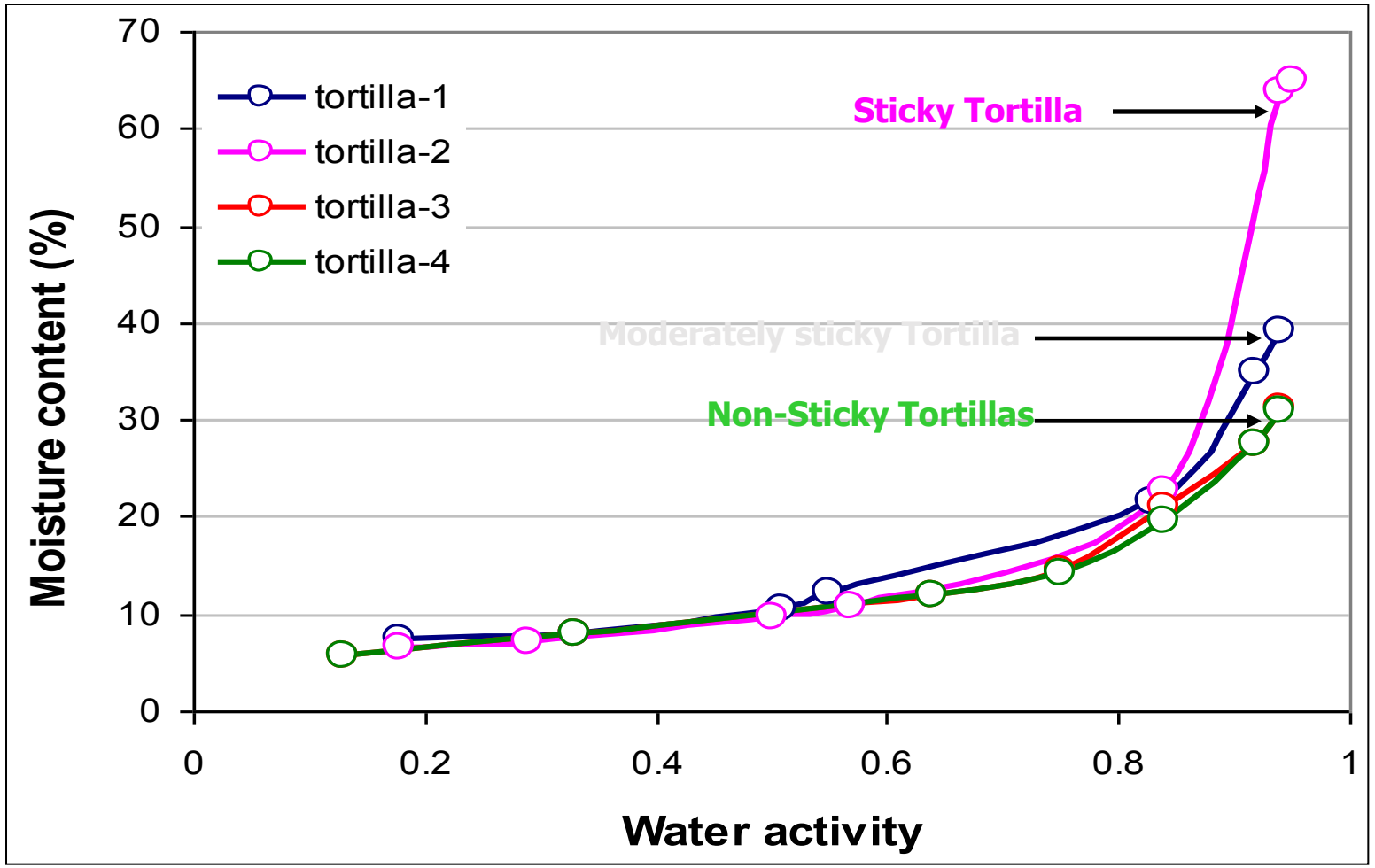

(Different colors indicate different commercial products)

PURDUE UNIVERSITY

Biocompatible spherical nanoparticles and nanotubes

- Biocompatible nanoparticles from natural biopolymers (carbohydrates and proteins)
- protein and carbohydrate polyelectrolytes are a desirable choice
- nanoparticles with unique physical, chemical, and biological characteristics can be made.
- Methods for the preparation of bio-nanoparticles :
  - Desolvation
  - Coacervation
  - Emulsification

PURDUE UNIVERSITY

Nanoparticulation of Starch

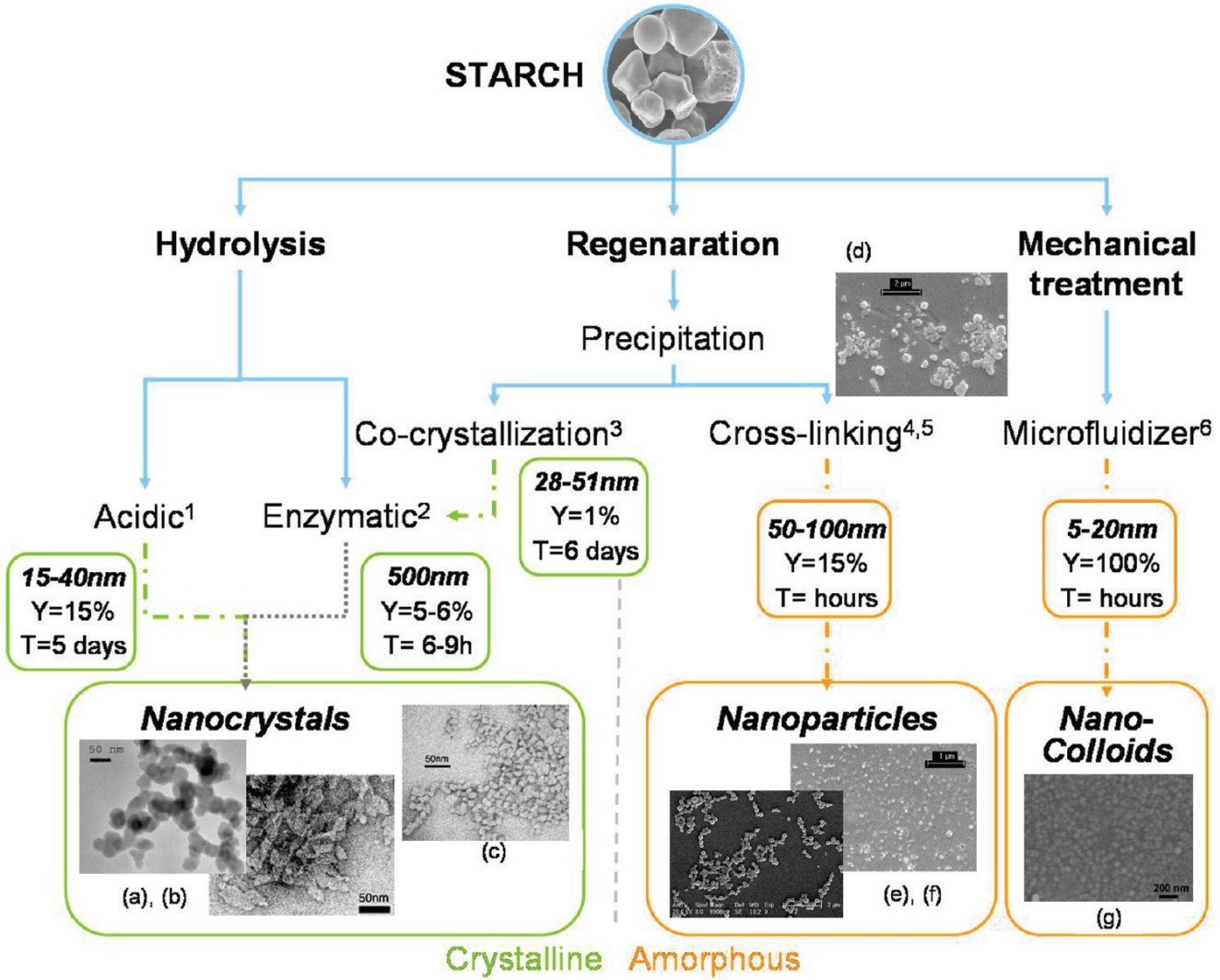

References: Putaux et al., 2003 and Le Corre, Bras, Dufresne, 2010

PURDUE UNIVERSITY

Quantum dots: application as food structure and microorganisms detection tools

- QDs are semi-conductor materials that have a core-shell structure

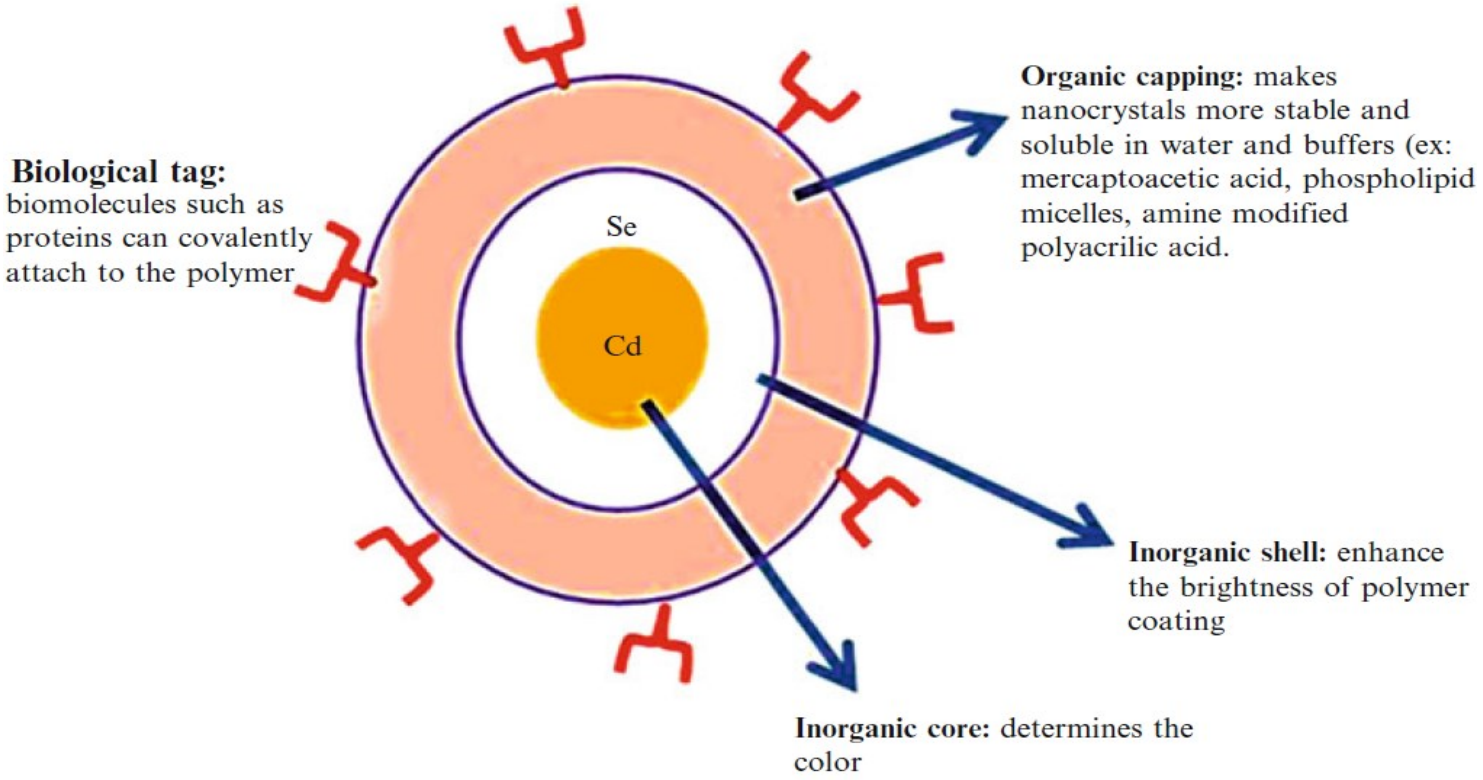

Multifunctional quantum dots can be used to target and image complex systems simultaneously (Luecha, J., Sozer, N., Kokini, J. L. 2013)

PURDUE UNIVERSITY

Distribution of gluten in baked bread

- Merged fluorescence and differential interference contrast (DIC) images of QD labeled gluten proteins from top–center–bottom sections of baked bread samples are shown.
- The top and bottom sections showed a great deal of ungelatinized starch granules surrounded by an uneven gluten network.
- Parts of the gluten network was dense, as evidenced by the darker yellow color observed.

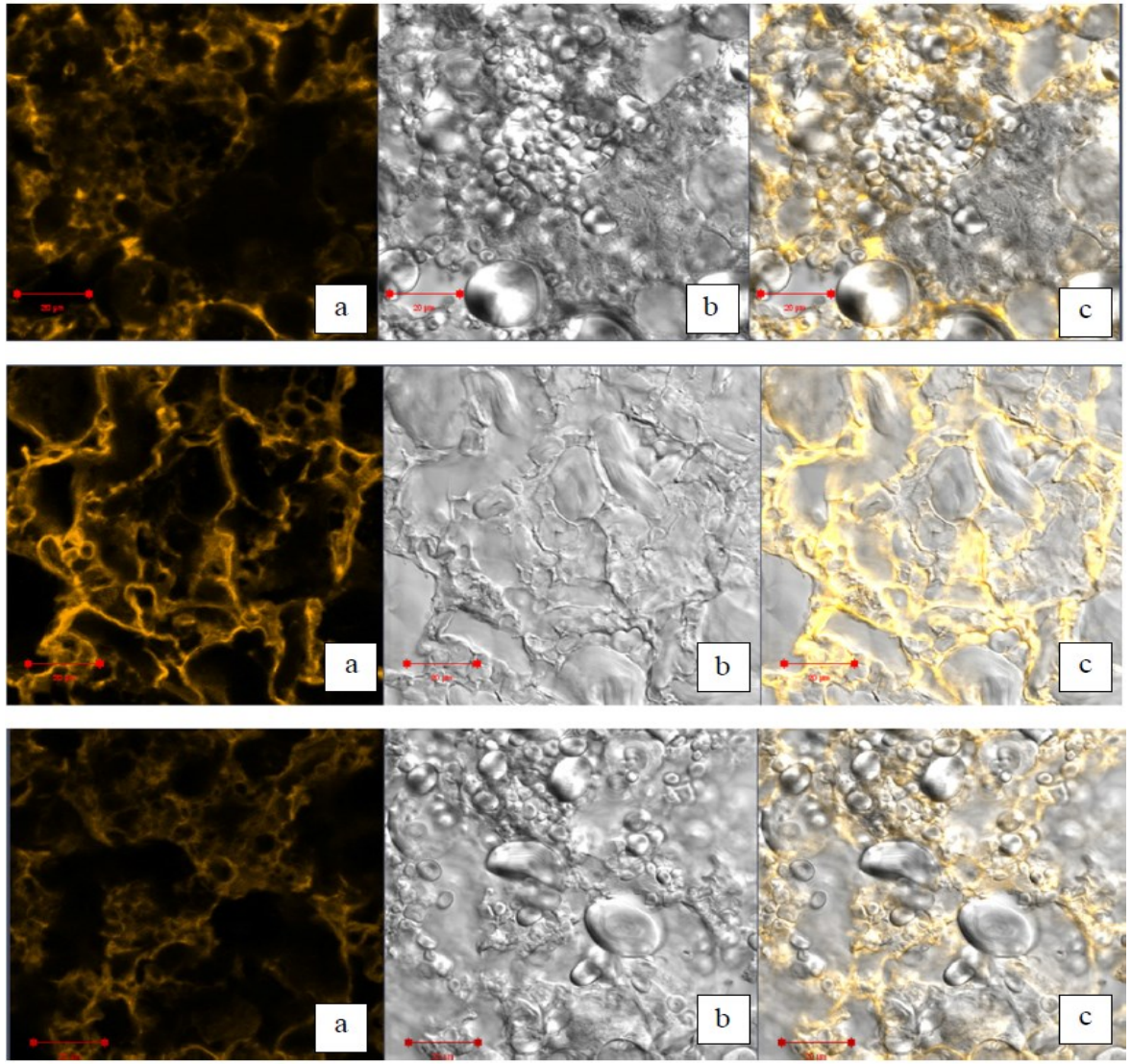

Bread sample (top–center–bottom cross-sections of bread) labeled with QDs 40× objective. a) Fluorescence image; b) DIC image; c) merged fluorescence–DIC image (Sozer and kokini, 2014).

PURDUE UNIVERSITY

No photo bleaching and no contamination of the background with quantum dots in comparison with Rhodamine 6B

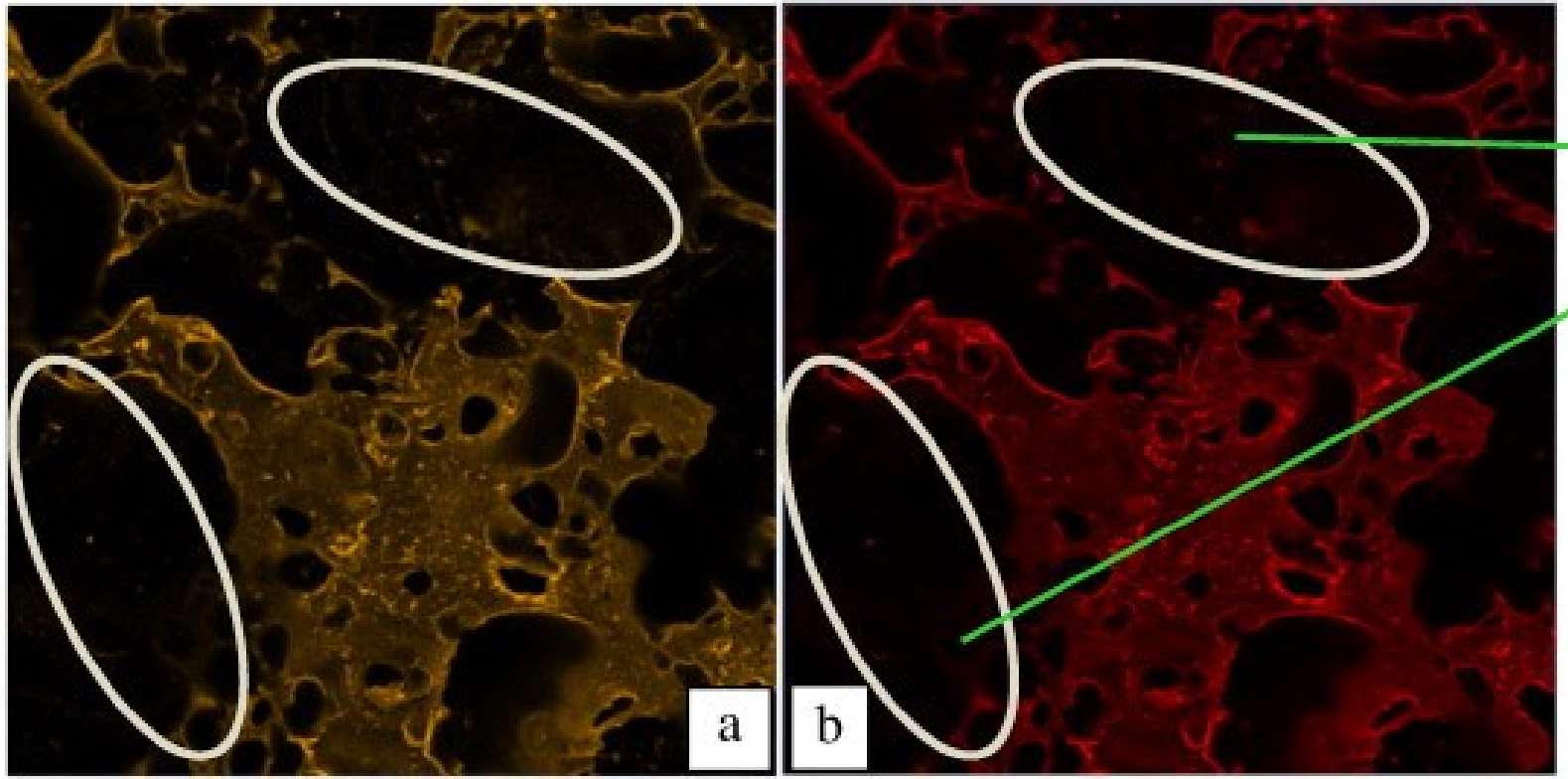

No contamination of the background by QDs (black background with no fuzziness)

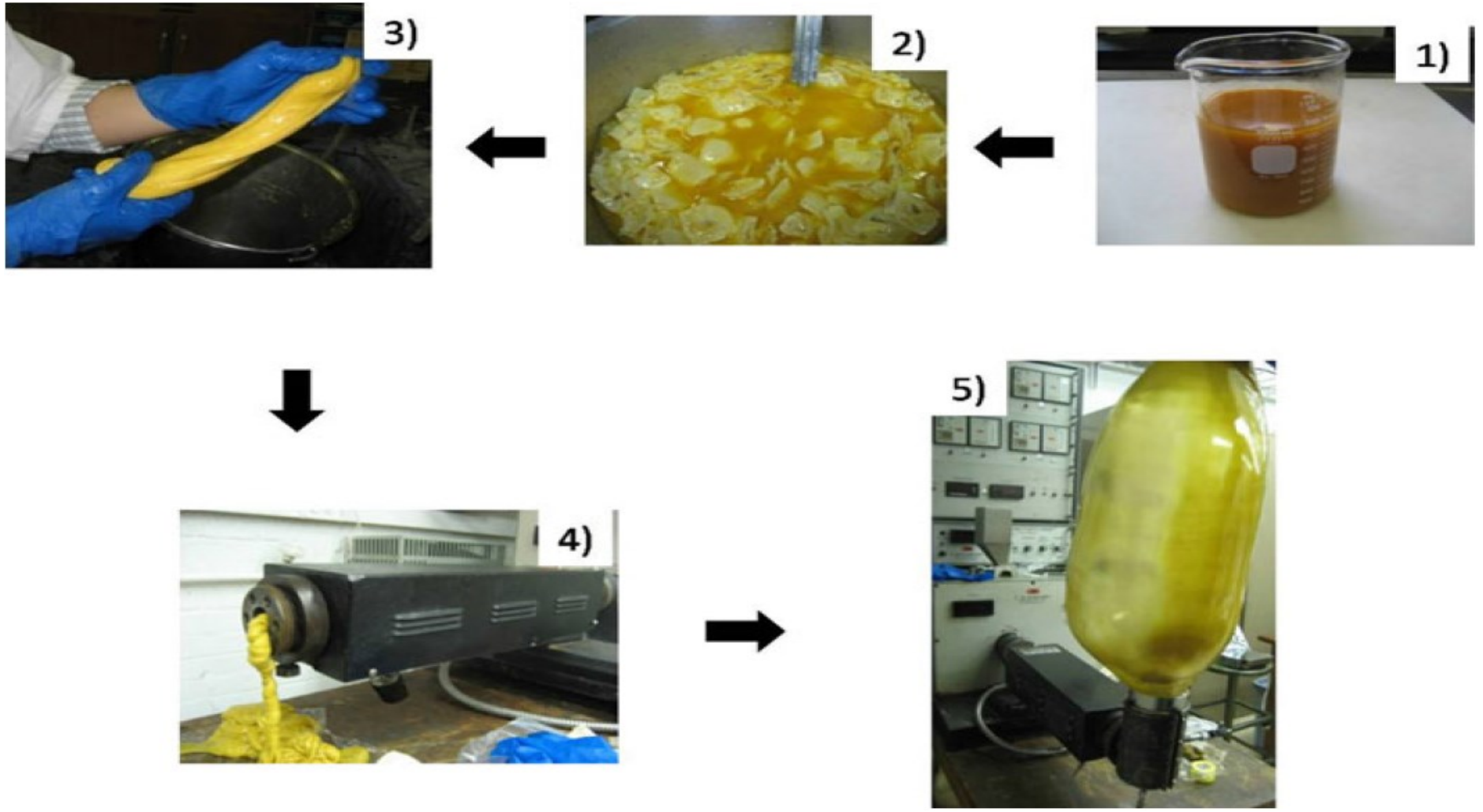

The steps of the blown extrusion technique including 1 zein MMT solution, 2 precipitation, 3 resin formation, 4 cold extrusion, and 5 balloon formation (Luecha, Sozer, and Kokini, 2010).

TEM images show that both montmorillonite/zein nanocomposite preparation methods form partially exfoliated structures

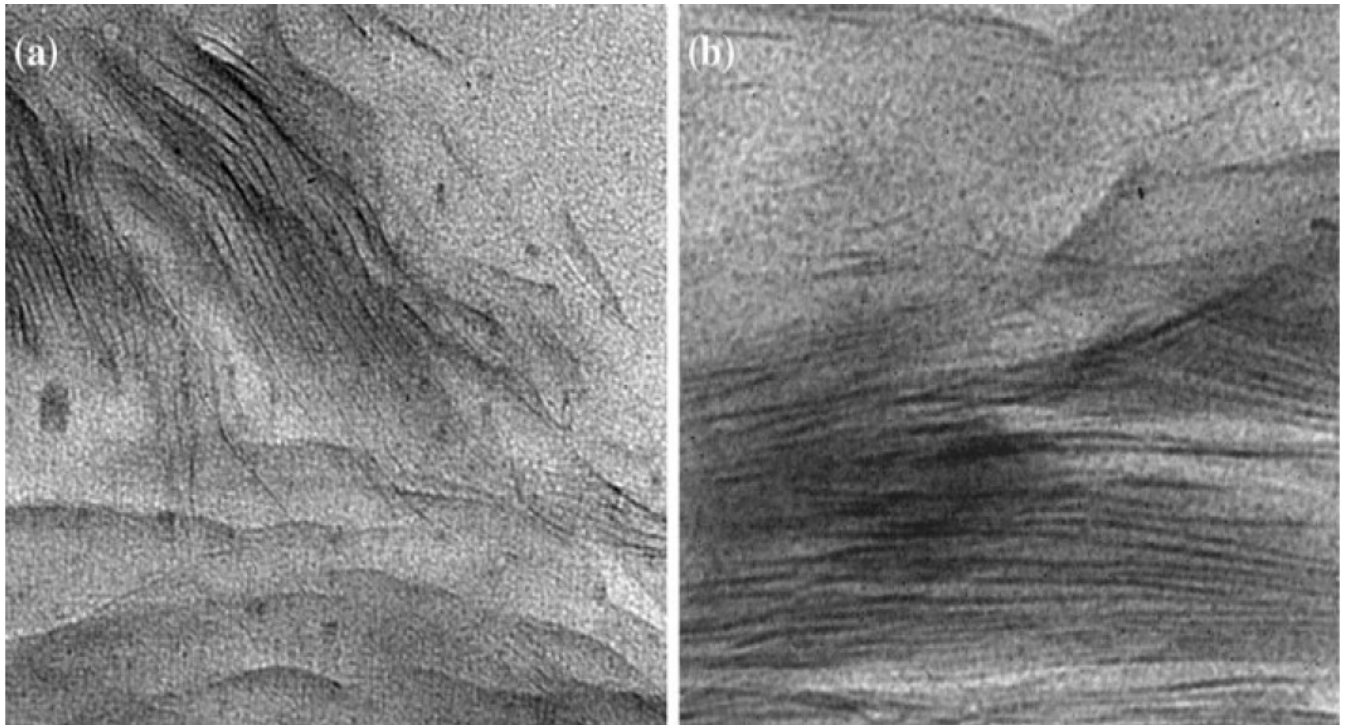

- TEM images of a) solvent cast zein MMT nanocomposite films with 5 wt% of MMT, and b) blown extrusion zein MMT nanocomposite films with 5 wt% of MMT (Luecha, Sozer, and Kokini, 2010).

Measurement of biaxial rheological properties

Bubble inflation method

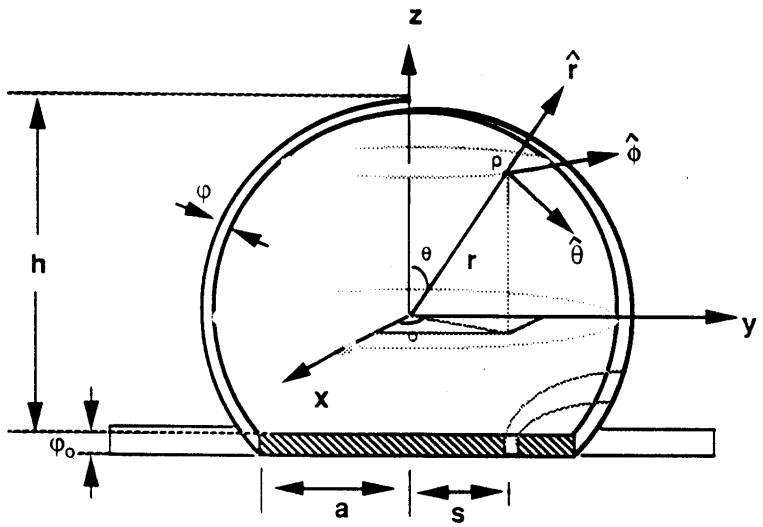

Lubricated film method

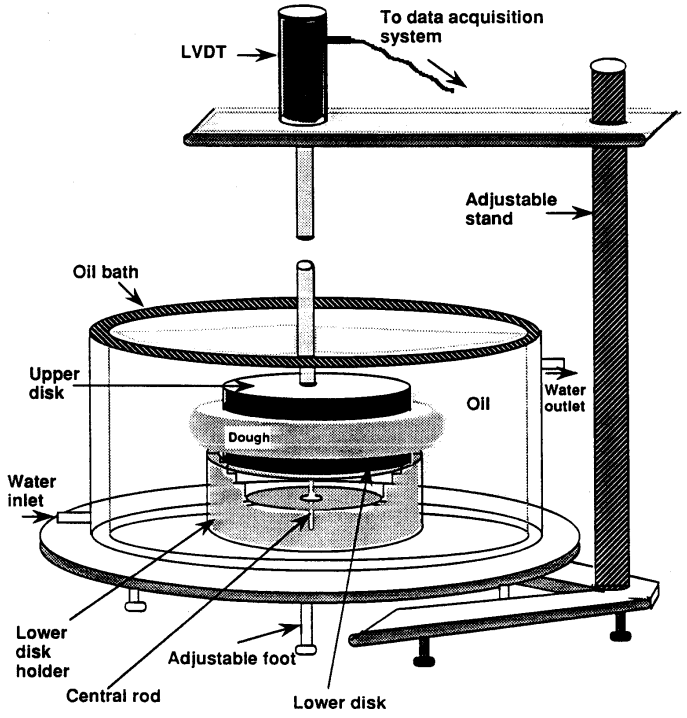

Transient properties of wheat flour dough–bubble inflation data

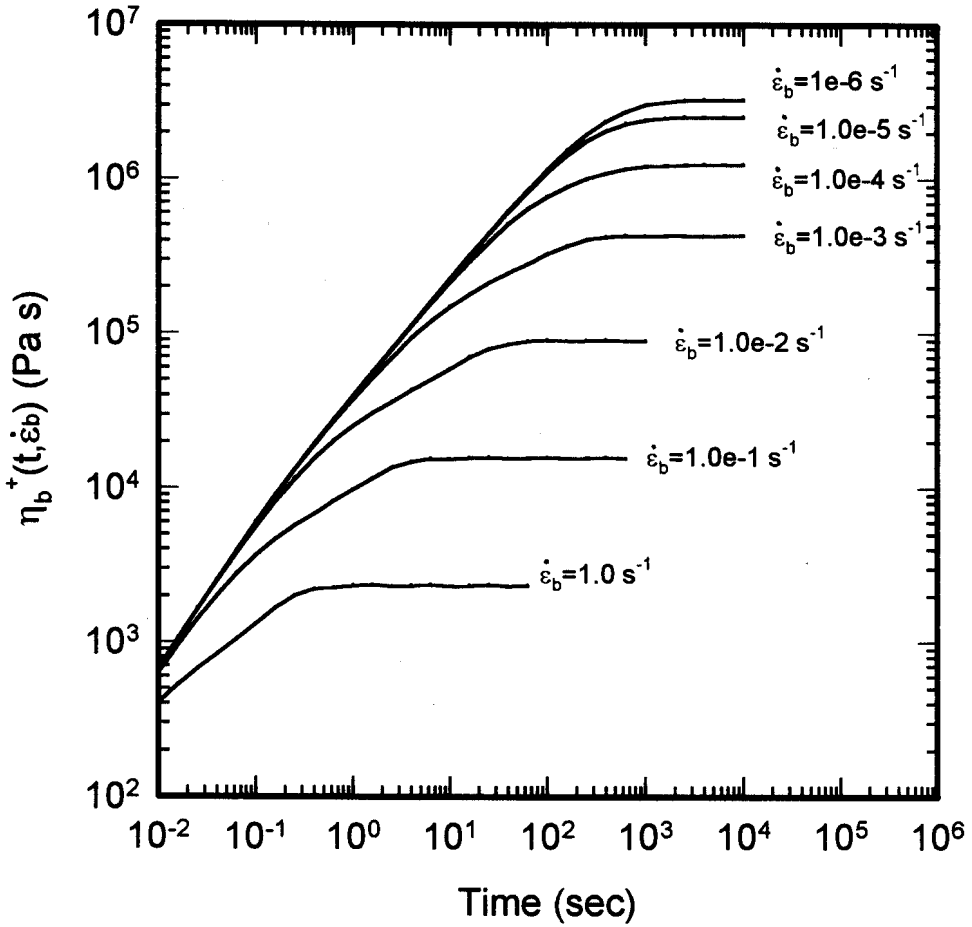

Agreement between squeeze flow and bubble inflation measurements

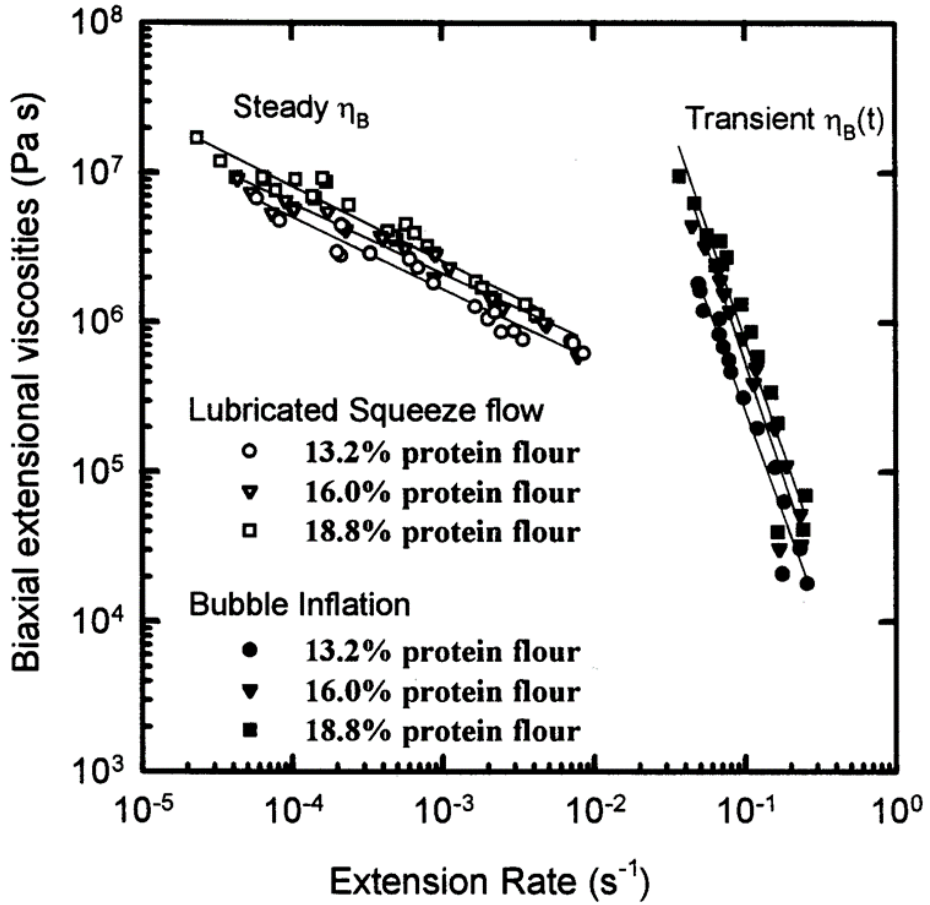

Relationships between shear and extensional viscosities

- A dimensionless ratio, the Trouton number (N_T), is used to compare the relative magnitude of extensional and shear viscosities:

$$N_T = \frac{\text{extensional viscosity}}{\text{shear viscosity}}$$

- The Trouton ratio for a Newtonian fluid in uniaxial (η_E), biaxial (η_B) and planar (η_P) extensions:

$$\eta = \frac{\eta_E}{3} = \frac{\eta_B}{6} = \frac{\eta_P}{4}$$

(Dealy, 1984)

PURDUE UNIVERSITY

Effect of Water Activity on the Instrumental Stickiness

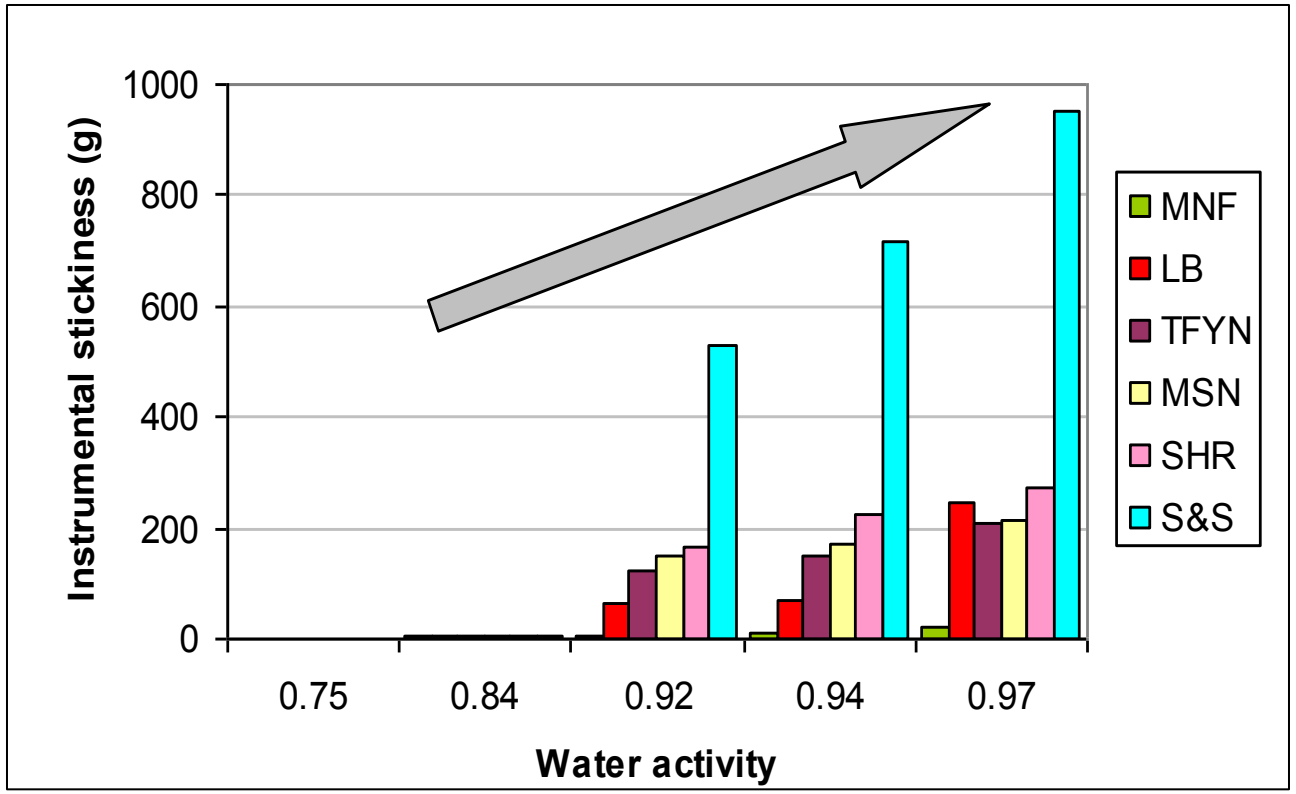

MNF: Manny's Fajita Tortilla
TFYN: Toufayan Plain Wrap
SHR: Sahara Wrap

LB: La Banderita Tortilla
MSN: Mission Tortilla
S&S: Stop & Shop Tortilla

PURDUE UNIVERSITY

Effect of cellularity on average number of peaks in extruded snacks

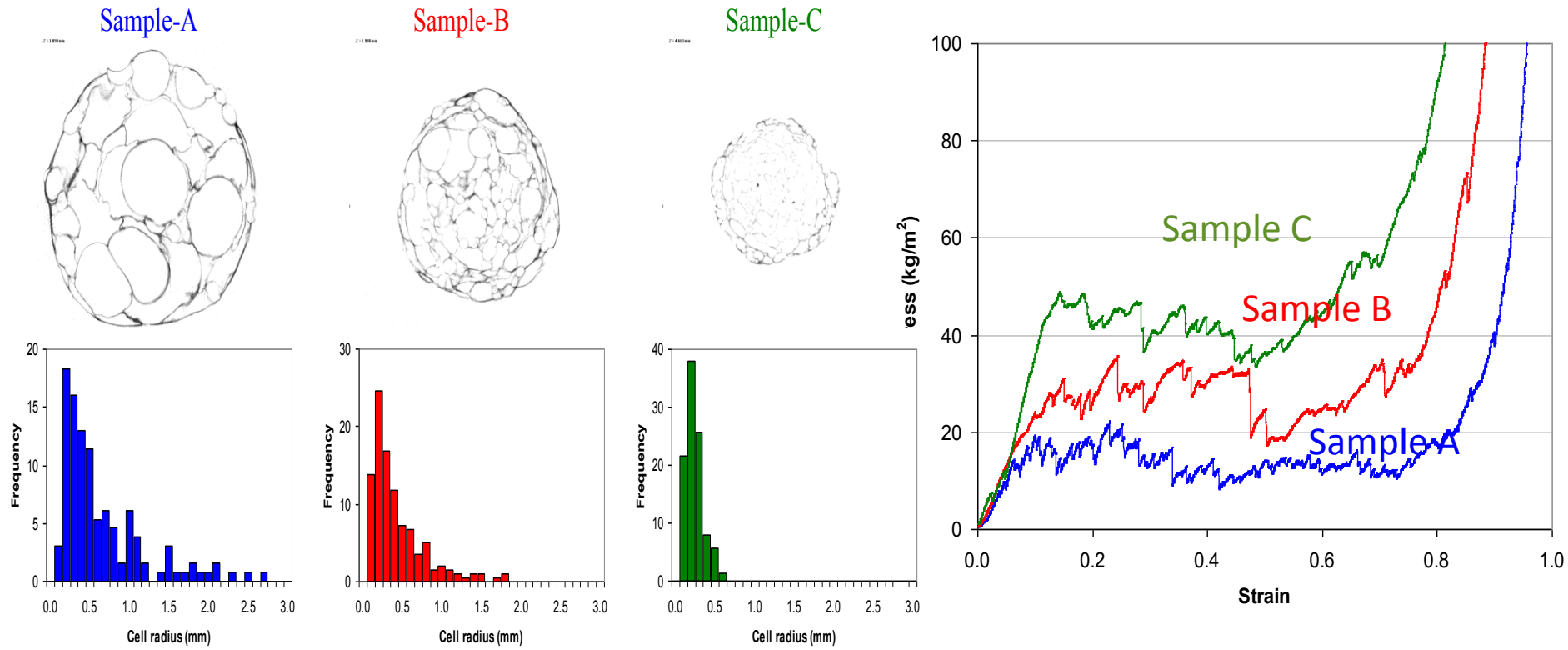

Average cell size and cell size distribution affect fracture behavior significantly.

Distribution of gliadin around gas cells where the fluorescence intensity is highest relative to bulk dough.

The peaks' whiteness height is due to quantum dot fluorescence intensity

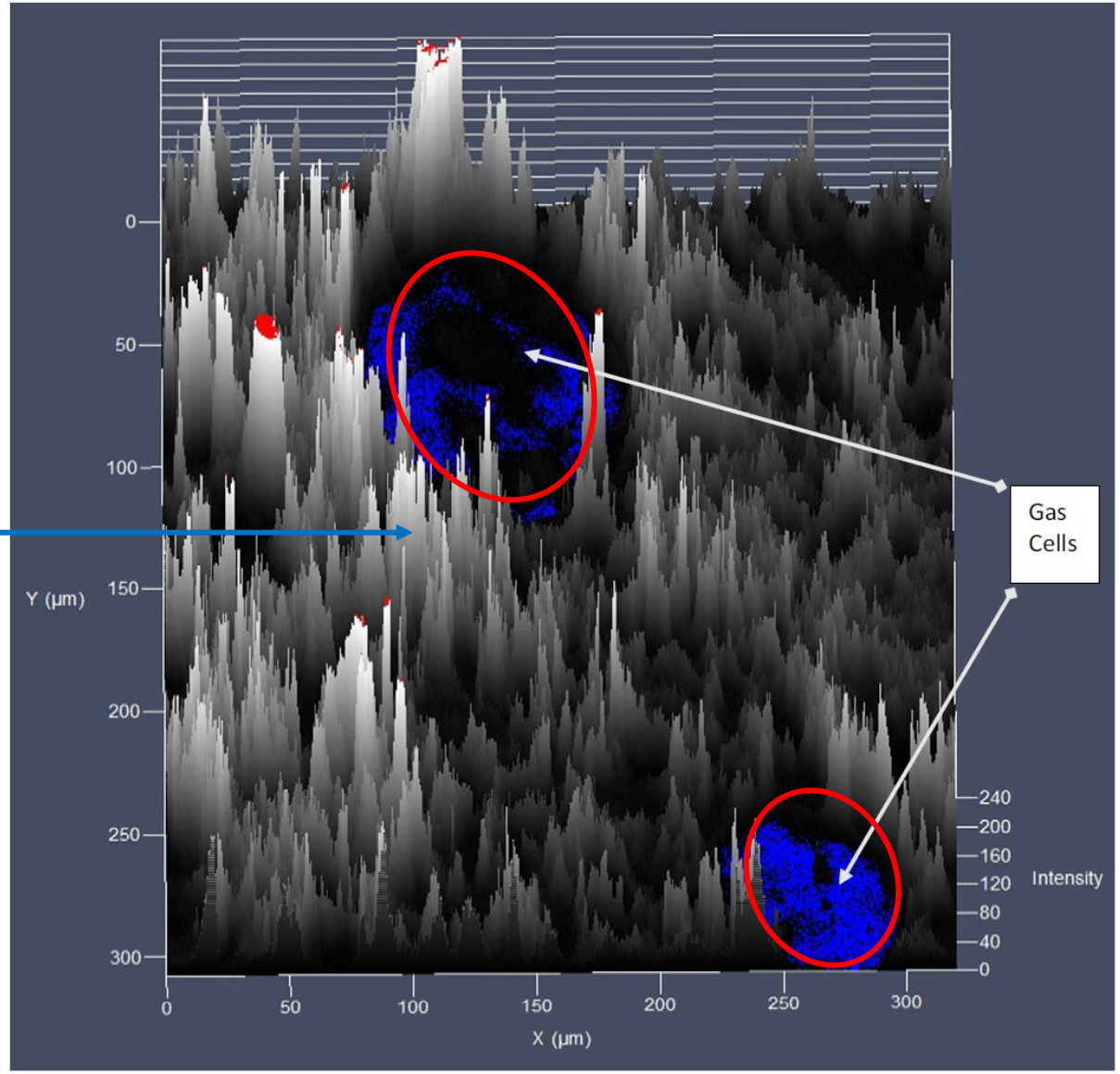

State diagram for an extruded meat–starch matrix (two Tgs)

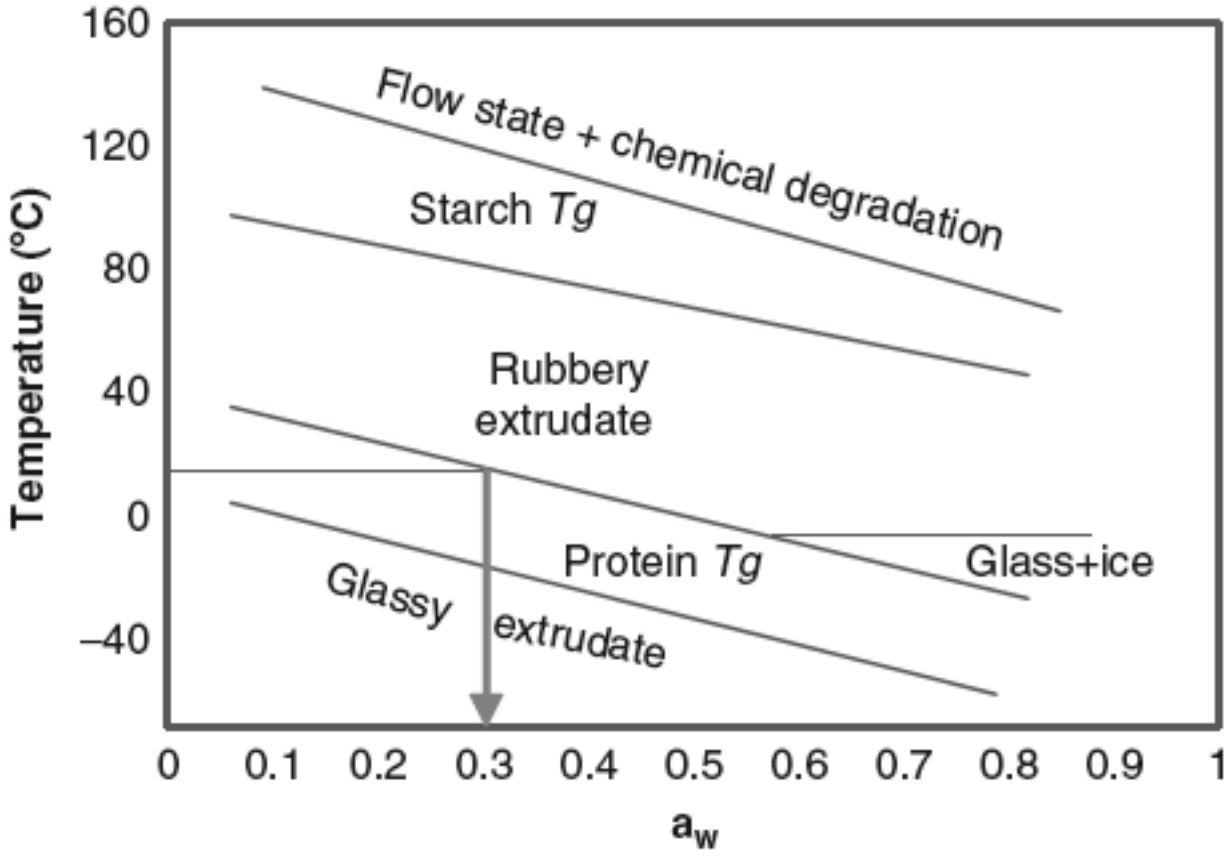

Hypothesis for the mechanism of microwave expansion

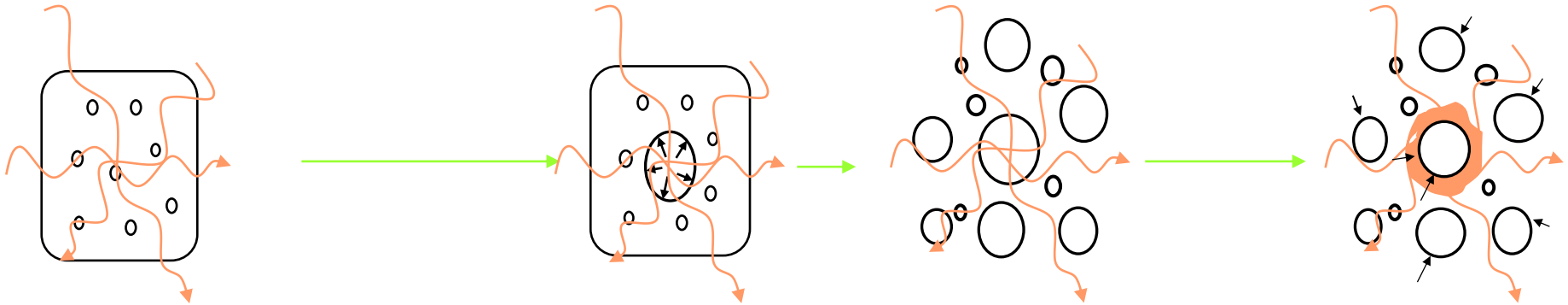

1. Water vaporizes, creating locally a high pressure; bubbles form at nuclei.

2. The glassy matrix undergoes a phase transition to a rubbery matrix where the bubbles grow; if the matrix is too soft, collapse occurs.

3. Under further heating, with moisture loss samples begin to burn.

Biaxial extension during expansion and bubble growth

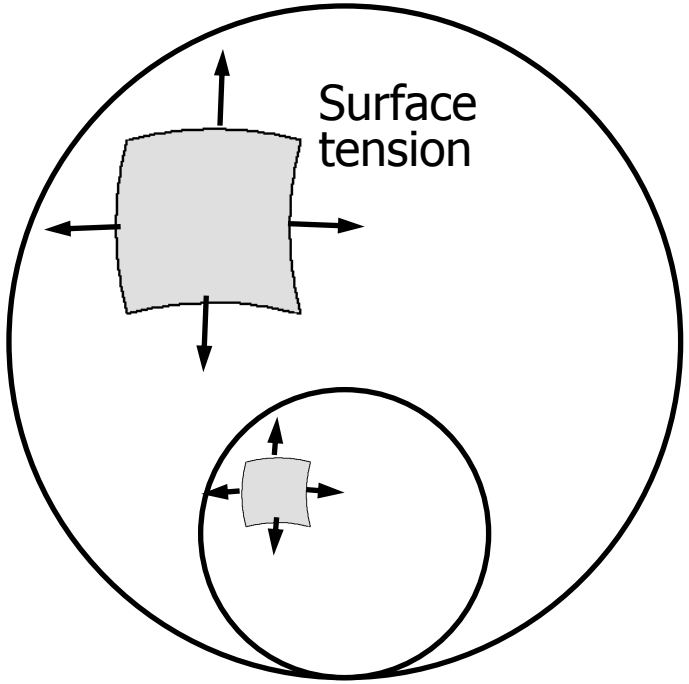

Biaxial extension
during bubble growth

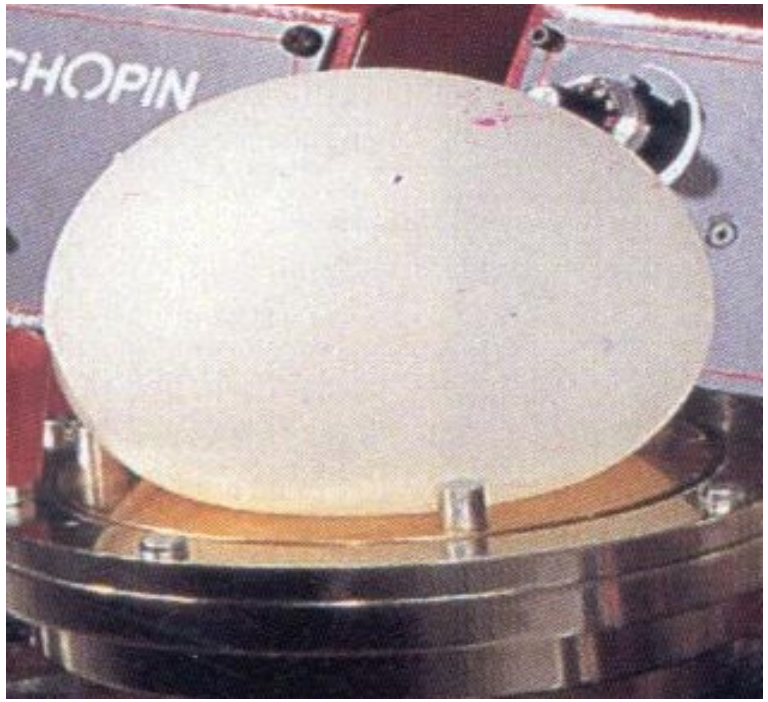

Important phenomena in extrudate expansion

- **Extrudate swell -** the phenomenon that governs the diametral expansion of extrudates in the absence of blowing agents. It is caused by elastic recovery.

- **Bubble growth** – in a high viscosity mass, it is mainly determined by the driving force and the resistance to deformation.

- **Bubble collapse** – determines the final extrudate expansion in high moisture and low viscosity materials.

PURDUE UNIVERSITY

Gliadin Tg using DSC

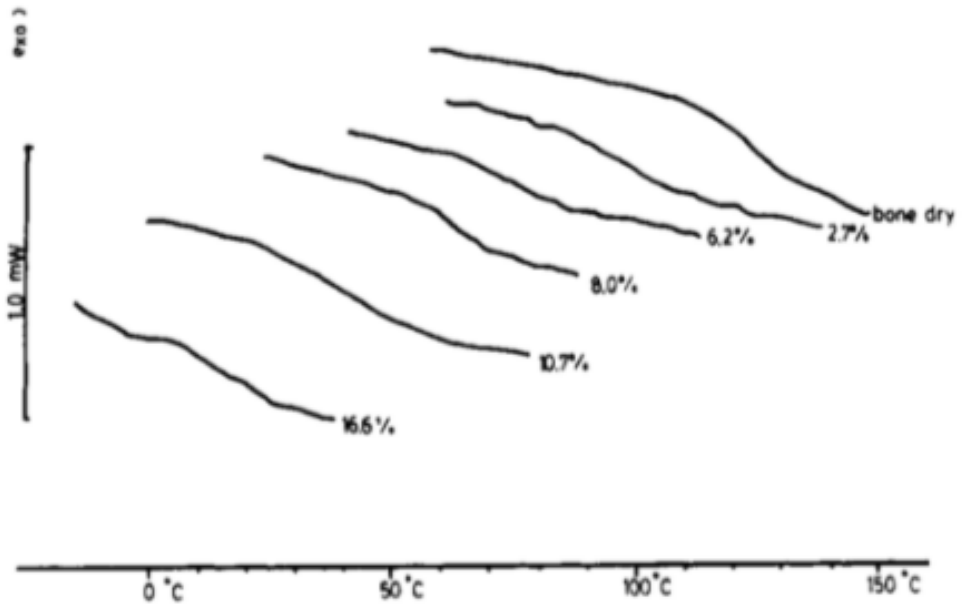

Figure 3. Differential scanning calorimetry curves for gliadin at different moisture contents.

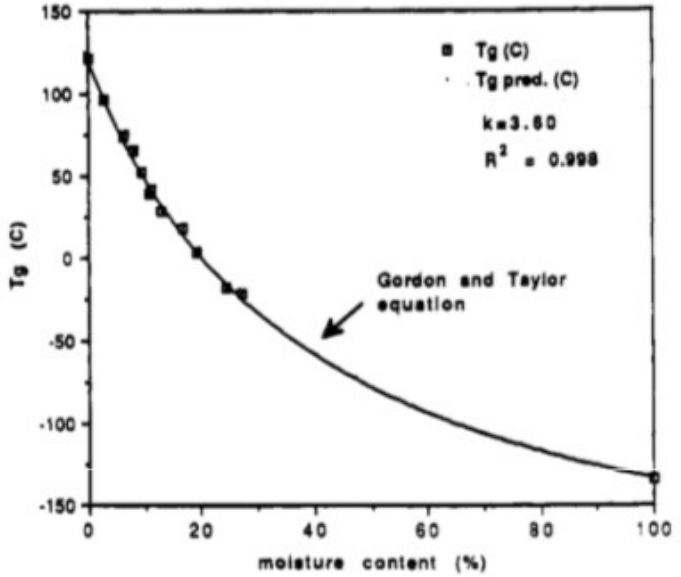

Figure 5. Gordon–Taylor fit for the glass transition in the Sigma gliadin state diagram.

Table II. Glass Transition Temperatures of Gliadin at Different Moisture Contents Determined by Differential Scanning Calorimetry

equilibrium moisture content ± 0.5 (%)	glass transition temperature (T_g) ± 2.5 (°C)
0.0	121.25
2.7	96.5
6.2	73.4
8.02	64.9
10.7	39.4
16.62	17.4